ER8515S

GEOLOGICAL SURVEY EXPLANATORY REPORT

SHEET 41

ST HELENS

JRVEY 1:50 000 EXPLANATORY REPORT • 41 (8515S) • ST HELENS • 1992 • ISBN 0 7246 2099 0

TASMANIA DEPARTMENT OF MINES

COVER PHOTOGRAPH

Aerial view of St Helens, looking north. Medeas Cove at left and Georges Bay at right. Granite and adamellite intrusions occupy the foreground and higher ground in distance. The low ground around the township is underlain by Tertiary and Quaternary sediments.

Tasphoto Services

TASMANIA DEPARTMENT OF MINES

1992

GEOLOGICAL SURVEY EXPLANATORY REPORT

SHEET 41 (8515S)

ST HELENS

by M. P. McClenaghan, B.Sc. (Hons), Ph.D., N. J. Turner, B.Sc. (Hons) and J. L. Everard, B.Sc. (Hons)

with contributions by P. R. Williams, B.Sc. (Hons), Ph.D.,

and an appendix on Economic Geology by N. J. Turner, B.Sc. (Hons)

DEPARTMENT OF MINES
GPO BOX 56, ROSNY PARK, TASMANIA 7018

ISBN 0 7246 2099 0

McCLENAGHAN, M. P.; TURNER, N. J.; EVERARD, J. L. 1992. Geological atlas 1:50 000 series. Sheet 41 (8515S). St Helens. *Explan. Rep. geol.Surv. Tasm.*

ISBN 0 7246 2099 0

TECHNICAL EDITOR: E. L. Martin

TEXT INPUT: Lisa Doran, Jan Howie, Anne Taylor

LINE ART / CAD: J. S. Ladaniwskyj, A. McGuinness, R. M. Turvey

CONTENTS

LIST OF FIGURES

LIST OF TABLES

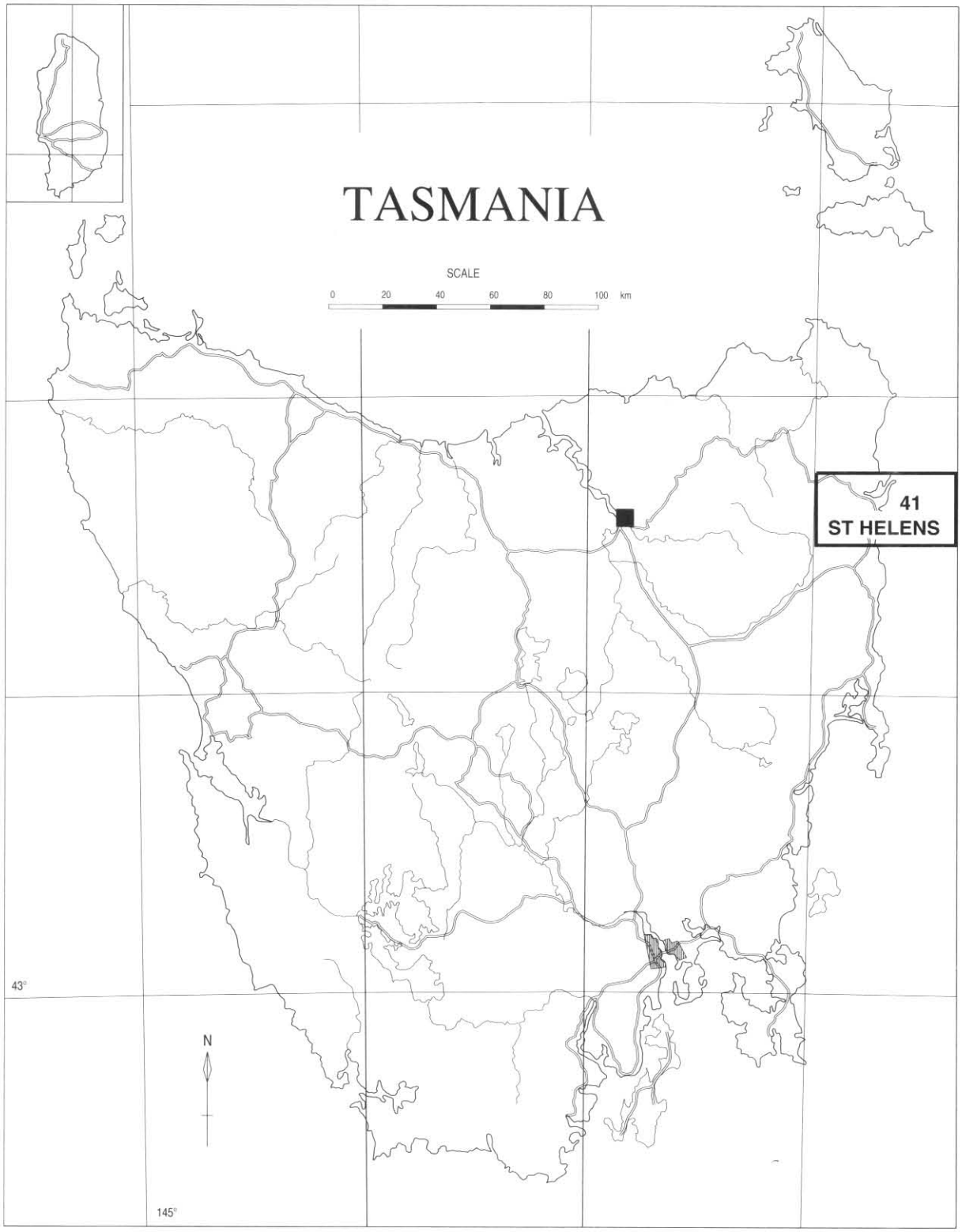

Figure 1. Location of the St Helens Quadrangle

5 cm

INTRODUCTION

The St Helens map sheet is situated on Tasmania's east coast, between latitudes 41°15′ and 41°30′S and longitudes 148° and 148°30′E (fig. 1). The Tasman Sea covers nearly half the area of the map sheet. The largest settlement, St Helens (population 1149 at the 1986 census), is connected to Hobart and Launceston by the Tasman Highway or via Fingal, by the Esk and Midland Highways. Other minor centres are Scamander at the mouth of the Scamander River and Pyengana near the Tasman Highway in the extreme north-west of the map sheet.

Precipitation occurs throughout the year but with a winter maximum. St Helens receives an average annual rainfall of 781 mm. Rainfall is greater in the higher western parts of the map sheet. Agriculture is confined to the lower ground near the Scamander River, the coastal plain, the area surrounding St Helens, the low ground near the George River and the Pyengana area. The remainder of the map sheet is covered with dry sclerophyll forest, with some wet sclerophyll and rain forest in the higher wetter areas.

Fishing, tourism, farming and forestry provide most of the local employment. Secondary services associated with fishing have developed in St Helens such as ship's chandlery, boat building and repairs, and marine electrical work. St Helens together with Scamander is one of the major east coast holiday centres and there is a well developed hospitality industry. Farming is mixed beef, dairy and sheep farming. Integrated logging operations are currently being carried out by Australian Pulp and Paper Manufacturers to provide logs for saw milling and for pulp. Radiata pine plantations are established in the Skyline Tier areas between St Helens and Scamander and in the extreme south-west corner of the map sheet.

No mining occurs in the map sheet at present but in the past there was extensive alluvial tin mining in the Tertiary sedimentary rocks west of St Helens. Minor tin, copper, lead, zinc and silver mineralisation in the area south-west of St Helens and gold and silver mineralisation in the area near Hogans Road [EQ880164] were worked in the past but did not provide any significant mines.

The area is well served with secondary roads and four-wheel drive tracks constructed for forestry and logging operations. The only area with difficult access is the high ground with thick rain forest centred around Billy of Tin Tier area [EQ850215] in the west of the map sheet.

The map sheet was mapped between 1981 and 1986 by M. P. McClenaghan, N. J. Turner and P. R. Williams, and the 1:50 000 geological map was published in 1987.

M. P. McClenaghan, N. J. Turner and J. L. Everard compiled the following report based on their own work and a report and notes of P. R. Williams. The geologists mainly responsible for each section are named with the section-heading; other geologists responsible for any given information are referred to by their initials within parentheses.

PHYSIOGRAPHY

The easternmost part of the map sheet consists of a partly rejuvenated coastal plain with a gentle easterly dip, extending south from near St Helens to Henderson Lagoon. It is covered by a thin veneer of Tertiary sedimentary rocks that have been partly dissected. The widest part of the plain is at Dianas Basin where it is 3–5 km wide and it tapers to the south having a width of 1–2 km at Scamander. The coastal margin is lined with sand dunes and beaches. The dunes are best developed in the north and form a zone about 0.5 km wide with dunes to 20 m high (Peron Dunes) on the peninsula south-west of St Helens Point. Several lagoons and barred basins occur to the west of the dunes (Henderson, Wrinklers, Jocks Lagoons and Dianas Basin).

West of the coastal plain in the south a youthful trellised drainage pattern has developed in a low mountainous region with typical V-shaped valleys which is dominantly underlain by Mathinna Beds. The drainage pattern has been influenced by structural features of the rocks such as prominent jointing and faulting rather than by differential erosion of rock types.

The northern part of the area has more subdued relief and is dominantly underlain by granitoid rocks partly covered by a thin layer of Quaternary and Tertiary sedimentary rocks which form Thureau's lead (Jack, 1964*b*). The drainage pattern was dominantly controlled by jointing and faulting with small areas of Mathinna Beds showing greater resistance to erosion than surrounding granitoids and forming upstanding ridges.

The western part of the map sheet is part of the dissected, flat-lying pre-Permian surface with a thin layer of Permian sedimentary rocks overlying the Mathinna Beds and granitoids on the interfluves of several streams.

The major rivers draining the area are the Avenue and Scamander Rivers in the south and the Golden Fleece Rivulet and the George River in the north. Jennings (1968*a*) showed that the Scamander River is only shallowly incised into its valley, and that its meandering course is caused by resistant bars of Mathinna Beds. He also, in agreement with Twelvetrees (1911) and Walker (1957), suggested that when the river previously flowed at a higher level it followed a course through Henderson Lagoon before joining the sea farther south. The Tertiary rocks in the north of the area probably follow the course of the former George River and its tributaries and lie to the south of the present river.

PREVIOUS WORK

Until recently geological work on St Helens map sheet was mainly concerned with ore deposits in the Tertiary sedimentary rocks (Jennings, 1968*a*, 1968*b*) and in the Mathinna Beds of the Scamander mineral field (Montgomery, 1893*b*; Smith, 1897; Twelvetrees, 1900*a*, 1911; Waller, 1901; Henderson, 1939, 1941; Jack, 1964*a*; Urquhart, 1968; Groves and Baker, 1971; Groves, 1972). Walker (1957) mapped the granitoid–Mathinna Beds boundaries in the eastern part of the area and Williams (1959) described sedimentary structures in the Mathinna Beds in the Scamander River area. McDougall and Leggo (1965) provided data on isotopic ages of granitoids in the St Helens area. Cocker (1977) subdivided the granitoids in the area immediately around St Helens and Rb-Sr geochronological and Sr isotopic work by Cocker (1982) included data on granitoids from the St Helens area.

STRATIGRAPHY

Mathinna Beds (Silurian (?) – Devonian)

NORTHERN PART OF ST HELENS MAP

M. P. McClenaghan

Introduction

The name Scamander Quartzite and Slate was used by Walker (1957) for the pre-Permian sedimentary rocks in the area between St Helens and the St Marys Pass on the St Marys map sheet. The term Mathinna Beds was later used for pre-Permian sedimentary rocks in north-eastern Tasmania (Banks, 1962). A graptolite of probable Pragian age (late early Devonian) has been recorded from the Mathinna Beds near Scamander (Rickards and Banks, 1979) and an indication of the sedimentation age of the Mathinna Beds in the St Helens map sheet.

The Mathinna Beds consist of interbedded sequences of poorly sorted sandstone, siltstone and mudstone with the sandstone and siltstone volumetrically dominant. Low grade regional dynamic metamorphism has recrystallised the clay matrix in the sediments to muscovite and chlorite which define the cleavage. Petrological descriptions of the Mathinna Beds from the St Helens map sheet are given by Walker (1957) and Williams (1959). Williams (1959) has described sedimentary structures including flute casts, drag marks, load casts and flame structures, festoon current bedding, and convoluted folding from the Scamander Road area [FQ030090]. Williams (1959) concluded that the sedimentary features suggest deposition from turbidity currents that came from an area to the south-west of Scamander.

Scamander Plantation area

P. R. Williams

An extensive area of the Mathinna Beds in the Scamander Plantation [FQ030160] is shallowly dipping and not intensively folded (essentially for 3 km in an E-W direction). This allows for the stratigraphic relationships in the Mathinna Beds to be determined. Three subdivisions have been established; a sandstone dominated succession, interbedded sandstone and mudstone successions and mudstone successions.

Sandstone dominated successions contain several sandstone beds greater than 0.4 m thick and the sequence as a whole has a sandstone to mudstone ratio of greater than one. Two distinct beds have been recognised within the sandstone-dominated succession, aiding in the correlation of these successions. At FQ018164 a very coarse-grained sandstone bed approximately 7 m thick contains abundant shale and other rock fragments as well as quartz grains. Some fragments near the base of the bed are up to 150 mm in length. The bed is graded. A similar thick sandstone bed crops out at FQ026171 and probably also at FQ027176. The beds are probably the same unit. At FQ023170 a sequence of beds containing fragments of powdery white material about 5 mm in diameter in a green/grey matrix forms a very distinctive rock type. The same rock type occurs in float at FQ023163, confirming the correlation of these units.

Sandstone beds in the sandstone dominated sequence commonly show load-casting, basal scours and graded bedding. Some beds show partial Bouma sequences (A-C) with an E or D division overlying sandstone with a sharp contact.

Sandstone bed thickness in the interbedded sandstone and mudstone sequences is usually less than 0.4 m and the sandstone to shale ratio is about one. Sandstone beds usually begin with the B division (laminated) and many have ripple cross-lamination on the top of the bed. Bedding is laterally continuous, and flute marks are rare. A few beds show good graded bedding.

The mudstone sequences are composed dominantly of mudstone, and have only rare siltstone interbeds, which occur as trains of isolated ripple-marks. Occasional thin sandstone laminae (up to 50 mm) in discrete packets are either ripple trains or plane laminated. They are continuous over several metres of outcrop. Very rare plane laminated beds up to 160 mm thick occur, and may represent overbank deposits from very large turbidite flows.

In the area sandstone units appear to occur at 20 to 40 m intervals and are about 20 to 60 m thick. In comparison to the rate of deposition on modern submarine cones, these figures are consistent with accumulation of sandstone in depositional lobes of a submarine fan, followed by migration of those lobes leading to the formation of overbank mudstone. Variation in bed thickness has been observed, and in sandstone sequences is thickening-upwards. Thinning-upwards sequences are also present.

SOUTHERN PART OF ST HELENS MAP

N. J. Turner

Introduction

Mathinna Beds (Banks, 1962) is the general name given to the sedimentary succession in north-east Tasmania which is intruded by the widespread Devono- Carboniferous granitoids. Discussions of the overall succession comprising the Mathinna Beds are given in Baillie, Powell, Banks and Hills (1989) and in Powell, Baillie, Conaghan and Turner (in press).

In the eastern part of the St Helens quadrangle the Mathinna Beds are represented by the Scamander Formation (Walker, 1957) of interbedded mudstone, siltstone and poorly sorted sandstone. The Scamander Formation extends from near the town of St Helens southwards past Scamander into the St Marys quadrangle where it is overlain unconformably by the extrusive part of the St Marys Porphyrite (Turner and Calver, 1987). Rocks similar to those in the Scamander Formation also comprise the Mathinna Beds in other parts of the St Helens and St Marys quadrangles.

Sedimentology

E. Williams (1959) recognised the turbiditic character of sandstone and coarse siltstone in a section of the Scamander Formation exposed in cuttings along the Upper Scamander Road around EQ030090. He described the poor sorting which characterises the sandstone and coarse-grained siltstone, the typical grading of sandy and silty beds, the profusion of current markings on the soles of these beds and the occurrence of small scale cross lamination in the upper parts of many graded beds. Current markings on soles comprise flute casts and casts of linear drag marks, all showing modification due to loading with flame structures being produced in many instances through intrusion of mudstone into overlying sandstone at cusps in the sole structures. Sandy and silty layers vary in thickness from about 0.02 m to about 3 m with interbedded mudstone, usually grey, ranging in thickness from a few millimetres to 3.7 m. The sedimentological features of the Scamander Formation at Upper Scamander Road are also typical of the Mathinna Beds elsewhere in the southern part of St Helens quadrangle.

Powell *et al.* (in press) carried out detailed stratigraphic logging of Mathinna Beds sections at EQ023156 which is within the area described by P. R. Williams (this volume), at EQ053090 which includes the quarry at the southern end of the old Scamander Bridge, at EQ028091 which is within E. Williams' (1959) area beside the Upper Scamander Road, and at EQ991082 which is on the Forestry Commission's S Road about 3 km north of the southern edge of St Helens quadrangle. The data collected included bed thickness and Bouma divisions, grain size, palaeocurrent indicators and modal sandstone composition.

The sandstone beds in all four localities consist of typical Bouma subdivisions and a bed may commence with division A or B or C. Beds comprising divisions A, B, A + B and A + B + C range from thin to thick whilst beds consisting of division C are usually only a few centimetres thick though, together with interbedded mudstone (C + D + E) they may comprise several metres of section.

The turbidite units in the four measured sections, and elsewhere in St Helens quadrangle, tend to occur as 'packets' of beds which display some unifying characteristic. For example, in the northern locality at EQ023156 the 13 m measured section comprises a lower packet of moderately thick (under 0.5 m) sandstone beds

with common mudstone interbeds and an upper packet, or interval, of relatively thick (0.5–1 m), generally coarser grained sandstone beds with less interbedded mudstone. The upper interval resembles channel or channel-lobe transition facies whereas the lower interval resembles lobe facies. The 32.5 m section which includes the quarry at Scamander also contains packets characterised by thick (up to 4 m), relatively coarse-grained sandstone and packets characterised by much thinner sandstone/siltstone beds with more common mudstone interbeds. Modal composition of sandstone at Scamander is quartzose sublithicwacke whereas in the northern locality it is sublithicwacke and lithicwacke.

Intervals of thickly-bedded (up to 3.8 m) sandstone and intervals of relatively thinly-bedded sandstone, siltstone and mudstone again characterise the 40 m section logged at the Upper Scamander Road locality. However, the 20 m section logged at EQ991082 on S Road is much more uniform. It comprises fine- to medium-grained sandstone beds up to 0.8 m thick together with fairly evenly distributed mudstone interbeds. This section probably represents lobe facies deposits near the channel-lobe transition. At both Upper Scamander Road and S Road the modal composition of sandstone is sublithicwacke to lithicwacke but most rocks contain less feldspar than the similar lithologies in the northern locality at EQ023156.

Sandstone compositions

Sandstone similar to the varieties identified by Powell *et al.* (in press) is widespread in St Helens quadrangle. Quartzose sublitharenite is present at EQ884084 and EQ906104, west of Catos Dyke, at EQ950102 just east of Catos Dyke, and at EQ001060 east of S Road. Monocrystalline quartz is dominant in these rocks with some larger grains displaying good rounding and smaller grains being angular. Grains of accessory zircon and tourmaline also may show good rounding. This good rounding of quartz, zircon and tourmaline is presumed to have been a feature of some of the deposits from which the turbidity currents were derived. Muscovite, plagioclase, untwinned feldspar and uncommon rock fragments comprise the other relatively coarse-grained constituents in the quartzose lithicwacke whilst fine-grained muscovite and quartz comprise the matrix. The rock fragments include porphyritic, felsic volcanics in which the glassy matrix has recrystallised producing 'snowflake' texture.

Volcanic wacke of quite different composition to the sandstone varieties of Powell *et al.* (in press) occurs at EQ070156 and EQ077162 on the beach north of Beaumaris. The outcrops are small but of good quality and display sedimentological features typical of the Mathinna Beds. In particular, poorly sorted sandstone and siltstone occur in graded beds of up to about 0.5 m thickness and are interbedded with mudstone. The sandstone/siltstone beds comprise Bouma A, B and C subdivisions. Also near EQ077162 there are interbedded, thin, cross-laminated Bouma C subdivisions and mudstone which comprise an approximately 1.5 m thick section in isolated outcrop.

Hand specimens of the volcanic wacke are dark grey and contain abundant white feldspar grains which are up to 2 mm across in the basal parts of some Bouma A divisions. In contrast, quartzwacke which occurs on the southern part of Beaumaris Beach at EQ066131 and EQ066121 is pale grey and no feldspar is discernible in hand specimen. This rock is similar to the pale coloured quartzose litharenite in the logged section at Scamander. The sublitharenite and litharenite which occur in the other logged sections of Powell *et al.* (in press) are commonly of medium grey colour and sparse feldspar is usually evident in the basal parts of thicker, coarser grained Bouma A subdivisions particularly in the northern locality.

Though further mapping would be required for proof, it seems that the quartzose sandstone beds in the eastern part of St Helens quadrangle occupy a distinct stratigraphic unit which extends south from Beaumaris Beach to Scamander then north along Skyline Ridge. The unit appears to overly the volcanic wacke near Beaumaris and the sublithicwacke and lithicwacke in the northern locality of Powell *et al.* (in press) since the regional plunge of folds is to the south.

In thin section the volcanic wacke from a Bouma A subdivision at EQ070156 contains 25% (volumetric estimate) of very fine-grained matrix which appears to have been predominantly phyllosilicate with little quartz. The matrix now consists of thermal metamorphic biotite. Sand grains comprise 75% of the rock and range in size up to 0.8 mm across. They consist of estimated volumetric proportions of 20% quartz, 40% feldspar and 15% rock fragments. Quartz grains are angular to moderately rounded though the grain margins have been pitted by reaction with the matrix. No typically volcanic quartz grains were recognised. Both lamellar twinned and untwinned feldspar are present and the grains range in shape from angular and anhedral to moderately rounded and subhedral to almost euhedral. Zircon is an accessory mineral.

Rock fragments in the volcanic wacke include mudstone, now metamorphosed, and granoblastic chert but are mainly volcanic. The volcanic fragments consist of subhedral to euhedral phenocrysts of plagioclase and untwinned feldspar in a subtrachytic groundmass of fine-grained plagioclase laths with interstitial crystalline, felsic material. Hornblende occurs as interstitial material in some fragments and may show alteration to chlorite and opaque material. Hornblende also occurs as inclusions in some plagioclase phenocrysts and as uncommon detrital grains. Probably the overall composition of the volcanic rock fragments is andesitic though further work is desirable to confirm this.

Palaeocurrents

Powell *et al.* (in press) showed that oppositely-directed palaeocurrents were involved in the deposition of the turbiditic sandstone beds in the eastern part of the St Helens quadrangle. Their data combined with data collected during the mapping of St Helens quadrangle (fig. 2) defines two sedimentational units separated by a NNW-SSE boundary. The boundary is approximately parallel to the generally NNW and SSE palaeocurrent directions in the respective sedimentational units west and east of the boundary. It is also approximately parallel to the overall fold axis trend in the southern part of St Helens quadrangle (fig. 26).

The sedimentational units may be stratigraphically distinct or they may be laterally equivalent and detailed investigation of the boundary is necessary to determine this. The data to hand provides little indication of interdigitation of the two units along the boundary though an isolated example of southerly directed palaeocurrent occurs amongst the northerly palaeocurrents in the westerly sedimentational unit (fig. 2). This isolated example derives from two beds in a bold outcrop on the south-east bank of Binns Creek near FQ000084. Sandstone comprising the beds contains markedly more feldspar than sandstone in beds with opposite palaeocurrent direction in the surrounding area. The estimated composition of the sandstone is marginal between lithic feldspathic arenite and subfeldspathic arenite.

There is a considerable range of sandstone compositions deposited by SSE-directed currents in the easterly sedimentational unit. The range includes volcanic wacke, litharenite and sublitharenite, quartzose sublitharenite and

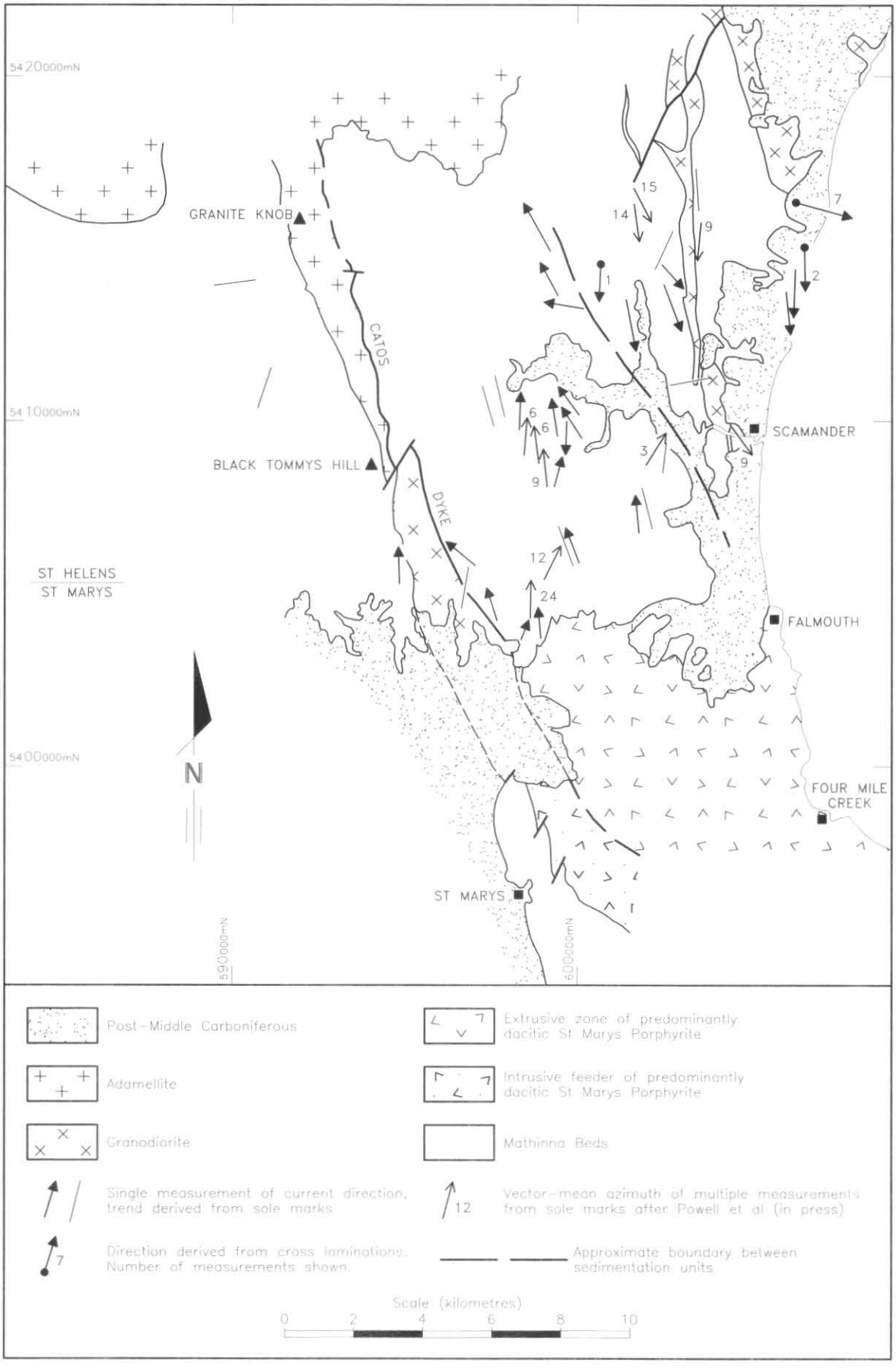

Figure 2. Palaeocurrent directions in the Mathinna Beds derived from sole marks (casts of flutes, longitudinal furrows and ridges) and from cross laminations. Each measurement has been rotated to the horizontal using the dip and strike of the bed in which the measurement was made and the statistical fold axis for the structural subarea in which the bed occurs (see Figure 26). The dip direction of cross bed sets when bedding is horizontal is taken as the current direction.

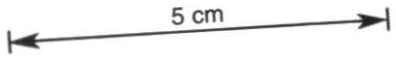

quartzwacke. In the western sedimentational unit the sandstone deposited by NNW currents varies from litharenite to sublitharenite to quartzose sublitharenite and quartzwacke. Powell *et al.* (in press) note that feldspar is relatively low in most of the sublitharenite and litharenite deposited by NNW directed currents. The further work described here has identified sandstone types of much more feldspar-rich character than previously known and has shown firstly, that they were deposited by SSE directed currents and secondly, that they may interdigitate with the sandstone types deposited by NNW flowing turbidity currents.

Fossils

Fossils of Early Devonian age occur near Scamander and on Skyline Ridge (Walker, 1957; Banks, 1962; Rickards and Banks 1979). The localities are in the sedimentation unit characterised by palaeocurrents directed to the SSE.

In the quarry at EQ053090 near the southern end of the old bridge at Scamander there are fragmental, transported corals, polyzoans, brachiopods and crinoids of Early Devonian age in turbiditic sandstone. Upstream from the bridge on the northern side of the Scamander River near EQ051094 there is siltstone which contains a Devonian assemblage of corals, brachiopods, bivalves, a conularid, cephalopods and dacryoconarids.

A graptolite species occurs in brown siltstone and black siltstone along part of a road on Skyline Tier near EQ034118 (Rickards and Banks, 1979). The species is *Monograptus aequabilis* cf. *notoaequabilis* indicating a probable age of early Pragian (late Siegenian).

Fragments of vascular plants are known from Scamander, Upper Scamander and cuttings on S Road. They may be of Late Silurian or Devonian age (see Baillie *et al.*, 1989). A graptolite of upper Middle Silurian age occurs in the western part of St Helens quadrangle (Rickard, Davidson and Banks, in prep.) near Golden Ridge.

Parmeener Supergroup (Ps)

N. J. Turner

Scattered, thin intervals of Parmeener Supergroup cap ridges in the south western part of St Helens quadrangle. The base of the succession rests unconformably on Mathinna Beds and has a regional dip of some 2° towards 140°E. The base ranges in elevation from about 500 m at EQ841138 near Hogans Road to around 200 m at EQ922056, close to the southern edge of the quadrangle.

At the southern edge of St Helens quadrangle the beds are continuous with the basal unit of the Parmeener Supergroup in the adjacent St Marys quadrangle. This unit consists of freshwater quartz sandstone, shale and conglomerate passing up into marine, poorly sorted sandstone and mudstone (Castleden and Calver *in* Turner *et al.*, 1984). Only the lower or freshwater part of the unit appears to be present in St Helens quadrangle where the maximum preserved thickness of beds is no more than about 35 m.

On the basis of scattered exposures the succession in St Helens quadrangle includes lower beds of very coarse-grained, well-sorted, feldspathic, quartz sandstone and granule conglomerate with thin lenses of pebble and cobble conglomerate. The pebbles and cobbles are well rounded and consist of vein quartz and indurated Mathinna Beds sandstone. Sand grains and granules are angular and both feldspar and quartz appear to be mainly of coarse-grained granitic provenance. Thin bedded shale occurs above these lower beds in places as does well-sorted, coarse-grained, sparkling, quartz sandstone containing scattered granules and small pebbles. The sandstone contains muscovite and minor feldspar. Sandstone beds in parts of the succession are around 600 mm thick and are cross laminated.

Tertiary deposits

M. P. McClenaghan

Several patches of partly consolidated Tertiary sedimentary rocks (Ts) lie unconformably on Mathinna Beds and granitoid rocks in the areas immediately to the west and east of St Helens. The Tertiary rocks west of St Helens follow the course of the former Georges River and have been termed Thureau's Lead (Montgomery, 1893*a*; Jack, 1964). The lead starts in the Terryvale Marsh area [EQ925255] and extends north to the George River. It the bends to the east and continues for about 4 km before swinging south and following the same course as the Argonaut Creek. It reaches Medeas Cove after passing south of a prominent granitoid hill at FQ014245. Twelvetrees (1904) and Walker (1957) suggested that the former river course may have reached the coast through Dianas Basin, but Cocker (1977) on the basis of the location of basement granitoid outcrops and seismic and gravity traverses, considered that it crossed the coast in the Stieglitz area [FQ090240]. At EQ955293 erosion has removed the sedimentary rocks between two areas of outcrop though a narrow connection may exist between granitoid outcrop found at EQ960292 and EQ956296 (see Proline auger drilling results, Jennings, 1968*b*).

Jack (1964) reported that the type of sediments found by drilling in the former river course were dominantly sandy clay and clayey sand, with occasional gravel and sand beds. Cemented clay and gravel beds were found at deeper levels. Heavy mineral concentrates from the drill samples were zircon, pyrite, garnet, ilmenite, siderite, pleonaste and small amounts of cassiterite and magnetite. Cassiterite, garnet, zircon and ilmenite were concentrated at higher levels. Surface outcrops show that the poorly consolidated sands consist dominantly of quartz and weathered feldspar and that pale buff to white clay lenses are kaolinitic material derived from feldspar, together with a little mica.

The sediments are about 80 m thick near St Helens at FQ032249 and reach a depth of about 75 m below sea level. Cocker (1977) reported a sediment thickness of 120 m near Stieglitz at FQ098238.

Basalt (Tb) was encountered in bore holes near the base of the sedimentary sequence in the area west of St Helens (Jack, 1964) and consists of at least two flows.

Spores from a sample of sediment collected at EQ984269 about 9 m above the basal basalt indicate an Early Oligocene age (Harris, 1968).

Large areas of the Tertiary sedimentary rocks along the course of the former river have been mined for tin. These areas are indicated by an overprint on the map.

Rare small areas of extremely hard rock termed silcrete (Tss) occur in the sediments (e.g. at FQ048218) and consist of coarse quartz grains cemented with silica.

Cainozoic deposits (Cpl)

N. J. Turner

Quartzose sand and gravel deposits extend from the southern part of St Helens quadrangle near Hendersons Lagoon northwards to Dianas Basin along the seaward side of the coastal ranges. The deposits form a veneer on the lower slopes of the ranges, reaching a maximum elevation of about 110 m which corresponds to a marked change in slope angle. The deposits are strongly dissected by the present drainage system.

Walker (1957) grouped the sand and gravel with deposits (Ts) in Thureau's Deep Lead which is west of St Helens

(Jack, 1964) McClenaghan, this volume). Mid-Tertiary spores are present in the lead (Harris, 1968). They are also present in deposits (Ts) on the south eastern shore of Georges Bay (Forsyth, 1989) which are either in, or adjacent to, the probable eastward extension of the lead (Cocker, 1977). The Georges Bay fossil locality is in a fairly large tract of materials which are compositionally similar to the deposits designated Cpl and which occupy a similar range of elevations. Thus, it would appear that Ts and Cpl are of equivalent age.

The relative age of the Tertiary materials in Thureau's Deep Lead and its probable eastward extension compared with the age of the similar materials around Dianas Basin and to the south is unclear because the two sets of materials appear to be the products of different depositional systems. Thureaus Deep Lead is a palaeo-river estuary whereas the overall relationship between the distribution of Cpl, height above sea level and change of slope angle strongly suggests the influence of raised sea level.

Effects on deposition and coastal slopes due to raised Pleistocene sea levels are evident in Boobyalla quadrangle (Baillie *et al.*, 1979), Eddystone quadrangle (Baillie, 1984) and St Marys quadrangle (Turner *et al.*, 1984) where there are deposits in similar settings to Cpl though the elevations of the change of slope and of the highest deposits are variable. This variability may be due to tilting and/or faulting. The maximum elevation of about 110 m in St Helens quadrangle is relatively high.

Evidence of a high erosional base level indicative of raised sea level is not confined to the coastal part of St Helens quadrangle. Lag of Mathinna Beds cobbles and boulders occurs at about 80 m elevation at FQ017085 in the Scamander River valley upstream of the coastal ranges. Similar lag also occurs at 80 m elevation at FQ016133 near the South Orieco prospect and on spurs between there and Hospital Corner on the Scamander River. Other small patches of elevated sandy gravels occur in the upper reaches of the Scamander and Avenue Rivers, though the steeply incised, youthful nature of the terrain suggests that such older, unconsolidated deposits would mostly have had limited longevity. There is scope for additional accurate mapping of these occurrences.

In the St Helens area there is little doubt that the topographically lower deposits in Ts are of fluviatile or estuarine origin. However, it seems likely that the topographically higher deposits have been affected by a high sea level stand of about 110 m. The maximum elevation of Ts south of Georges Bay is about 85 m, at FQ014266 it is 80 m, at EQ997273 it is 120 m, at EQ963250 it is 90 m and at Terryvale Marsh it is about 100 m. These values are within the range of maximum elevations displayed by Cpl along the eastern side of the coastal ranges.

IGNEOUS ROCKS

Devonian granitoid rocks

NORTHERN PART OF THE ST HELENS MAP

M. P. McClenaghan

PETROLOGY AND FIELD CHARACTERISTICS

Introduction

The granitoids of the St Helens area form the southern part of the Blue Tier Batholith which is a composite, essentially post-kinematic, granitoid mass intruded at high level. Biotite igneous ages range from 370 to 395 Ma (Cocker, 1982). Granitoid rocks in the area range from diorite to alkali-feldspar granite. The classification used is that of Streckeisen (1973) with the modification that the term adamellite is used for the part of the 'granite' field with over 35% plagioclase.

Sparsely porphyritic coarse-grained biotite-hornblende granodiorite (Dbgsp)

This rock type together with the biotite granodiorite (Dbgbsp), biotite adamellite (Dba) and biotite granite (Dbrpc) forms part of the earliest intrusive body in the area surrounding Georges Bay. It corresponds to the Georges River Granodiorite defined by Cocker (1977).

On the west and north sides it has been intruded by younger granitoids and on the south and south-west sides it has intrusive margins against the Mathinna Beds.

The contact of the granodiorite with the Mathinna Beds on the eastern side of Launceston Creek between EQ977224 and EQ994243 is clearly dipping south-west at a moderate angle based on the relationship of the boundary to the topography. This boundary passes under Tertiary sedimentary rocks to the north and then emerges south of St Helens at FQ022228 and passes along the lower slopes of a NW-trending ridge. The boundary is well exposed over a small distance in a small stream at FQ030205 and it is clear that it dips west at a moderate angle only slightly greater than the grade of the stream. Farther to the east the boundary is displaced north by the intrusion of a substantial N-S granodiorite dyke. The boundary east of the dyke trends south-east along the lower slopes of low hills between FQ041219 and FQ066167. Small patches of the granodiorite are exposed near Beaumaris (e.g. at FQ056145) and as far south as FQ066119 on the coast within the Mathinna Beds suggesting that the main mass of the granodiorite may be close to the surface in that area. Other contacts between the granodiorite and the Mathinna Beds occur on the coast north of Dianas Basin near FQ092204. These features suggest that the granodiorite/Mathinna Beds boundary east of the dyke is irregular and gently dipping and that the granodiorite throughout the area is not far from the roof of the intrusion.

The granodiorite in the Binalong Bay and Baretop area has been shown on the map as being part of this unit because its characteristics are similar to the granodiorite in the areas described above. Cocker (1977) included this area with a later intrusion of variably porphyritic coarse- to fine-grained biotite-hornblende granodiorite (Dbgp). Since there is considerable overlap in the characteristics of these granodiorites unequivocal identification is not possible. Cocker's view is supported by the geochemical similarity of two whole rock analyses from this area to the later granodiorite rather than to the earlier (see geochemistry section for discussion of this point).

The granodiorite is generally a coarse-grained dark grey rock with sparse plagioclase phenocrysts. Mafic minerals generally constitute about 15% of the rock with biotite dominant over amphibole. Prominent euhedral amphiboles occur in some outcrops and good outcrops usually show mafic-rich bands and variable amounts of fine-grained dioritic xenoliths. In the area bordering the George River north of St Helens a strong apparent lineation on horizontal surfaces is developed defined by the elongation of quartz aggregates and the alignment of mafic minerals.

In thin section the granodiorite consists of plagioclase, quartz, K-feldspar, biotite and amphibole with accessory ilmenite, sphene, apatite, allanite and zircon. Plagioclase commonly contains distinct rounded core areas which have abundant sericite alteration while the rim zones are clear. The core regions are unzoned or only slightly zoned but vary between crystals and rock specimens from An_{58} to An_{41}. The rim zones are strongly zoned and range from An_{47} to An_{22} with rare rims of An_{10}. The K-feldspar is

microcline and crystallised last as it encloses all other mineral species. Amphibole is present as patches of small crystals in various orientations and as large euhedral crystals. Cocker (1977) recorded clinopyroxene associated with amphibole from a sample at FQ032270. Biotite occurs as isolated crystals and also as patches of small crystals. The biotite patches are often associated with the amphibole and the biotite is occasionally present as small patches enclosed in the amphibole. Minor chloritic alteration of the biotite is sometimes present and occasionally thin strips of prehnite are developed along the biotite cleavages. Quartz is present as isolated large crystals and in composite small crystal patches. Ilmenite is usually associated with biotite. In some specimens ilmenite enclosed by biotite has a thin rim of sphene. Zircon and apatite are also present as inclusions in biotite. Modal analysis presented by Cocker (1977) indicate that the composition of the rock type ranges from granodiorite to adamellite.

Representative mineral analyses are presented in Table 1 and biotite and amphibole compositions are plotted in Figures 3 and 4. Biotite is pleochroic with X = pale brown and Y, Z = dark red/brown, and it plots in the centre of the biotite field. Amphibole has pale to dark green pleochroic colours and ranges from close to actinolite in composition to hornblende with a small edenite component.

Within the area of outcrop of the granodiorite near St Helens there occur a number of approximately oval areas (<1.5 km long) where the granodiorite has been strongly altered to produce rock ranging in composition from granodiorite to monzodiorite and monzonite. These bodies correspond to the Priory Monzonite of Cocker (1977). Several bodies but not all, are adjacent to small bodies of biotite adamellite (Dba) which occur in the same general area.

The altered rock is coarse-grained with dark green amphibole and pink or white feldspar. Quartz and biotite are usually not seen in hand specimen. Thin dark green veining is commonly present and also occurs in the otherwise unaltered neighbouring granodiorite. The change from unaltered granodiorite takes place within a few metres.

In thin section the thin dark veining in granodiorite near altered rock can be seen to consist of amphibole. In the more altered rock plagioclase is present as large cloudy crystals and is usually albite but small amounts of oligoclase is also present in some samples. Small grains of epidote are frequently present in the altered plagioclase and also occur in granular patches and veins. Amphibole occurs as thin veins, large composite patches and as thin needle shaped crystals. Radiating growth patches of amphibole laths are also common. K-feldspar is microcline and is less abundant than in the granodiorite. Biotite is present as a minor component or is absent. Where present it is strongly altered and often associated with ilmenite and sphene with the sphene sometimes rimming the ilmenite. Quartz is present in a few specimens as a minor component. Accessory allanite, zircon and apatite are also present. The vein, needle and radiating growth of the amphibole suggest that the rock has undergone metasomatic alteration. The lack of quartz compared to the granodiorite indicates considerable desilicification.

Representative mineral analyses are presented in Table 2 and biotite and amphibole compositions are plotted in Figures 3 and 4. Biotite has the same pleochroic colours as for the unaltered rock and plots in the same area on the diagram. Amphibole also shows a similar compositional range to that in the unaltered rock.

Fine- to coarse-grained biotite adamellite (Dba)

This adamellite occurs as a number of small bodies near St Helens within the area of the biotite-hornblende granodiorite (Dbgsp) and corresponds to the Medeas Cove Adamellite of Cocker (1977). The two largest bodies are elongated in a north-east direction. Boundary relationships with the granodiorite were not seen. A marginal variant of the granodiorite at EQ985228 which is gradational with the main mass of the granodiorite, resembles the adamellite and suggests that the adamellite may be part of the same intrusive body as the granodiorite.

The adamellite is a light pink, fine- to coarse-grained rock with varying amounts of biotite. In some areas it resembles aplite and in others it has pegmatitic patches.

In thin section it consists of quartz, K-feldspar, plagioclase and biotite. The K-feldspar is microcline and the plagioclase shows zoning (An_{47}–An_{16}). The plagioclase is considerably altered to sericite and the biotite is widely altered to chlorite. Minor amounts of sphene are associated with altered biotite. Inclusions of zircon and apatite are common in the biotite. Accessory allanite was identified in one sample.

Representative mineral compositions are presented in Table 3 and biotite compositions are plotted in Figure 4. Biotite compositions in the adamellite resemble those of biotites in the surrounding granodiorite (Dbgsp) (see table 1, 3 and fig. 3) and are dissimilar to the compositions of biotites from other nearby adamellite bodies such as the biotite-minor muscovite adamellite (Dbasc) (see table 6 and fig. 3). This supports the suggestion that the adamellite is part of the same intrusive body as the granodiorite.

Very abundantly porphyritic with small K-feldspar phenocrysts, medium- to coarse-grained biotite granite (Dbrpc)

Rocks of this type are exposed in the eastern Georges Bay area and correspond with the Grants Points Granite of Cocker (1977). The boundary with the biotite-hornblende granodiorite (Dbgsp) is exposed at Skeleton Bay [FQ102322] and Wilson Bay [FQ083283] where the transition occurs gradually over several metres.

The biotite-hornblende granodiorite (Dbgsp) in this area was considered by Cocker (1977) to be part of a later intrusion of variably porphyritic coarse- to fine-grained biotite-hornblende granodiorite (Dbgp). Cocker's view is supported by the geochemical similarity of two whole rock analyses from this area to the later granodiorite rather than to the earlier (see geochemistry section for discussion of this point).

The granite is a medium- to coarse-grained medium dark grey rock with very abundant small K-feldspar phenocrysts (25–40 mm). Biotite-rich bands are common in some areas and sparse small fine-grained darker dioritic xenoliths are frequently present. The very abundant feldspar phenocrysts often show alignments on horizontal surfaces and are the most characteristic feature of the rock type.

In thin section the rock consist of quartz, K-feldspar, plagioclase and biotite with accessory muscovite, apatite and zircon. The K-feldspar is microcline and has many small inclusions of plagioclase, biotite and quartz. The cores of plagioclase crystals have abundant sericite alteration and the rims are clear and zoned. The biotite is usually partly altered to chlorite. Cocker (1977) reported small (<1%) quantities of hornblende from this rock type. Representative mineral analyses are presented in Table 4. Biotite compositions are plotted in Figure 3 and show that they are similar to biotite from the Dbgsp, Dba and Dbgbsp rock types. It is described as a granite following

Table 1. REPRESENTATIVE MINERAL ANALYSES FROM THE SPARSELY PORPHYRITIC COARSE-GRAINED BIOTITE-HORNBLENDE GRANODIORITE (Dbgsp)

		hornblende			biotite	
No.		MSH123-3/1	MSH76-9/1		MSH76-5/3	MSH123-7/1
SiO_2		48.70	44.87		34.88	36.50
TiO_2		0.57	1.19		4.05	3.70
Al_2O_3		5.76	7.10		14.3	14.78
Cr_2O_3		0	0		0	0
Fe_2O_3		7.25	5.87		0	0
FeO		7.79	18.31		27.21	19.93
MnO		0.54	0.62		0.31	0.27
MgO		14.28	7.20		6.73	11.34
CaO		11.92	10.89		0	0
Na_2O		0.62	1.18		0	0
K_2O		0.5	0.81		8.72	9.53
H_2O		2.07	1.96		3.81	3.94
		O = 23			O = 22	
Tet	Si	7.063	6.852	Tet	5.492	5.554
	Al	0.097	1.148		2.508	2.446
	Σ	8	8		8	8
Oct M1-3	Al	0.048	0.131	Oct	0.146	0.205
	Ti	0.063	0.136		0.479	0.423
	Fe^{+3}	0.791	0.674		Fe^{+2} 3.583	2.536
	Cr	0	0		0	0
	Fe^{+2}	0.945	2.338		Mn 0.041	0.035
	Mn	0.067	0.081		Mg 1.579	2.571
	Mg	3.086	1.639		Σ 5.827	5.771
	Σ	5	5		Ca 0	0
XM1-3		0	0		Na 0	0
M4	Ca	1.852	1.782		K 1.751	1.851
	Na	0.148	0.218		Σ 1.751	1.851
	Σ	2	2		OH 4	4
A	Na	0.027	0.130		Mg* 0.31	0.50
	K	0.093	0.158			
	Σ	0.120	0.288			
	OH	2	2			
	Mg*	0.77	0.41			

	plagioclase				K-feldspar
	core	core	rim	rim	
No.	MSH88-6/1	MSH126-7/1	MSH76-7/2	MSH123-2/1	MSH76-7/3
SiO_2	55.27	59.1	57.8	72.04	65.58
TiO_2	0	0	0	0	0
Al_2O_3	27.40	26.31	27.21	17.78	18.5
FeO	0	0	0	0	0
MnO	0	0	0	0	0
MgO	0	0	0	0	0
CaO	12.13	8.03	9.15	1.71	0
Na_2O	4.76	6.43	5.67	8.33	0.45
K_2O	0.43	0.13	0.17	0.14	15.47
			O = 32		
Si	9.998	10.528	10.326	12.426	12.048
Al	5.845	5.525	5.730	3.616	4.007
Na	1.671	2.219	1.964	2.787	0.162
Ca	2.351	1.533	1.752	0.316	0
K	0.099	0.003	0.039	0.031	3.625
Σ	19.964	19.834	19.810	19.175	19.842
An	0.58	0.41	0.47	0.10	0

Cocker (1977) though a modal analysis using the different boundary values used in this report, places it marginally in the adamellite field.

Sparsely porphyritic medium- to coarse-grained biotite granodiorite (Dbgbsp).

This rock type corresponds to the Akaroa Granodiorite of Cocker (1977) and occurs in the areas bordering the mouth of Georges Bay. Boundaries are exposed with the biotite granite (Dbrpc) at FQ116302, FQ095268, FQ100267 and FQ134297 where they can be seen to be gradational over several metres.

The granodiorite is a medium- to coarse-grained medium dark grey rock with sparse small K-feldspar phenocrysts (<25 mm) and rare larger ones (up to 70 mm). The rock generally has a speckled appearance due to the dispersed biotite flakes. Biotite-rich layers are common and widely dispersed biotite clots are present. Rare finer grained dioritic xenoliths also occur. In some areas (e.g. FQ128295) the biotite-rich layers have sharp boundaries on one side and pass into zones with abundant small K-felspar phenocrysts resembling the abundantly porphyritic biotite granite (Dbrpc) on the other side. Similar mineral layering occurs in the coastal outcrops from Binalong Bay [FQ094324] to Dora Point [FQ113300] and include rhythmic mineral and sized graded layering as also reported by Cocker (1977). Cocker (1977) interpreted such layering as evidence for flow and gravitational settling within the magma.

In thin section the rock consists of quartz, plagioclase, K-feldspar and biotite with accessory muscovite, apatite and zircon. The plagioclase has sericite and sometimes epidote alteration in the cores with clear zoned rims. The K-feldspar is microcline and has inclusions of plagioclase, biotite and quartz. The biotite is extensively altered to chlorite. Representative mineral analyses are presented in Table 5 and biotite compositions are plotted in Figure 3. Modal analysis presented by Cocker (1977) show that the composition ranges from granodiorite to adamellite.

Porphyritic to seriate to equigranular coarse-grained biotite-minor muscovite adamellite (Dbasc)

The adamellites form part of a large body which extends from the Hogans Road area [EQ920170] in the central part of the map sheet to the Mt Pearson area [FQ335035] in the

Table 1. REPRESENTATIVE MINERAL ANALYSES FROM THE SPARSELY PORPHYRITIC COARSE-GRAINED BIOTITE-HORNBLENDE GRANODIORITE (Dbgsp) *(continued)*

	Sphene	Ilmenite
	MSH76-5/1	MSH72-5/1
SiO_2	31.21	0
TiO_2	35.7	52.2
Al_2O_3	2.26	0
Cr_2O_3	0	0
Fe_2O_3	0	0
FeO	0.6	42.93
MnO	0	4.85
MgO	0	0
CaO	30.23	0
Na_2O	0	0
K_2O	0	0
H_2O	0	0
	O = 18	O = 6
Si	3.672	0
Al	0.313	0
Ti	3.159	1.817
Mn	0	0.208
Mg	0	0
Ca	3.811	0
Σ	11.01	4.012

$Mg^* = Mg/(Mg + Fe^{+2})$.
O is the oxygen number used to calculate the structural formulae.

Blue Tier map sheet to the north and correspond to the Mt Pierson Adamellite of Cocker (1977). The western boundary of the body is intrusive into Mathinna Beds and stretches in a NNE direction from EQ947082 to EQ888298. The boundary is straight and steep and it seems possible that its attitude was structurally controlled. Along the south-east margin of the body between EQ928178 and EQ977224 it is also intrusive into Mathinna Beds while farther north as far as EQ995309 the country rock is biotite-hornblende granodiorite (Dbgsp). Farther north of this the boundary with the granodiorite is displaced eastwards along a younger NW-trending granodiorite dyke. In the Launceston Creek area at EQ980230 the contact between the adamellite and the granodiorite is well exposed and quartz and feldspar pegmatitic patches, present in the marginal adamellite, vein into the granodiorite showing that the adamellite is later. The remainder of the boundary with the granodiorite is not exposed.

Throughout the northern parts of the adamellite body the rock is coarse-grained and light grey with very abundant K-feldspar crystals which in some areas are distinctly larger than the matrix grains but mostly have a continuous range in size with the matrix. The large feldspars define a widespread apparent lineation on horizontal surfaces. The biotite is often present in small clumps as well as isolated crystals.

A broad zone occurs in the south-east margins of the body in which the rock has a pink colour and the biotite is strongly altered. In some specimens the biotite is no longer visible and the coarse quartz grains are present in a pink feldspar matrix. Within this zone irregular-shaped intrusions of fine- to medium-grained granitoid occur which become more abundant as the margin of the body is approached. At the boundary the granitoid is fine- to medium-grained with quartz phenocrysts. Sparse patches of quartz and feldspar pegmatite also occur. At some points (e.g. EQ969168) abundant flakes of pale brown mica is present. Miarolytic cavities, partly filled with tourmaline and quartz are also present together with quartz and quartz/tourmaline veins. The boundary between the marginal zone and the main part of the body is gradational and there are a number of small areas of pink granite at a distance from the marginal zone. The marginal zone granitoids correspond with the Constable Creek Granite of Cocker (1977).

In thin section the adamellite consists of coarse-grained quartz, K-feldspar, plagioclase and biotite. K-feldspar is in the form of large perthitic orthoclase crystals and smaller microcline crystals. Plagioclase frequently has core zones of uniform composition which is cloudy due to abundant sericite alteration and is surrounded by less altered oscillatory zoned rims. Core regions are of andesine and oligoclase composition with rim compositions close to albite. Typical mineral compositions are presented in Table 6 and biotite compositions are plotted in Figure 3. Biotite is close to annite and siderophyllite in composition and is quite different from biotites from the granodiorites and older adamellite (Dba) and granite (Dbrpc). The biotite is pleochroic with X = medium dark grey/brown and Y, Z = light brown.

The fine- to medium-grained granitoid intrusions consist of a granular mass of quartz, K-feldspar and plagioclase with a little altered biotite. Plagioclase is albite in composition and the K-feldspar is microcline. Rare patches of manganese-rich garnet are present.

Representative mineral analyses are presented in Table 6.

Variably porphyritic coarse- to fine-grained biotite hornblende granodiorite (Dbgp)

This rock type forms dyke-shaped bodies ranging up to 3 km wide. It corresponds to the Scamander Tier Granodiorite of Cocker (1977). The eastern dyke extends from the mouth of the Scamander River at FQ048089 to the shores of Moulting Bay at FQ065275 where it attains its greatest thickness of one kilometre. The southern part of the dyke intrudes Mathinna Beds and in the north, near St Helens, it cuts the sparsely porphyritic coarse-grained biotite-hornblende granodiorite (Dbgsp). A thin (300 m) WNW extension of the dyke occurs at its northern end which follows the boundary between the granodiorite and the porphyritic to seriate to equigranular biotite adamellite (Dbasc). In the Apteds Creek [EQ943315] to Terryvale [EQ272925] area the dyke extends southwards and has a maximum width of 3 km. The western boundary in this area comes against a body of the porphyritic to seriate to equigranular adamellite (Dbasc). On the north-west margin it has a boundary with a porphyritic biotite adamellite (Dbapc). Farther south separated from these outcrops a thin strip of the same type of granodiorite occurs near Holloways Hill [EQ937143] where it comes against Mathinna Beds in the east side and porphyritic to seriate to equigranular biotite adamellite (Dbasc) and quartz feldspar porphyry (Dbp) on the west side. South of a north-east trending fault in the Catos Creek area [EQ070954] outcrop is about one kilometre wide and has Mathinna Beds on both sides.

The eastern dyke is well exposed along large parts of its length but outcrop on the west north-west dyke and western dyke is less complete. The boundaries on the narrow parts of the dykes are well defined and appears to be steep on the basis of their straight trace across the topography and the steep attitude of small parts of the boundary directly observed. Chilling of the granodiorite can be seen at many places and the dykes are younger than the sparsely porphyritic coarse-grained biotite-hornblende granodiorite (Dbgsp) and the porphyritic to seriate to equigranular biotite adamellite (Dbasc). The granodiorite in the Binalong Bay and Baretop area indicated on the map as the Dbgsp rock type was considered by Cocker (1977) as part of the granodiorite dyke and therefore part of the Dbgp rock type. The overlap in characteristics of these granodiorites makes unequivocal identification impossible. The apparent lack of any chilling in the granodiorite at the contact with the

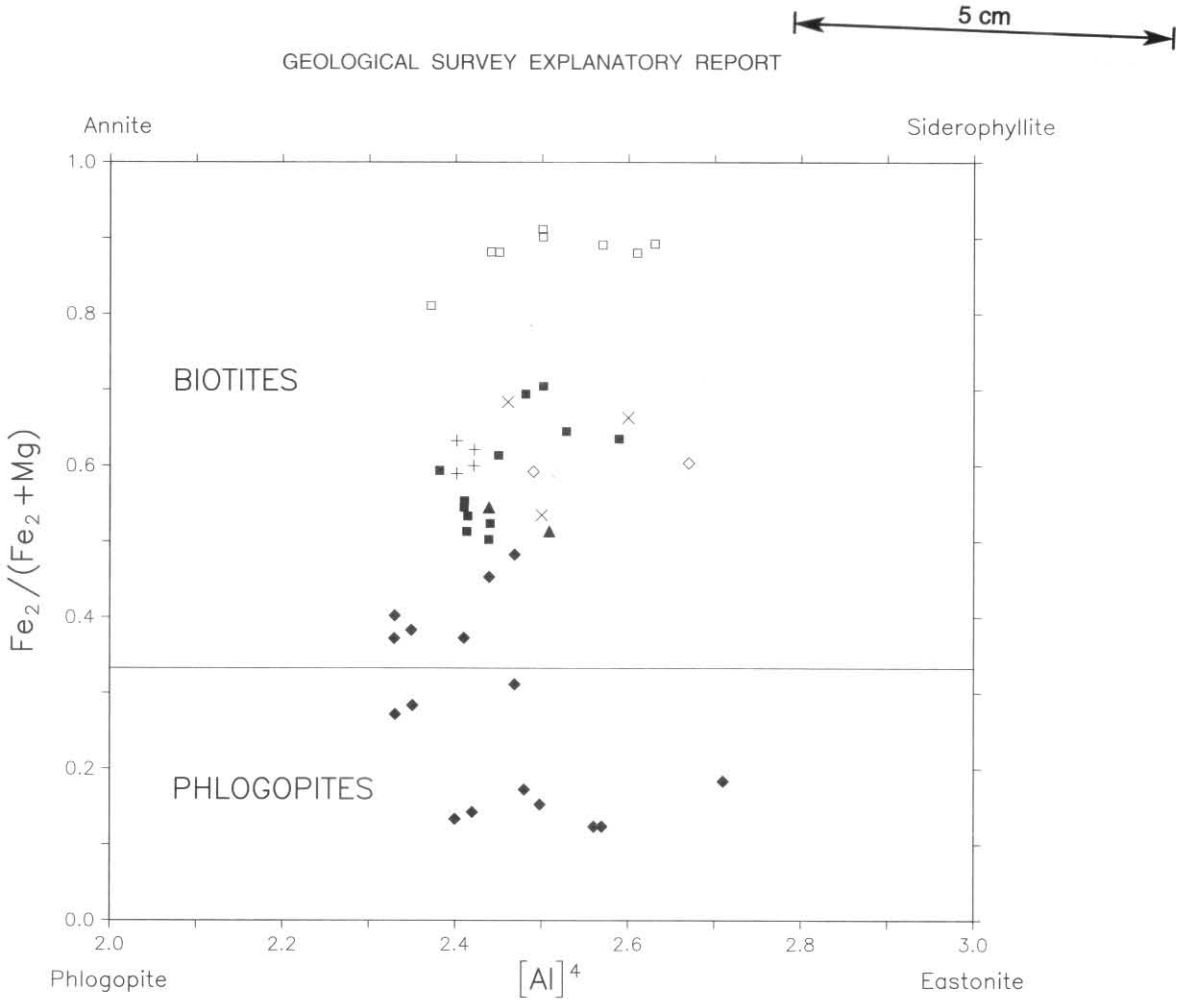

Figure 3. Mica compositions from the St Helens map sheet. □ Dbasc, + Dbgp, × Dbgsp (albitised monzodiorite to monzonite areas), ◇ Dbgbsp, ■ Dbgsp and Dbrpc, ▲ Dba, ◆ Dbdc.

biotite adamellite (Dbasc) between FQ047293 and FQ074321 is surprising if it is part of the dyke and supports the interpretation shown on the map. Cocker's view is, however, supported by the geochemical similarity of the two whole rock analyses from this area to the later granodiorite rather than the earlier (see geochemistry section for discussion of this point).

The granodiorite is a variably porphyritic, coarse- to fine-grained dark grey rock. It is fine grained where the margins have been chilled against the country rock in a zone generally about 5–10 m wide. Areas where the chilling at the boundary have been observed are indicated on the map. The central parts of the dykes are coarse grained. The texture of the granodiorite shows considerable variability. At FQ033200 in the Scamander Tier area, immediately at the contact the fine-grained granodiorite contains abundant quartz phenocrysts (5 mm) and several metres away from the contact abundant plagioclase phenocrysts (<10 mm) also occur. In the central parts of the dykes the plagioclase phenocrysts form a continuous size range with the matrix. Occasionally amphibole crystals, slightly larger than matrix, can be identified. In some parts of the dyke large K-feldspar phenocrysts are very abundant and amphibole is less common or absent. These areas are distinguished on the map. At FQ037224 blocks of coarse grained biotite adamellite with large K-feldspar showing seriate texture resembling the Dbasc rock type are present, surrounded by medium-grained granodiorite with a fine- grained, thin, chilled zone at the contact. This is an accidental xenolith brought up by the dyke. Other xenoliths of coarse-grained equigranular granodiorite occur a short distance farther south at FQ035213. Fine-grained small dioritic xenoliths can be seen in areas of good exposure. Rare xenoliths of Mathinna Beds occur in the eastern dyke in the Scamander Tier area but in the WNW dyke and its extension to the Terryvale and Apteds Creek area they become very abundant. In these areas outcrop is poor and there is a complex intermingling of granodiorite and Mathinna Beds float. The areas of abundant Mathinna Beds xenoliths have been distinguished on the map.

K-feldspar phenocrysts in some areas show alignment on horizontal surfaces approximately parallel to the dyke walls (e.g. at FQ031200). This is particularly marked near Moulting Bay at FQ065266 where there is an alignment of elongate mafic mineral concentration parallel to the K-feldspar trend. It seems probable that these features are produced by flow.

In thin section the granodiorite consists of plagioclase, quartz, K-feldspar, biotite and amphibole with accessory ilmenite, sphene, allanite, apatite and zircon. The fine- and medium-grained samples are porphyritic with very abundant quartz and plagioclase phenocrysts. Amphibole and biotite phenocrysts are less common. K-feldspar phenocrysts are microperthitic orthoclase and are extremely abundant in some samples. The plagioclase phenocrysts are generally euhedral showing oscillatory zoning. Some phenocrysts have core regions bordered by thin zones rich in fine sericite. The quartz phenocrysts are commonly embayed. Amphibole often occurs in composite patches in association with biotite and quartz. Biotite and amphibole also occur as isolated small phenocrysts. The matrix is formed from the same minerals with K-feldspar being subordinate to plagioclase and generally showing microcline twinning.

Modal analyses by Cocker (1977) show that the rock type is a granodiorite. Representative mineral analyses are presented in Table 7 and biotite and amphibole compositions are plotted in Figures 3 and 4. Biotite is pleochroic with X = pale brown and Y, Z = dark

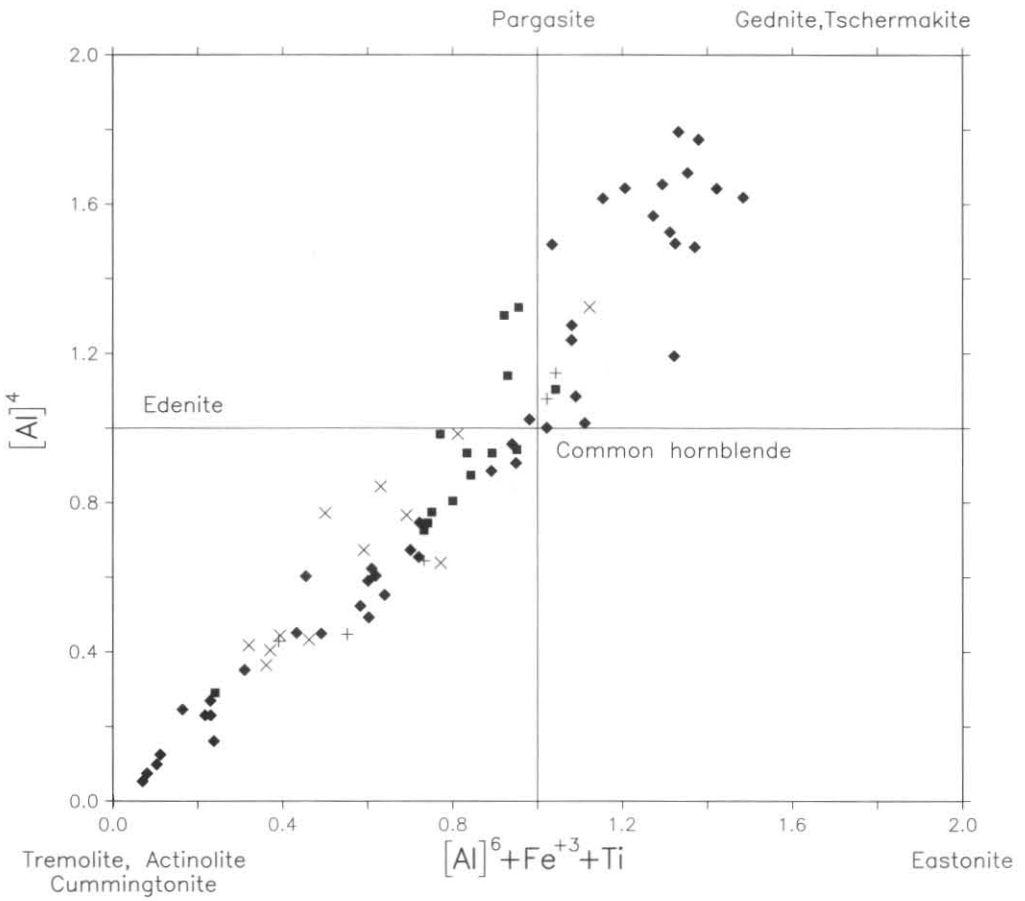

Figure 4. Amphibole compositions from the St Helens map sheet. + Dbgp, × Dbgsp (albitised monzodiorite to monzonite areas), ■ Dbgsp and Dbrpc, ◆ Dbdc.

red/brown, and it plots in the centre of the biotite field. Amphibole has pale to dark green pleochroic colours and ranges from close to actinolite in composition to hornblende with a small edenite component.

Coarse-grained diorite (Dbdc)

This rock type occurs as several small bodies, in the west of the map sheet in the area immediately north of Trafalgar Flat [EQ870184]. The bodies are included within, or are associated with, small patches of strongly hornfelsed Mathinna Beds. The diorite and the Mathinna Beds bodies occur within an adamellite pluton (Dbapc) and lie in a zone parallel to its margin. The field occurrence suggests that the diorite intruded the Mathinna Beds and that they were both subsequently transported by the adamellite to their present position as rafts. An additional small body of diorite occurs at EQ873263 intruded into Mathinna Beds outside the adamellite pluton.

The diorite shows considerable compositional range. In thin section the most basic sample (MSH22) is composed of large anhedral amphiboles enclosing olivine, orthopyroxene, clinopyroxene and biotite. Olivine and pyroxene occur as irregularly shaped grains and patches with slightly rounded outlines. Amphibole is variable in composition. Thin rims of cummingtonite are present around some of the olivine and orthopyroxene while clinopyroxene is surrounded by irregularly-shaped patches of very pale green actinolite set in darker green amphibole which grades into hornblende. Biotite is pale brown and forms only a minor proportion of the rock. Accessory minerals are apatite, pyrite, ilmenite and spinel. The latter mineral is present as minute inclusions in olivine where it is chromium rich, and also as small isolated grains of iron-rich spinel. Apatite occurs as sparse anhedral pale brown/mauve grains. Minor chloritic alteration is also present. Mg* values of cummingtonite are similar to those of olivine and orthopyroxene while those of actinolite match the clinopyroxene. Typical mineral analyses are presented in Table 8.

In less basic parts of the body samples contain plagioclase and quartz, and olivine and orthopyroxene are absent. Amphibole is present as large anhedral crystals and has inclusions of anhedral grains of clinopyroxene, plagioclase and biotite. Quartz is intergranular and biotite is more abundant and darker brown. Amphibole has a range of composition from actinolite to hornblende. Plagioclase contains altered cores rich in sericite with sharp boundaries with clear slightly zoned rims. There is a gap in compositional ranges between the cores (An_{77}–An_{93}) and the rims (An_{42}–An_{51}). Accessory minerals are apatite, pyrite, ilmenite zircon and prehnite. The latter mineral occurs as thin strips along the cleavage in biotite.

In the least basic samples amphiboles are smaller and clinopyroxene is absent but otherwise the rock is similar to that described above. Typical mineral analyses from less basic samples are presented in Table 9.

Strongly foliated medium- to coarse-grained biotite granodiorite (Dbgbf)

This rock type forms a small body near Pyengana [EQ270850] where it has intruded Mathinna Beds. It is the eastern part of the Pyengana Pluton described by Groves (1977). The granodiorite is a medium- to coarse-grained, dark grey rock with a strongly developed alignment of elongated biotite and quartz patches. Fine-grained dioritic xenoliths are elongated parallel with the mineral

Table 2. REPRESENTATIVE MINERAL ANALYSES FROM THE ALBITISED MONZODIORITE TO MONZONITE AREAS OF THE SPARSELY PORPHYRITIC COARSE-GRAINED BIOTITE-HORNBLENDE GRANODIORITE (Dbgsp)

		amphibole			biotite	
No.		MSH127-4/1	MSH145-2/3		MSH127-3/1	MSH145-2/4
SiO_2		46.21	49.29		35.38	35.91
TiO_2		0	0.36		2.74	1.17
Al_2O_3		7.75	5.25		15.41	16.43
Cr_2O_3		0	0		0	0
Fe_2O_3		5.17	4.79		0	0
FeO		18.64	11.55		26.08	22.76
MnO		1.57	0.44		0.97	0.28
MgO		6.29	12.99		6.78	11.16
CaO		11.04	12.18		0	0
Na_2O		0.63	0.43		0	0
K_2O		0.73	0.45		8.8	8.37
H_2O		1.97	2.05		3.83	3.92
		O = 23			O = 22	
Tet	Si	7.031	7.233	Tet	5.54	5.491
	Al	0.969	0.767		2.46	2.509
	Σ	8	8		8	8
Oct M1–3	Al	0.42	0.137		0.385	0.454
	Ti	0	0.04		0.323	0.135
	Fe^{+3}	0.592	0.527	Oct	Fe^{+2} 3.416	2.91
	Cr	0	0		0	0
	Fe^{+2}	2.372	1.411		Mn 0.128	0.036
	Mn	0.202	0.055		Mg 1.582	2.543
	Mg	1.427	2.829		Σ 5.835	6.077
	Σ	5.014	5		Ca 0	0
XM1-3		0.014	0		Na 0	0
M4	Ca	1.801	1.908		K 1.759	1.633
	Na	0.185	0.092		Σ 1.759	1.633
	Σ	1.986	2		OH 4	4
A	Na	0	0.031		Mg* 0.32	0.47
	K	0.142	0.084			
	Σ	0.142	0.115			
	OH	2	2			
	Mg*	0.38	0.67			

	Plagioclase		K-feldspar	Epidote		Sphene	Ilmenite
No.	MSH122-4/1	MSH145-7/2	MSH122-5/1	MSH130-1/1		MSH127-8/1	MSH145-5/1
SiO_2	68.75	63.12	65.29	38.21		31.33	0
TiO_2	0	0	0	0		33.14	52.18
Al_2O_3	20.08	23.53	18.60	25.11		3.26	0
Cr_2O_3	0	0	0	0		0	0
Fe_2O_3	0	0	0	11.19		0	0
FeO	0	0	0	0		1.50	41.84
MnO	0	0	0	0		0	5.97
MgO	0	0	0	0		0	0
CaO	0.36	4.78	0	23.57		30.76	0
Na_2O	10.81	8.43	0.66	0		0	0
K_2O	0	0.14	15.45	0		0	0
H_2O	0	0	0	1.92		0	0
	O=32			O = 25		O = 18	O = 6
Si	11.965	11.145	12.010	Si 6.018	Si	3.942	0
Al	4.12	4.898	4.033	Al 0	Al	0.454	0
Na	3.648	2.887	0.235	S 6.018	Ti	2.942	1.986
Ca	0.067	0.904	0	Al 4.663	Fe^{+2}	0.148	1.771
K	0	0.032	3.627	Fe^{+3} 1.327	Mn	0	0.256
Σ	19.799	19.866	19.905	Cr 0	Mg	0	0
An	0.02	0.24	0	Σ 5.99	Ca	3.891	0
				Mn 0	Σ	11.133	4.014
				Mg 0			
				Ti 0			
				Ca 3.978			
				Na 0			
				K 0			
				Σ 3.978			
				OH 2			

Mg* = Mg/(Mg + Fe^{+2}).
O is the oxygen number used to calculate the structural formulae.

alignment. Sparse large K-feldspar phenocrysts are present in some outcrops.

In thin section the granodiorite consists of plagioclase, quartz, K-feldspar and biotite with accessory zircon and apatite. Plagioclase shows zoning and is andesine. K-feldspar is finely perthitic orthoclase. Quartz forms granular patches intergranular to the plagioclase and biotite crystals. K-feldspar crystallised late as it encloses the other major minerals. Fracturing and bending of the biotite is common. Minor alteration of the biotite to chlorite is present together with small amounts of prehnite formed along the biotite cleavages.

Porphyritic coarse-grained biotite and biotite minor muscovite adamellite (Dbapc)

This rock type is present as two large bodies in the north-west part of the map sheet. The more southerly of

Table 3. REPRESENTATIVE MINERAL ANALYSES FROM THE FINE- TO COARSE-GRAINED BIOTITE ADAMELLITE (Dba)

		Biotite		Plagioclase		K-feldspar
No.		MSH128-5/1		MSH128-1/1	MSH128-1/2	MSH128-2/3
SiO_2		35.82		57.59	65.25	65.23
TiO_2		2.53		0	0	0
Al_2O_3		15.08		27.2	22.11	18.51
Cr_2O_3		0		0	0	0
Fe_2O_3		0		0	0	0
FeO		25.24		0	0	0
MnO		0.53		0	0	0
MgO		7.87		0	0	0
CaO		0		9.31	3.16	0
Na_2O		0		5.77	9.35	0.31
K_2O		9.07		0.13	0.13	15.95
H_2O		3.85		0	0	0
		O = 22			O = 32	
Tet	Si	5.582	Si	10.3	11.465	12.019
	Al	2.418	Al	5.735	4.579	4.021
	Σ	8	Na	1.999	3.185	0.111
Oct	Al	0.382	Ca	1.784	0.595	0
	Ti	0.296	K	0.030	0.029	3.749
	Fe^{+2}	3.289	Σ	19.848	19.853	19.901
	Cr	0	An	0.47	0.16	0
	Mn	0.069				
	Mg	1.828				
	Σ	5.835				
	Ca	0				
	Na	0				
	K	1.804				
	Σ	1.804				
	OH	4				
	Mg*	0.36				

Mg* = Mg/(Mg + Fe^{+2}).
O is the oxygen number used to calculate the structural formulae.

these bodies is centred on the Billy Tin Tier area [EQ850215] and extends into the Alberton map sheet to the west. The other, northern body crops out in the Organ Hill [EQ845314] and Mother Hill [EQ904310] area and is on the southern edge of a large pluton mostly cropping out in the Blue Tier and Ringarooma map sheets.

The southern body has a boundary against the Mathinna Beds and the strongly foliated medium- to coarse-grained biotite granodiorite (Dbgbf). The adamellite crosses the granodiorite/Mathinna Beds boundary at EQ854260 showing that it is younger than the granodiorite. In the southern part of the body [EQ870190] a large (3 km long) patch of hornfelsed Mathinna Beds and coarse-grained diorite (Dbdc) occurs within the adamellite area and is approximately parallel to the boundary. This is probably a raft. Near this area the adamellite/Mathinna Beds boundary has a distinct projection into the adamellite. This may be a partial screen between two adamellite bodies of similar character which have coalesced to form the southern body.

The northern adamellite body has boundaries along its southern margin, against Mathinna Beds, the porphyritic to seriate to equigranular coarse-grained biotite adamellite (Dbasc) body and the variably porphyritic coarse- to fine-grained biotite hornblende granodiorite (Dbgp). The cross-cutting relationship the northern adamellite body has to the boundaries between these rock bodies indicates that it is a later intrusion.

The adamellite is a medium dark grey coarse-grained rock with abundant large (<50 mm) K-feldspar phenocrysts. The phenocrysts often show alignments defining apparent lineations on horizontal surfaces. Biotite is prominent as small clots and isolated crystals. There is a slightly greater proportion of biotite and less common K-feldspar phenocrysts in the southern part of the southern mass which supports the suggestion that this part of the body might be a separate pluton. It was not however, possible to map out a boundary for this slight difference in character between the southern and northern part of the body.

In thin section the adamellite consists of plagioclase, quartz, K-feldspar and biotite with accessory zircon, apatite and muscovite. Plagioclase is of oligoclase to andesine composition with slight zoning and is usually slightly altered to sericite. K-feldspar phenocrysts are perthitic and usually constitute 10–15% of the rock. They range in size up to about 50 mm long and contain abundant zones of small plagioclase inclusions aligned parallel to crystal boundaries which are anhedral. Muscovite, biotite and quartz inclusions are also present in the K-feldspar phenocrysts. Muscovite flakes always occur within or adjacent to K-feldspar. Biotite shows minor alteration to chlorite. Modal analyses from the northern body on the Blue Tier and Ringarooma map sheets (table 2, rock type 3, McClenaghan and Williams, 1982) indicate that the rock type is an adamellite.

Porphyritic fine-grained biotite-muscovite adamellite with abundant small plagioclase phenocrysts (Dbapf)

Rocks of this type occur in the north-west corner of the map sheet and form the edge of sheet-like bodies that are substantially in the Blue tier map sheet and were described by McClenaghan and Williams (1982). The rock bodies are intruded into the coarse-grained biotite adamellite (Dbapc).

The rock type occurs in two variants. The first is a fine-grained light grey rock with abundant small(<10 mm) plagioclase, sparse larger (<20 mm) K-feldspar and abundant quartz phenocrysts (<5 mm). This variant is exposed in a small area in the extreme north-west corner of the map sheet. In thin section the fine-grained matrix consists of quartz, K-feldspar and plagioclase. Small amounts of apatite and topaz (<1%) are often present as well as muscovite, chlorite and ilmenite. Subhedral plagioclase phenocrysts sometimes have narrow rims composed of myrmekitic intergrowths and contain sparse inclusions, notably quartz and rarely biotite and chlorite. Quartz phenocrysts are subhedral, and in most specimens contain only rare biotite inclusions. Subhedral K-feldspar

Table 4. REPRESENTATIVE MINERAL ANALYSES FROM THE VERY ABUNDANTLY PORPHYRITIC WITH SMALL K-FELDSPAR PHENOCRYSTS, MEDIUM- TO COARSE-GRAINED BIOTITE GRANITE (Dbrpc)

		Dbrpc biotite		Dbrpc plagioclase core
No.		MSH96-3/1		MSH96-4/1
SiO_2		35.70		64.18
TiO_2		3.73		0
Al_2O_3		17.83		22.96
Cr_2O_3		0		0
FeO		22.2		0
MnO		0.32		0
MgO		6.98		0
CaO		0		3.86
Na_2O		0		8.99
K_2O		9.32		0
H_2O		3.92		0
		O = 22		O = 32
Tet	Si	5.465	Si	11.296
	Al	2.535	Al	4.763
	Σ	8	Na	3.068
Oct	Al	0.682	Ca	0.729
	Ti	0.430	K	0
	Fe^{+2}	2.841	Σ	19.856
	Cr	0	An	0.19
	Mn	0.042		
	Mg	1.592		
	Σ	5.587		
	Ca	0		
	Na	0		
	K	1.820		
	Σ	1.820		
	OH	4		
	Mg*	0.36		

Mg* = Mg/(Mg + Fe^{+2}).
O is the oxygen number used to calculate the structural formulae.

phenocrysts contain inclusions of muscovite, biotite, plagioclase and quartz. Modal analyses (table 2, type 5, McClenaghan and Williams, 1982) indicate that the rock type is adamellite.

The second variant is much lighter coloured, rich in muscovite with variable development of plagioclase and quartz phenocrysts, and occurs over a larger area at the northern edge of the map sheet in the area around EQ870328. In thin section the matrix consists of perthitic K-feldspar, quartz, plagioclase, muscovite and biotite. Plagioclase is variable in composition (An_{0-13}, table 1, McClenaghan and Williams, 1982). Biotite is frequently largely altered to muscovite and sometimes chlorite. Muscovite is also present as an alteration product of K-feldspar and as large irregular flakes associated with minor amounts of topaz. The amount of feldspar and muscovite is highly variable, and in some cases the rock is composed almost entirely of quartz and muscovite.

Leucocratic muscovite granite (Dbgm)

Rocks of this type occur as numerous dykes in the area surrounding Georges Bay. The dykes range in width up to about 30 m with steep dipping margins (e.g. at FQ133283) and have intruded all the granitoid types of the area including the granodiorite dyke (Dbgp) at FQ043238. This is the most westerly occurrence of the dykes. The dykes trend in various directions but an approximate east-west direction is most common.

The granite is a coarse-grained, very leucocratic rock with prominent muscovite. Pegmatitic patches with quartz, feldspar and tourmaline at the dyke margins are common and sometimes there are thin tourmaline veins extending into the country rock.

In thin section the granite consists of a granular mass of quartz, plagioclase, K-feldspar and muscovite. Plagioclase shows cloudy alteration or abundant sericite, has only slight zoning and is oligoclase or albite composition. K-feldspar is microcline and encloses quartz and plagioclase. Muscovite is abundant and is present as large and small patches some of which are replacement of microcline. Patches of tourmaline associated with topaz are common and a little-altered biotite is present in some samples. Cocker (1977) reported andalusite from these dykes in the St Helens Point area and at FQ135297 andalusite (XRD determination) was found as coarse patches of crystals in pegmatitic material included within one of the granite intrusions. A modal analysis (Cocker, 1977) from a dyke in the St Helens Point area [FQ132296] indicates that it is granite.

Quartz-plagioclase-hornblende porphyry (Dbhp)

Minor dykes of this rock type occur at a number of localities [FQ045220, FQ027210, FQ008258] intruding the sparsely porphyritic coarse-grained biotite-hornblende granodiorite (Dbgsp). The dykes are fine grained dark grey with abundant phenocrysts of amphibole, plagioclase and quartz. They appear to correspond to the dyke suite described as lamprophyres by Cocker [1977), who presented two chemical analyses and suggested that they may be related to the granodiorites which they intrude.

Quartz-feldspar porphyry (Dbp)

The principal occurrence of this rock type is as a narrow dyke shaped intrusion trending NNW close to the eastern margin of a south-projecting narrow wedge of the porphyritic to seriate to equigranular coarse-grained adamellite body (Dbasc) at EQ929160. It is at its widest (0.5 km) near its northern end. A small dyke of the same rock type occurs in the George River at FQ052274 where it has intruded granodiorite (Dbgsp).

It is a fine-grained light to medium dark grey rock with abundant feldspar and quartz phenocrysts. In thin section quartz phenocrysts show slightly corroded margins, plagioclase phenocrysts are slightly zoned and K-feldspar phenocrysts are finely perthitic. Rare biotite phenocrysts are also present. The matrix consists of quartz, plagioclase, K-feldspar and minor biotite. Sparse grains of opaque minerals are associated with the biotite.

Aplitic granite (Dbaa)

Minor veins and small dykes of fine-grained leucocratic rock consisting almost entirely of quartz and feldspar but sometimes with minor mica occur intruding granite (Dbrpc) in coastal outcrops at Skeleton Bay [FQ105322] and St Helens Point [FQ135297].

SUMMARY OF INTRUSIVE EVENTS

The mapped distribution of rock types and the field relationships described in the previous sections allows the order of intrusion of some of the major bodies to be recognised in the St Helens area. In the east and north part of the map sheet the bodies in order of intrusion are as follows:

(1) A largely granodiorite body consisting of biotite hornblende (Dbgsp), biotite granodiorite (Dbgbsp), biotite adamellite (Dba) and biotite granite (Dbrpc) in the area surrounding Georges Bay (George River intrusive phase).

(2) A coarse-grained biotite adamellite (Dbasc) body lying to the west and north of St Helens (Mt Pierson intrusive phase).

Table 5. REPRESENTATIVE MINERAL ANALYSES FROM THE SPARSELY PORPHYRITIC MEDIUM- TO COARSE-GRAINED BIOTITE GRANDIORITE (Dbgbsp)

		plagioclase		K-feldspar			biotite
		core	rim				
No.		MSH108-2/3	MSH108-3/2	MSH108-4/2			MSH108-3/1
SiO_2		57.32	63.89	64.01			34.95
TiO_2		0	0	0.19			2.32
Al_2O_3		27.53	21.47	18.07			19.30
Cr_2O_3		0	0	0			0
Fe_2O_3		0	0	0			0
FeO		0	0	0			22.66
MnO		0	0	0			0.34
MgO		0	0	0			8.34
CaO		9.31	2.95	0			0
Na_2O		5.72	9.23	0.42			0
K_2O		0.12	0.30	15.28			8.16
P_2O_5		0	0.18	0			0
H_2O		0	0	0			3.94
			O = 32				O = 22
	Si	10.25	11.46	12.02	Tet	Si	5.33
	Al	5.80	4.54	4.00		Al	2.67
	Na	1.98	3.21	0.42		Σ	8
	Ca	1.78	0.57	0	Oct	Al	0.79
	K	0.03	0.07	3.66		Ti	0.26
	Σ	19.84	19.85	20.01		Fe^{+2}	2.89
	An	0.47	0.15	0		Cr	0
						Mn	0.04
						Mg	1.89
						Σ	5.87
						Ca	0
						Na	0
						K	1.58
						Σ	1.58
						OH	4

		chlorite		sphene
No.		MSH108-2/4		MSH108-2/2
SiO_2		24.90		31.05
TiO_2		0		32.32
Al_2O_3		22.47		4.64
Cr_2O_3		0		0
Fe_2O_3		0		0
FeO		29.36		2.66
MnO		0.62		0
MgO		11.37		0.80
CaO		0		28.33
Na_2O		0		0
K_2O		0		0
P_2O_5		0		0.20
H_2O		11.27		0
		O = 28		O = 18
Tet	Si	5.30	Si	3.65
	Al	2.70	Al	0.64
	Σ	8	Ti	2.86
Oct	Al	2.94	Fe^{+2}	0.26
	Ti	0	Mn	0
	Fe^{+3}	0	Mg	0.14
	Cr	0	Ca	3.57
	Fe^{+2}	5.23	Σ	11.12
	Mn	0.11		
	Mg	3.61		
	Ca	0		
	Na	0		
	K	0		
	Σ	11.89		
	OH	16		

$Mg^* = Mg/(Mg + Fe^{+2})$
O is the oxygen number used to calculate the structural formulae

(3) Biotite hornblende granodiorite (Dbgp) dyke shaped bodies lying to the south, north and west of St Helens. These bodies have been considered to be the plutonic equivalent of the St Marys Porphyrite (Dpr, Dpm) an ash-flow tuff occurring in the St Marys map sheet (Higgins *et al.*, 1986) (Scamander Tier intrusive phase).

(4) A porphyritic coarse-grained biotite adamellite (Dbapc) body outcropping in the north-west part of the map sheet and forming the southern margin of a large body mostly present in the Ringarooma and Blue Tier map sheets (Poimena intrusive phase).

(5) Fine-grained biotite-muscovite adamellite bodies in the north-west part of the map sheet which are the continuation of sheet and dome shaped bodies mostly occurring in the Blue Tier map sheet.

In the western part of the map sheet a porphyritic coarse-grained biotite adamellite body centred on the Billy of Tin Tier ridge [EQ850215] is later than the strongly foliated biotite granite (Dbgbf) body of the Pyengana area. Its order of intrusion can not be related to the bodies in the eastern part of the map sheet.

AGE OF INTRUSION

The age of the various intrusive phases in the St Helens and neighbouring areas has been reviewed by McClenaghan and Higgins (in preparation). Figure 5 reproduced from that work shows the range of biotite K-Ar and biotite-total rock Sr-Rb dates for the various intrusive phases. For average K-Ar ages (fig. 5*a*) the Scamander Tier intrusive phase has almost the same range as the earlier George River intrusive phase and the Mt Pierson phase appears younger than it. The Poimena phase is distinctly younger. The age range of the Mt Pierson phase contradicts the unequivocal geological

Table 6. REPRESENTATIVE MINERAL ANALYSES FROM THE PORPHYRITIC TO SERIATE TO EQUIGRANULAR COARSE-GRAINED BIOTITE-MINOR MUSCOVITE ADAMELLITE AND ASSOCIATED FINE- TO MEDIUM-GRAINED PINK BIOTITE GRANITE INSTRUSIONS (Dbasc, EASTERN BODIES)

		coarse-grained adamellite				fine-grained granite intrusion	
		biotite	siderophyllite	annite	muscovite		garnet
No.		MSH180-4/1	MSH187-2/1	MSH188-4/1	R1020-2/3		R1023-5/2
SiO_2		35.94	35.47	34.94	49.44		36.18
TiO_2		3.99	0.66	0.37	0		0
Al_2O_3		16.21	20.1	20.47	31.27		21.06
Cr_2O_3		0	0	0	0		0
Fe_2O_3		0	0	0	0		0
FeO		26.29	27.91	28.84	3.87		26.26
MnO		1.04	0.86	0.75	0		16.02
MgO		3.48	2.13	1.80	0.77		0
CaO		0.23	0		0.20		0.24
Na_2O		0	0		0.42		0
K_2O		8.99	9.03	9.02	9.53		0
P_2O_5		0	0	0	0		0.24
H_2O		3.83	3.83	3.81	4.5		0
			O = 22				O= 24
Tet	Si	5.624	5.554	5.498	6.582	Si	5.952
	Al	2.376	2.446	2.502	1.418	P	0.033
	Σ	8	8	8	8	Al	0.015
	Al	0.615	1.265	1.294	3.489	Σ	6
	Ti	0.470	0.078	0.044	0	Al	4.069
Oct	Fe^{+2}	3.440	3.655	3.795	0.431	Fe^{+3}	0.015
	Cr	0	0	0	0	Fe^{+2}	3.597
	Mn	0.139	0.114	0.100	0	Mn	2.233
	Mg	0.811	0.498	0.422	0.153	Ca	0.043
	Σ	5.475	5.610	5.655	4.073	Σ	9.957
	Ca	0.038	0	0	0.028		
	Na	0	0	0	0.109		
	K	1.795	1.804	1.810	1.618		
	Σ	1.833	1.804	1.810	1.755		
	OH	4	4	4	4		
	Mg*	0.19	0.12	0.10	0.26		

	central part of coarse-grained body		marginal part of coarse-grained body feldspars				fine-grained granite intrusion	
	core	rim						
No.	MSH180-6/1	MSH180-7/1	R1020-3/2	MSH188-5/1	MSH187-5/1	MSH187-1/1	R1023-1/2	R1023-1/1
SiO_2	60.34	65.77	63.36	65.82	64.02	6.49	68.47	65.66
TiO_2	0	0	0	0	0	0	0	0
Al_2O_3	25.32	21.88	23.41	21.78	22.92	18.3	19.85	18.14
Cr_2O_3	0	0	0	0	0	0		0
Fe_2O_3	0	0	0	0	0	0		0
FeO	0	0	0	0	0	0		0
MnO	0	0	0	0	0	0		0
MgO	0	0	0	0	0	0		0
CaO	6.79	2.47	4.48	2.48	3.87	0	0.48	0
Na_2O	7.39	9.66	8.42	9.71	8.79	0.23	11.10	0.49
K_2O	0.15	0.21	0.33	0.21	0.41	15.98	0.09	15.71
				O = 32				
Si	10.727	11.540	11.185	11.550	11.288	12.061	11.948	12.083
Al	5.307	4.526	4.871	4.506	4.763	3.973	4.084	3.935
Na	2.548	3.287	2.881	3.302	3.003	0.083	3.755	0.174
Ca	1.294	0.465	0.847	0.466	0.731	0	0.091	0
K	0.034	0.047	0.075	0.048	0.092	3.756	0.020	3.689
Σ	19.91	19.865	19.858	19.872	19.878	19.872	19.898	19.881
An	0.34	0.12	0.23	0.12	0.20	0	0.02	0

$Mg^* = Mg/(Mg + Fe^{+2})$.
O is the oxygen number used to calculate the structural formulae.

evidence as to the order of intrusion. If resetting has taken place it is possible that some samples may have escaped being reset or have been less affected. In Figure 5*b* age ranges for the oldest sample from each phase is shown. This shows the George River, Mt Pearson and Scamander Tier phases as having very similar age ranges and the Poimena again being distinctly younger. The age ranges allow the four phases to have been intruded in the order indicated on geological grounds. The age of 397±4 Ma obtained from the muscovite granite dyke (Dbgm) intruding the George River pluton is the same as the oldest age from it and supports it having the oldest age of the intrusive phases. The age of 396±3.8 Ma from the southern part of the coarse-grained biotite adamellite (Dbapc) in the Billy Tin Tier area (Haleys New Country) is consistent with it being part of the Scamander Tier intrusive phase, as is suggested by its chemical composition (see geochemistry section).

For Sr-Rb data (fig. 5*c–d*) the average age ranges show a similar pattern, with the Mt Pierson phase being younger than its order of intrusion would suggest. Using maximum ages for each phase does not resolve this anomaly. Examination of the age range diagram (fig. 5) suggests that Sr-Rb ages are younger than K-Ar ages.

In order to obtain the age of intrusion of the dolerite dyke suite (Ddl), biotite was dated from two samples of granitoid collected adjacent (<300 mm) to dykes (fig.

Table 7. REPRESENTATIVE MINERAL ANALYSES FROM THE VARIABLY PORPHYRITIC COARSE- TO FINE-GRAINED BIOTITE HORNBLENDE GRANODIORITE (Dbgp)

		amphibole			biotite	
No.		MSH136-1/2	MSH136-1/3		MSH136-1/1	MSH36-1/1
SiO_2		55.87	46.05		35.88	36.33
TiO_2		0	0.94		3.86	4.21
Al_2O_3		0	7.23		14.10	14.07
Cr_2O_3		0	0		0	0
Fe_2O_3		0	6.49		0	0
FeO		12.49	15.38		24.43	23.07
MnO		0	0.06		0.37	0
MgO		16.92	9.06		8.35	9.11
CaO		12.62	10.49		0	0.16
Na_2O		0	1.31		0	0
K_2O		0	0.99		9.16	9.15
H_2O		2.10	2.00		3.86	3.89
		O = 23			O = 22	
Tet	Si	7.985	6.914	Tet	5.577	5.598
	Al	0	1.086		2.423	2.402
	Σ	7.985	8		8	8
Oct M1-3	Al	0	0.194		0.162	0.154
	Ti	0	0.106		0.451	0.488
	Fe^{+3}	0	0.734	Oct	Fe^{+2} 3.176	2.974
	Cr	0	0		0	0
	Fe^{+2}	1.493	1.931		Mn 0.048	0
	Mn	0	0.008		Mg 1.935	2.093
	Mg	3.604	2.027		Σ 5.771	5.709
	Σ	5.097	5		Ca 0	0.027
XM1-3		0.097	0		Na 0	0
M4	Ca	1.933	1.688		K 1.817	1.800
	Na	0	0.312		Σ 1.817	1.827
	Σ	1.933	2		OH 4	4
A	Na	0	0.069		Mg* 0.38	0.41
	K	0	0.190			
	Σ	0	0.259			
	OH	2	2			
	Mg*	0.71	0.51			

	plagioclase		K-feldspar
No.	MSH36-3/1	MSH36-3/2	MSH136-4/1
SiO_2	56.41	58.89	65.33
TiO_2	0	0	0
Al_2O_3	27.91	26.13	18.40
FeO	0	0	0
MnO	0	0	0
MgO	0	0	0
CaO	10.00	8.13	0.18
Na_2O	5.51	6.34	0.71
K_2O	0.17	0.52	15.38
		O = 32	
Si	10.122	10.518	12.024
Al	5.903	5.501	3.991
Na	1.918	2.195	0.252
Ca	1.923	1.556	0.035
K	0.039	0.118	3.611
Σ	19.905	19.888	19.913
An	0.50	0.41	0.01

Mg* = Mg/(Mg + Fe^{+2})
O is the oxygen number used to calculate structural formulae

5*a–b*). The ages of 386±4.2 Ma and 388±2.6 Ma are in agreement within the limits of error and suggest that the dolerites were intruded at about the same time as the granitoids. This is consistent with the geological evidence described above.

The data indicate that the first three intrusive phases took place from about 398 to 388 Ma but can not be clearly distinguished by dating. The Poimena phase of intrusion followed about 15 Ma later.

GEOCHEMISTRY

In Table 10 major and trace-element analyses are presented for samples collected in the area of the St Helens map sheet. Samples with numbers starting with 37 have been used to provide new analyses of rocks collected by Cocker (1971). Plots of chemical data include ten analyses (pers. comm., B. W. Chappell, 1989; TB1, TB2, TB7, TB8, TB9, TB10, TB22, TB23, TB34, TB36) from the area covered by the Blue Tier, St Helens and St Marys map sheets. An additional four unpublished analyses (742611, 762457, 762458, 762463) from the Blue Tier map sheet are included on the plots. Published chemical data from the St Marys map sheet (Turner and Calver, 1987) and other chemical data from the St Helens map sheet are discussed elsewhere in this report by N. J. Turner.

The chemical data are mainly from the first three phases of intrusion, the Georges River, Mt Pearson and Scamander Tier phases. The plutons of these three intrusive phases belong to two granitoid suites previously recognised on chemical, isotopic and petrographic character (McClenaghan, 1989). The George River phase rocks belong to the Gardens suite which will now be renamed the George River suite. The Mt Pearson phase rocks had previously been included in the Mussel Roe suite (McClenaghan, 1989) but is now considered more

Table 8. REPRESENTATIVE MINERAL ANALYSES FROM THE MOST MAFIC (MSH22) COARSE-GRAINED DIORITE (Dbdc)

	Olivine		Orthopyroxene	Clinopyroxene		Cummingtonite
No.	MSH22-2/3		MSH22-1/1	MSH22-12/1		MSH22-1/2
SiO_2	39.25		56.01	53.38		57.74
TiO_2	0		0	0		0
Al_2O_3	0		1.08	0.77		0.81
Cr_2O_3	0		0	0.51		0
Fe_2O_3	0		0.33	0		0
FeO	16.65		10.64	2.98		11.70
MnO	0.18		0.18	0		0.37
MgO	43.90		30.90	17.15		26.08
CaO	0		0.84	24.19		1.12
Na_2O	0		0	0		0
K_2O	0		0	0		0
H_2O	0		0	0		2.18
	O = 4		O = 6			O = 23
Si	0.994	Tet Si	1.973	1.981	Tet Si	7.948
Fe	0.353	Al	0.027	0.019	Al	0.052
Mn	0.004	Σ	2.000	2.000	Σ	8.000
Mg	1.656	Al	0.018	0.014	Al	0.8000
Σ	3.007	Ti	0	0	Ti	0
Mg*	0.82	Fe^{+3}	0.009	0	Fe^{+3}	0
		Cr	0	0.015	Oct Cr	0
		Oct Mg	1.622	0.931	M1-3 Mg	5.350
		Fe^{+2}	0.314	0.091	Fe^{+2}	1.347
		Mn	0.005	0	Mn	0.043
		Ca	0.032	0.944	Σ	6.820
		Na	0	0	XM1-3	1.820
		K	0	0	M4 Ca	0.166
		Σ	2.000	1.995	Na	0
		Mg*	0.84	0.91	Σ	1.986
					A Na	0
					K	0
					Σ	0
					OH	2
					Mg*	0.80

	Actinolite	Hornblende		Biotite		Spinel in olivine	Spinel outside olivine
No.	MSH22-2/1	MSH22-11/2		MSH22-4/1		MSH22-2/1	MSH22-3/1
SiO_2	56.31	43.70		39.38		0	0
TiO_2	0	1.60		1.74		1.01	0
Al_2O_3	2.35	12.34		15.84		20.77	64.83
Cr_2O_3	0.66	0.43		0.43		37.66	0
Fe_2O_3	0.47	8.37		0		6.55	0.83
FeO	3.56	0		6.29		28.55	19.92
MnO	0	0		0		0.51	0
MgO	21.81	17.05		22.48		4.74	14.24
CaO	12.65	11.95		0		0	0
Na_2O	0	1.50		0		0.20	0.16
K_2O	0	0.93		9.61		0	0
H_2O	2.18	2.11		4.22		0	0
	O = 23			O = 22		O = 4	
Tet Si	7.749	6.209	Tet Si	5.597	Si	0	0
Al	0.251	1.791	Al	2.403	Al	0.780	1.984
Σ	8.000	8.000	Σ	8.000	Cr	0.948	0
Al	0.130	0.277	Al	0.251	Fe^{+3}	0.235	0.024
Ti	0	0.171	Ti	0.185	Ti	0.024	0
Oct Fe^{+3}	0.049	0.895	Fe^{+2}	0.748	Σ	1.988	2.008
M1-3 Cr	0.072	0.049	Oct Cr	0.048	Mg	0.225	0.551
Mg	4.473	3.610	Mn	0	Fe^{+2}	0.761	0.432
Fe^{+2}	0.409	0	Mg	4.762	Mn	0.014	0
Mn	0	0	Σ	5.994	Ca	0	0
Σ	5.134	5.003	Ca	0	Na	0.012	0.008
XM1-3	0.134	0.003	Na	0	K	0	0
M4 Ca	1.866	1.819	K	1.743	Σ	1.012	0.992
Na	0	0.177	Σ	1.743	Mg*	0.23	0.56
Σ	2.000	2.000	OH	4			
A Na	0	0.236	Mg*	0.86			
K	0	0.169					
Σ	0	0.405					
OH	2	2					
Mg*	0.92	1.00					

Amphibole and pyroxene formulae calculated by the method developed by Papike *et al.* (1974) for maximum Fe^{+3}.
Ideal H_2O assumed for hydrous minerals and analyses recalculated to 100. Mg* = Mg/(Mg + Fe^{+2}).
O is the oxygen number used to calculate structural formulae.

likely that it is part of the Scamander Tier suite which also includes rocks from the Scamander Tier phase of intrusion.

The George River and Scamander Tier suite rocks range from metaluminous to weakly peraluminous with decreasing total iron content. The two suites plot on the typically calc-alkaline trend (fig. 6. Plots of various elements against total iron show slightly different approximately straight line trends (fig. 7) for each suite.

In the case of the George River suite the samples from the sparsely porphyritic biotite granodiorite (Dbgbsp) depart from the trend shown by most of the other rocks of the

Table 9. REPRESENTATIVE MINERAL ANALYSES FROM THE LESS BASIC COARSE-GRAINED DIORITE (Dbdc)

	Plagioclase					Clinopyroxene	
	rim		core				
No.	MSH23-3/1	MSH19-11/2	MSH19-11/1	MSH23-3/2		MSH43-3/2	MSH46-2/1
SiO_2	57.89	55.56	49.48	45.41		52.68	53.42
TiO_2	0	0	0	0		0	0
Al_2O_3	26.86	28.6	32.28	35.00		2.31	0.60
Cr_2O_3	0	0	0	0		0.83	0.29
Fe_2O_3	0	0	0	0		0.33	0
FeO	0	0	0	0		4.40	7.38
MnO	0	0	0	0		0	0.28
MgO	0	0	0	0		16.04	14.02
CaO	8.65	10.17	15.60	18.79		23.42	24.01
Na_2O	6.61	5.25	2.64	0.80		0	0
K_2O	0	0.41	0	0		0	0
H_2O	0	0	0	0		0	0
	O = 32					O = 6	
Si	10.352	9.991	9.032	8.369	Tet Si	1.934	1.987
Al	5.662	6.063	6.946	7.606	Tet Al	0.066	0.013
Ca	1.657	1.960	3.051	3.710	Tet Σ	2.000	2.000
Na	2.291	1.830	0.933	0.287	Oct Al	0.033	0.014
K	0	0.095	0	0	Oct Ti	0	0
Σ	19.962	19.939	19.962	19.972	Oct Fe^{+3}	0.009	0
An	0.42	0.50	0.77	0.93	Oct Cr	0.024	0.009
					Oct Mg	0.878	0.777
					Oct Fe^{+2}	0.135	0.229
					Oct Mn	0	0.009
					Oct Ca	0.921	0.957
					Oct Na	0	0
					Oct K	0	0
					Oct Σ	2.000	1.995
					Mg*	0.87	0.77

	Actinolite	Hornblende		Biotite		Prehnite	
No.	MSH23-2/2	MSH19-5/2		MSH20-2/6	MSH19-6/2		MSH23-7/1
SiO_2	54.00	45.51		36.71	39.25		43.56
TiO_2	0.30	1.76		3.42	3.35		0.36
Al_2O_3	2.76	11.61		16.08	15.75		23.64
Cr_2O_3	0.55	0.35		0	0		0.28
Fe_2O_3	1.73	6.31		0	0		0.99
FeO	8.55	4.99		19.41	11.46		0
MnO	0.28	0		0	0		0
MgO	17.50	14.23		11.75	17.36		0
CaO	12.00	11.50		0	0		26.81
Na_2O	0.21	1.15		0	0		0
K_2O	0	0.50		8.563	8.67		0
H_2O	2.12	2.10		3.99	4.15		4.35
	O=23					O=22	
Tet Si	7.644	6.506	Tet Si	5.522	5.667	Si	6.002
Tet Al	0.356	1.494	Tet Al	2.478	2.333	Al	0
Tet Σ	8.000	8.000	Tet Σ	8.000	8.000	Σ	6.002
Oct Al	0.105	0.463	Oct Al	0.374	0.348	Al	3.841
Oct Ti	0.032	0.190	Oct Ti	0.387	0.364	Fe^{+3}	0.103
Oct Fe^{+3}	0.184	0.679	Oct Fe^{+2}	2.442	1.383	Mg	0
Oct Cr	0.061	0.039	Oct Cr	0	0	Ti	0.038
Oct Mg	3.691	3.031	Oct Mn	0	0	Cr	0.030
Oct Fe^{+2}	1.012	0.596	Oct Mg	2.633	3.735	Σ	4.010
Oct Mn	0.034	0	Oct Σ	5.836	5.830	Ca	3.939
Oct Σ	5.119	4.998	Ca	0	0	Na	0
XM1-3	0.119	0	Na	0	0	K	0
M4 Ca	1.820	1.762	K	1.657	1.597	Σ	3.959
M4 Na	0.059	0.238	Σ	1.657	1.597	OH	4
M4 Σ	1.879	2.000	OH	4	4		
A Na	0	0.081	Mg*	0.52	0.73		
A K	0	0.090					
A Σ	0	0.171					
OH	2	2					
Mg*	0.76	0.70					

Mg* = Mg/(Mg + Fe^{+2}). O is the oxygen number used to calculate structural formulae.

suite by having lower SiO_2 and K_2O, and higher Al_2O_3, CaO, Na_2O and P_2O_5. This difference has probably been produced by metasomatic alteration as these rocks show considerable alteration of the more calcic rich plagioclase cores ($An_{0.47}$) to epidote and sericite, together with growth of clear more sodic plagioclase rims ($An_{0.15}$). Biotite is also extensively altered to chlorite.

Two other samples (37795, 37796) collected from the Binalong Bay area at FQ099327 and FQ066310 plot separately from the other samples for the intrusive phase for some elements. For the MgO, Y and Zr plots against total iron (fig. 7) these two samples (marked A and B on the plots) are more closely associated with the samples from the later intruded Scamander Tier suite rocks represented by the Dbgp rock type. This suggests that the rocks designated Dbgsp in the Binalong Bay – Baretop area may belong to the Dbgp rock group (see previous sections on petrology and field characteristics for discussion on this problem).

Two samples from the monzodiorite to monzonite bodies derived by a metasomatic process from the Dbgsp rock type are also plotted on the diagrams and show marked departures from the host granodiorite composition for

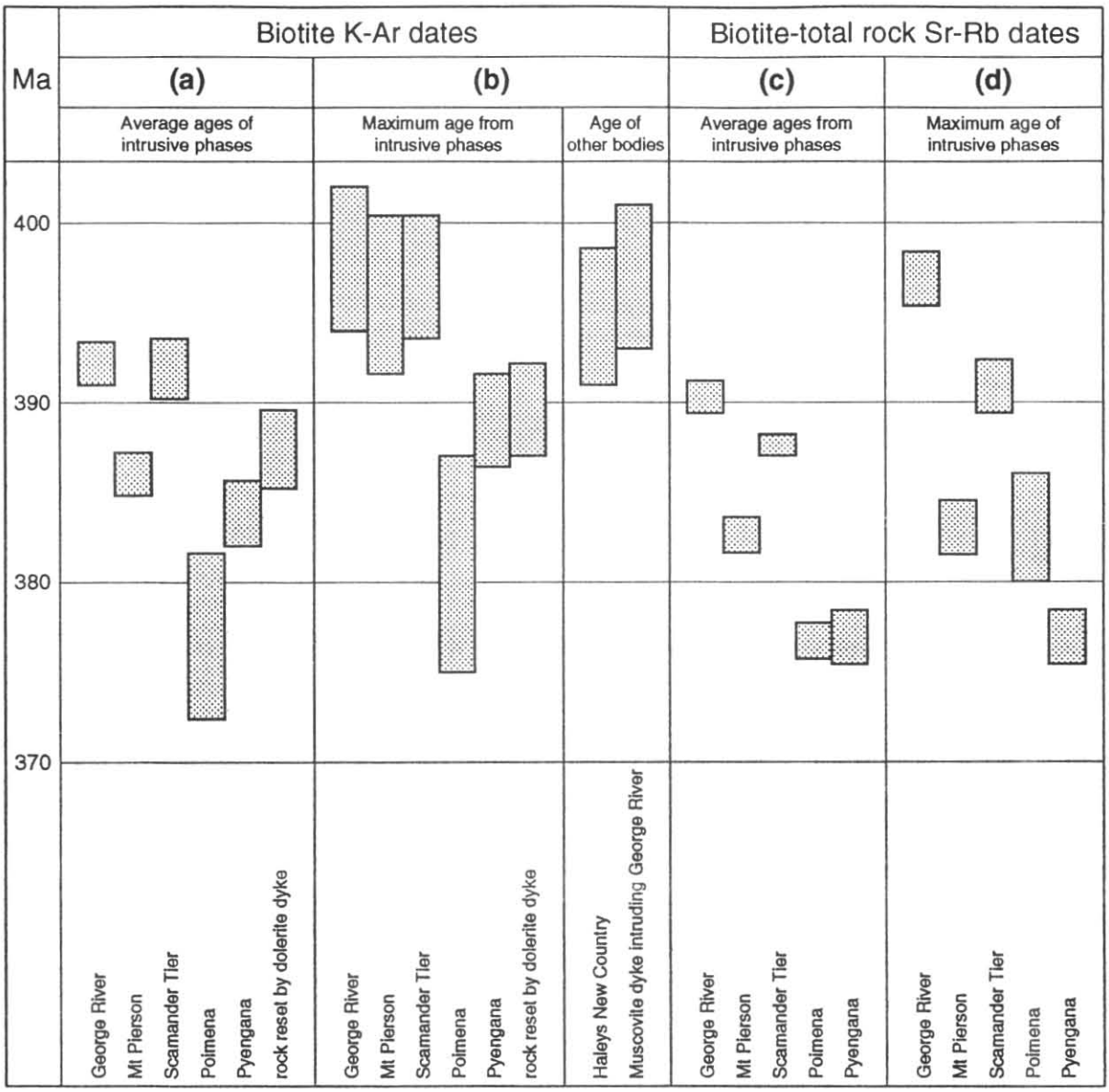

Figure 5. K-Ar and Sr-Rb dates for granitoid rocks. Error bars for 99% confidence level.

some elements. The metasomatic process has produced a large decrease in SiO_2 and a large rise in Al_2O_3 and Na_2O.

A single sample from the southern part of the coarse-grained biotite adamellite (Dbapc) in the Billy Tin Tier area plots (fig. 7) with the Scamander Tier suite rocks and may belong to that suite.

Elsewhere in the Lachlan fold belt the restite model (White and Chappell, 1977) has been used to classify granitoids into those derived from igneous source rocks (I-types) and sedimentary source rocks (S-types) (Hine *et al.*, 1978; Chappell, 1978; White and Chappell, 1983). Using the criteria of the restite model the George River and Scamander Tier suites are I-type granitoids. The presence of plagioclase with calcic core regions of approximately uniform composition surrounded by oscillatory and normal zoning has been suggested as indicating the presence of restite material (Chappell *et al.*, 1987). As the two suites contain plagioclase with distinct core zones and show approximately linear variation trends it is possible that their compositional variation was produced by restite/melt unmixing. Higgins *et al.*, (1986), however, favoured a fractional crystallisation model, based on a study of the Scamander Tier suite rocks.

The geochemistry of the coarse-grained diorite (Dbdc) bodies has been discussed by McClenaghan (1984) and will not be repeated here.

SOUTHERN PART OF ST HELENS MAP

N. J. Turner

FORM OF INTRUSIONS

Granitoids in the southern part of St Helens quadrangle comprise two, prominent, N-S trending linear bodies (fig. 8) and a number of very small bodies. Outcrop of the very small bodies is poor and their form is mainly unknown.

The prominent linear body which extends south from Scamander Tier along Skyline Tier to near Scamander is called Scamander Tier dyke. It appears to be a true dyke in that it is essentially parallel-sided and sheet-like though it is segmented at the southern end. Margins of the body are steeply-dipping and intrusive. They display narrow chilled zones but there are no readily discernible metamorphic aureoles.

The more westerly of the two prominent linear bodies extends south from Granite Knob to the southern edge of the map quadrangle. It is dyke-like and is called Catos Creek dyke but it is not a normal dyke, being strongly

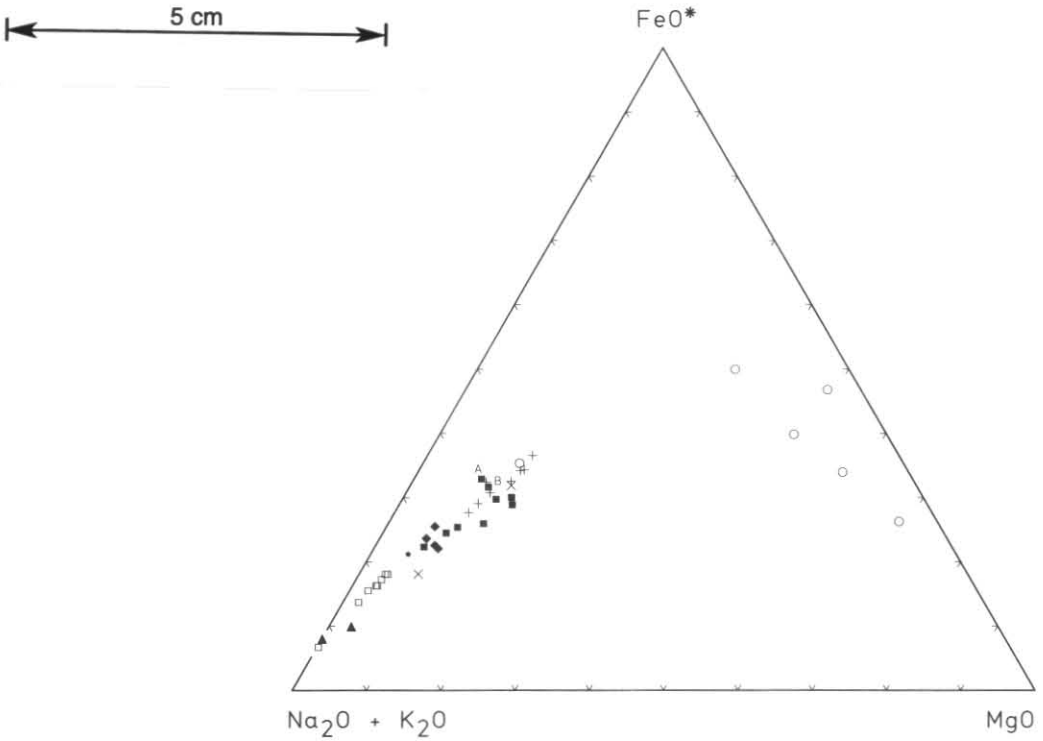

Figure 6. AFM diagram. FeO* is total iron as FeO. ○ Dbdc, ■ Dbgsp, ◇ Dbgbsp, ▲ Dba, ● Dbprc, × metasomatised Dbgsp – George River intrusive phase; □ Dbasc – Mt Pierson intrusive phase; + Dbgp, Dbr – Scamander Tier intrusive phase.

asymmetrical in a variety of ways. The steeply dipping eastern margin of the body has a chilled zone (fig. 9) but also shows evidence of fault movement and lacks a metamorphic aureole, except near EQ935150. In contrast, the western margin of the body dips moderately to steeply west, has no chilled margin, is simply intrusive and has a wide metamorphic aureole.

Catos Creek dyke is interpreted as part of the feeder to the extrusive rocks in the St Marys Porphyrite which lies south of the St Helens quadrangle and the eastern boundary of the dyke is regarded as a caldera subsidence fault (Turner *et al.*, 1986; Turner and Calver, 1987).

CATOS CREEK DYKE

Rock types

There is a dramatic change in the constituent rocks in Catos Creek dyke across the NE-trending fault which transects the dyke near Black Tommys Hill. South of the fault the dyke contains porphyritic granodiorite (Dbgp) whereas north of the fault similar hornblende-bearing porphyritic granodiorite is only present in a thin band along the eastern margin of the dyke where it is closely associated with porphyry (Dbp) which does not contain significant hornblende. Most of Catos Creek dyke north of the fault comprises coarse-grained adamellite (Dbasc) in which there are numerous microgranite intrusions.

Eastern contact of dyke

Informative sections across the eastern contact of Catos Creek dyke occur in St Helens quadrangle at EQ961072, EQ957086 (Catos Road), EQ948087 (Catos Road), EQ940122 and EQ943114. There are also important sections in St Marys quadrangle (Turner and Calver, 1987). These various sections provide evidence both of intrusion and of faulting. Elsewhere the nature of the contact is usually obscured due to poor exposure.

In all the above sections the rocks on the eastern side of the contact are thermally unmetamorphosed Mathinna Beds. At EQ957086 on Catos Road these unmetamorphosed rocks are in sharp contact with strongly thermally metamorphosed Mathinna Beds containing numerous granodiorite intrusions and thin migmatite veinlets. The sharp contact is inferred to be a fault. In the other sections the unmetamorphosed rocks are in contact with 'chilled' igneous rocks. In the immediate vicinity of these contacts the Mathinna Beds are brecciated though the amount of brecciated material may be small, as at EQ948087 and EQ943114.

At EQ940122, which is north of the fault near Black Tommys Hill, the section across the contact is well exposed in a road cutting. The Mathinna Beds 30 m from the contact are coherently bedded but they become progressively more broken by discrete fracture surfaces as the contact is approached. They are extensively but coarsely brecciated within 8 m of the contact and in a narrow (200 mm) zone at the contact the degree of comminution is extreme.

The strongly comminuted breccia in the narrow contact zone at EQ940122 contains small, highly angular fragments of Mathinna Beds mudstone and less prominent sandstone. The fragments are up to 10 mm across and are contained in a matrix of disaggregated Mathinna Beds. A minor component comprising feldspar and quartz grains of apparent igneous origin is also incorporated in the breccia. The Mathinna Beds fragments display strong alignment parallel to the contact. There appears to have been very little flattening associated with the development of the fabric in the breccia and microshears are absent. The absence of thermal metamorphism from the Mathinna Beds in the eastern part of the section and from the contact breccia is in marked contrast with the strong thermal metamorphism evident in a large (1.3 m) block of Mathinna Beds that occurs as a xenolith located 6 m inside the porphyry.

South of the fault near Black Tommys Hill there are similar contact relationships at EQ961072 though the quality of exposure is not so good. Finely comminuted breccia comprising angular fragments of Mathinna Beds

Table 10. WHOLE ROCK MAJOR AND TRACE ELEMENT ANALYSES OF ROCKS FROM THE ST HELENS MAP SHEET

Grid Ref.	EQ840330	EQ848273	FQ067132	EQ974226	FQ024292	FQ099327	FQ066310	FQ049234	FQ062258	FQ068183	FQ018283	FQ109266	FQ007256	FQ022255	FQ010266
Sample No.	MSH1	MAL7	SM5	37821	37828	37795	37796	37767	37769	37851	37768	37843	37764	37770	37766
Anal. No.	802628	802635	820333	841355	841356	841357	841358	841359	841360	841361	841362	841363	841365	841366	841367
Symbol	Dbapf	Dbgpf	SPsu	Dbasc	Dbgp	Dbgsp	Dbgsp	Dbgsp	Dbgsp	Dbgsp	Dbgsp	Dbgbsp	Dbgsp	Dba	Dbgsp
SiO_2	72.29	69.71	91.68	77.06	67.35	69.52	69.75	68.87	69.90	73.01	70.92	71.08	64.46	76.3	58.73
TiO_2	0.22	0.40	0.26	0.04	0.62	0.60	0.50	0.45	0.39	0.21	0.36	0.32	0.30	0.07	0.50
Al_2O_3	14.09	14.47	4.47	12.74	14.69	14.12	14.23	14.54	14.37	13.58	13.95	14.88	17.72	12.99	18.93
Fe_2O_3	0.33	0.90	0.07	0.28	0.33	0.13	0.29	0.49	0.37	0.17	0.33	0.16	0l67	0.12	0.59
FeO	1.41	2.62	0.27	0.36	4.06	3.58	3.19	2.86	2.86	2.01	2.52	2.16	1.98	0.84	4.21
MnO	0.03	0.06	0.01	0.02	0.08	0.06	0.06	0.09	0.07	0.04	0.05	0.04	0.10	0.06	0.23
MgO	0.45	1.29	0.41	0.03	1.67	1.03	1.18	1.62	1.68	0.64	1.41	0.81	1.13	0.31	2.03
CaO	1.04	3.04	0.01	0.56	3.98	3.03	3.36	3.69	3.46	2.31	2.91	2.74	2.56	1.05	4.47
Na_2O	2.80	1.90	0.06	3.64	2.55	2.68	2.69	2.62	2.68	2.74	2.56	3.67	6.68	3.30	4.79
K_2O	5.36	3.51	1.15	4.76	3.16	3.80	3.54	3.42	3.43	4.07	4.04	3.33	3.75	4.97	3.26
P_2O_5	0.17	0.10	0.02	0.02	0.14	0.14	0.13	0.12	0.11	0.06	0.08	0.10	0.10	0.02	0.15
SO_3	n.d.	n.d.	0.00	<0.01	<0.01	<0.01	<0.01	<0.01	<0.01	<0.01	<0.01	<0.01	<0.01	<0.01	<0.01
CO_2	0.15	0.15	0.10	0.08	0.07	0.03	0.04	0.06	0.03	0.08	0.04	0.06	0.05	0.07	0.08
H_2O^+	0.80	0.95	1.15	0.40	0.77	0.98	0.86	1.04	0.66	0.81	0.64	0.89	0.53	0.34	1.31
H_2O^-	0.22	0.31	0.00	0.07	0.04	0.06	0.02	0.04	0.03	0.02	0.02	0.02	0.03	0.04	0.03
Total	99.36	99.41	99.66	100.06	99.51	99.76	99.84	99.91	100.04	99.75	99.83	100.26	100.06	100.48	99.31
Sn	11	7	7	8	<3	4	4	5	3	0	4	8	24	14	122
Th	29	15	9	22	13	16	14	18	17	20	25	7	39	31	69
Sr	98	160	10	11	250	220	230	270	260	250	260	230	260	67	530
U	10	6	5	21	7	9	7	9	8	6	8	6	9	20	23
Rb	340	165	61	400	150	170	165	145	155	175	155	150	125	300	150
Y	19	31	14	125	33	38	37	20	21	33	11	22	15	30	25
Zr	150	140	280	80	210	195	200	140	140	130	135	130	145	66	260
Nb	11	7	4	13	9	9	10	6	8	10	8	8	7	8	17
Mo	<2	<2	<2	<2	<2	<2	<2	<2	<2	<2	<2	<2	<2	<2	<2
Ni	<3	6	<3	<3	5	3	3	6	<3	<3	5	<3	5	<3	15
Ba	480	540	260	19	620	680	660	580	560	800	1200	470	1200	155	900
Cr	<5	17	17	23	65	48	64	72	73	54	75	59	32	51	52
V	20	58	20	<3	120	78	87	95	93	40	71	46	56	12	102
Sc	<9	12	<9	<9	13	11	11	10	10	0	0	0	0	<9	<9
Pb	45	26	<4	43	15	18	16	74	16	23	15	16	14	48	31
As	14	11	<10	<10	<10	<10	<10	<10	<10	<10	<10	<10	<10	<10	<10
Bi	<5	<5	<5	5	5	5	<5	6	5	5	5	5	<5	<5	<5
Ga	19	16	5	15	16	18	16	14	15	15	11	15	13	11	17
Zn	52	56	4	52	75	70	67	130	51	29	43	49	50	25	190
Cu	10	23	9	<2	7	2	4	20	3	16	7	3	<6	4	2
Co	6	6	<6	<6	9	6	8	<6	8	<6	7	<6	7	0	6
Ce	n.d.	n.d.	n.d.	105	93	115	95	76	65	94	105	68	120	48	195
Nd	n.d.	n.d.	n.d.	30	29	37	31	17	21	32	25	19	30	8	62
La	n.d.	n.d.	n.d.	38	44	58	47	34	37	54	68	32	77	17	115
Ag	n.d.	n.d.	n.d.	<13	<13	<13	<13	<13	<13	<13	<13	<13	<13	<13	<13

Table 10. WHOLE ROCK MAJOR AND TRACE ELEMENT ANALYSES OF ROCKS FROM THE ST HELENS MAP SHEET (continued)

Grid. Ref.	FQ131283	FQ136297	FQ122291	FQ113296	FQ120320	EQ922265	EQ881164	EQ874263	EQ994255	FQ013251	EQ868199	EQ864182	EQ869197	EQ873195
Sample No.	MSH166	MSH167	MSH168	MSH170	MSH172	MSH177	MSH178	MSH181	MSH184	MSH185	MSH19	MSH20	MSH22	MSH23
Anal. No.	850175	850176	850177	850178	850179	850180	850181	850182	850183	850184	830678	830679	830680	830681
Symbol	Dbgm	Dbrpc	Dbgbsp	Dbgbsp	Ddl	Dbgp	Dbapc	Dbdc	Dbgsp	Dba	Dbdc	Dbdc	Dbda	Dbdc
SiO_2	74.25	73.08	71.29	71.49	51.99	69.63	71.40	51.96	69.86	70.95	51.87	48.8	47.20	53.97
TiO_2	0.16	0.35	0.40	0.39	1.43	0.58	0.58	1.03	0.50	0.36	0.47	0.96	0.31	0.54
Al_2O_3	14.31	13.29	14.17	14.33	14.72	13.96	12.98	9.35	13.92	13.47	10.77	17.63	6.88	12.23
Fe_2O_3	0.09	0.06	0.02	0.16	1.42	0.40	0.26	1.00	0.30	0.41	0.49	1.26	1.57	0.93
FeO	0.69	2.03	2.44	2.21	8.07	3.21	3.36	10.22	2.98	2.41	8.40	8.80	7.29	7.63
MnO	0.03	0.06	0.07	0.06	0.19	0.08	0.08	0.29	0.09	0.07	0.17	0.20	0.15	0.15
MgO	0.00	0.49	0.63	0.63	7.02	1.08	1.30	11.49	1.39	1.07	14.81	6.73	22.58	10.04
CaO	0.50	2.04	2.63	2.55	7.99	3.27	2.94	11.74	3.19	2.52	8.33	9.97	8.52	9.05
Na_2O	3.90	3.06	3.86	3.68	2.67	2.80	2.03	0.49	2.58	2.8	0.66	1.31	0.55	0.93
K_2O	4.77	4.05	2.65	3.22	1.21	3.44	3.12	0.37	3.67	4.27	1.45	1.53	0.92	1.53
P_2O_5	0.29	0.11	0.14	0.14	0.31	0.13	0.15	0.20	0.11	0.10	0.16	0.20	0.21	0.15
SO_3	0.19	0.08	0.08	0.09	0.37	0.08	0.09	0.09	0.08	0.08	0.08	0.07	0.3	0.39
CO_2	0.06	0.07	0.14	0.10	0.22	0.02	0.16	0.02	0.02	0.01	0.11	0.05	0.15	0.08
H_2O^+	0.83	0.76	1.12	0.89	2.50	0.75	1.38	1.94	0.74	0.71	2.23	2.12	2.03	2.02
H_2O^-	n.d.	n.d.	n.d.	n.d.	n.d.	n.d.	n.d.	n.d.	n.d.	n.d.	0.09	0.10	0.09	0.09
Total	100.07	99.53	99.64	99.94	100.11	99.43	99.83	100.19	99.43	99.33	100.09	99.73	98.75	99.73
Sn	18	<4	8	6	<4	4	<4	7	<4	<4	<3	5	<3	<3
Th	<4	15	9	9	5	11	15	<4	32	34	10	10	9	8
Sr	37	155	220	220	280	220	145	185	245	195	300	420	370	190
U	13	8	7	7	6	6	7	<5	7	11	2	2	2	4
Rb	270	210	155	150	67	155	130	17	150	175	59	61	30	74
Y	6	28	19	19	33	31	30	19	17	12	13	18	11	13
Zr	36	140	125	115	145	180	160	120	120	115	52	78	53	74
Nb	14	11	10	11	7	10	8	5	11	9	<3	<3	<3	<3
Mo	<2	<2	<2	<2	<2	<2	<2	<2	<2	<2	<2	<2	<2	<2
Ni	<3	<3	<3	<3	130	4	3	8	3	<3	120	12	280	18
Ba	115	400	360	420	290	580	620	105	580	480	420	400	430	200
Cr	92	92	99	89	330	110	130	630	130	100	1050	64	2100	390
V	3	27	36	33	230	65	68	370	65	48	185	290	145	220
Sc	<7	<7	8	5	23	9	13	80	11	<7	33	40	34	37
Pb	49	34	26	29	17	26	26	21	29	37	7	<4	<4	<4
As	<10	<10	<10	<10	<10	<10	<10	<10	<10	<10	62	18	<10	<10
Bi	7	<5	<5	<5	<5	<5	<5	<5	<5	<5	<5	<5	<5	<5
Ga	17	15	16	16	17	18	17	11	13	12	13	17	6	13
Zn	34	40	54	47	97	59	59	125	55	41	90	105	73	91
Cu	16	<3	<3	<3	31	<3	4	<3	<3	<3	15	15	29	19
Co	4	8	6	5	40	13	11	37	11	10	48	34	64	33
Ce	14	73	57	51	31	90	79	0	105	89	n.d.	n.d.	n.d.	n.d.
Nd	12	34	31	23	27	38	48	6	50	35	n.d.	n.d.	n.d.	n.d.
La	<9	37	25	28	9	51	41	<9	58	44	n.d.	n.d.	n.d.	n.d.
Ag	<8	<8	<8	<8	<8	<8	<8	<8	<13	<13	n.d.	n.d.	n.d.	n.d.

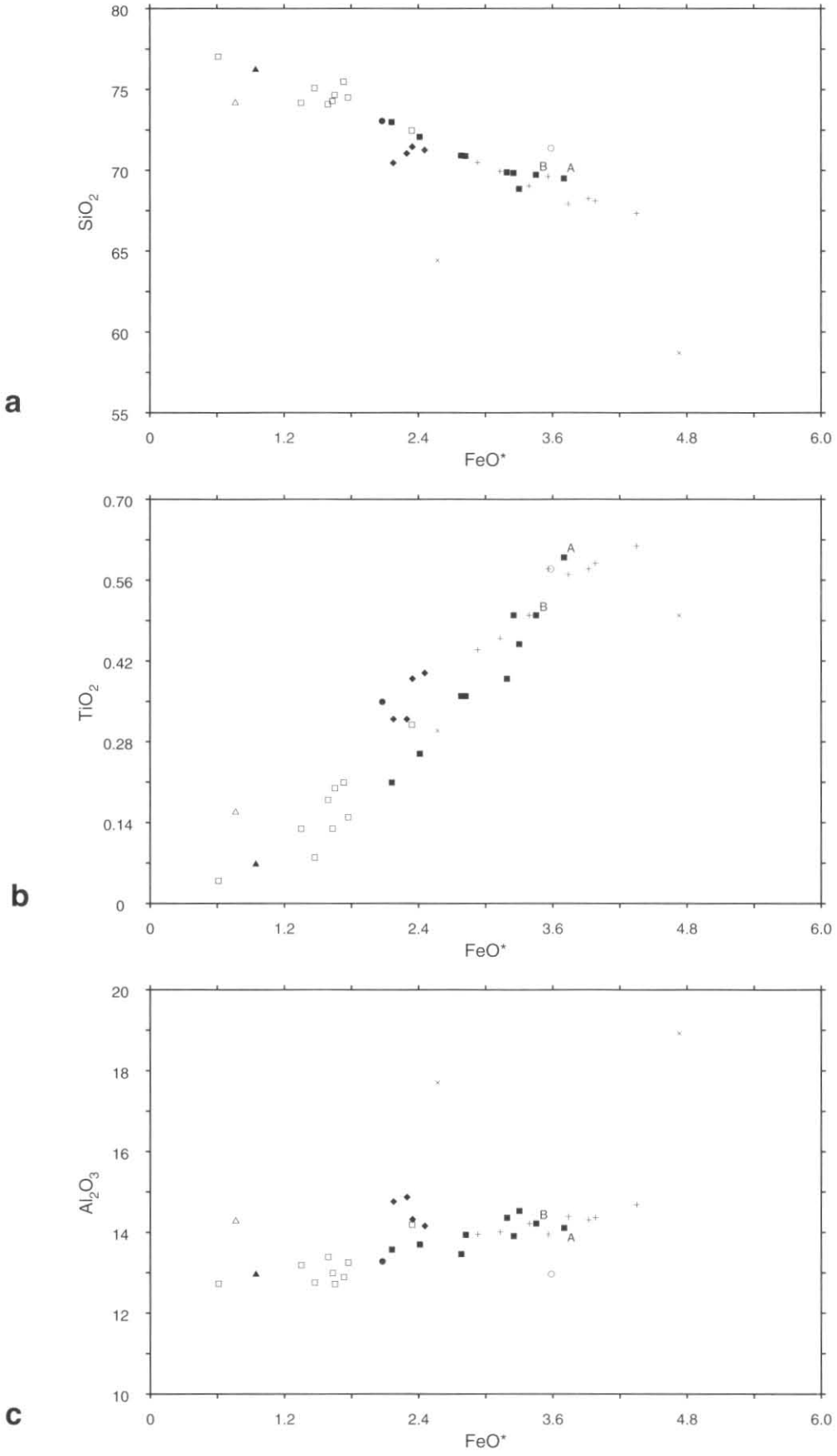

Figure 7a–c. Plots of major and trace elements against total iron as FeO (FeO*) for granitoid rocks from the St Helens map sheet and some associated rocks from the Blue Tier and St Marys map sheets.

○ Dbdc, ■ Dbgsp, ◇ Dbgbsp, ▲ Dba, ● Dbprc, × metasomatised Dbgsp – George River intrusive phase; □ Dbasc – Mt Pierson intrusive phase; + Dbgp, Dpr (St Marys map sheet) – Scamander Tier intrusive phase.

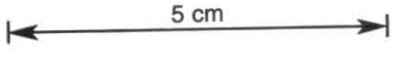

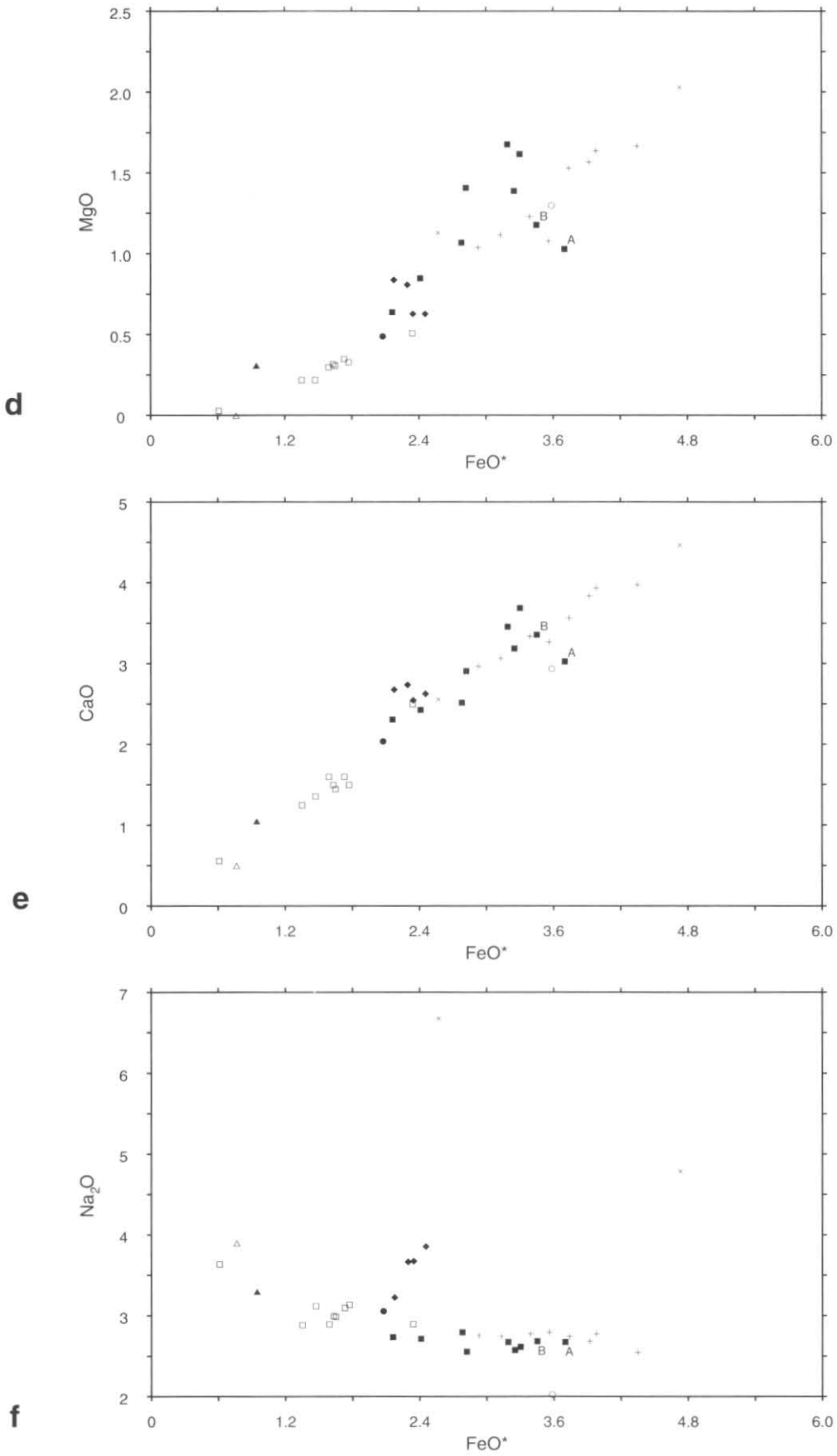

Figure 7d–f. Plots of major and trace elements against total iron as FeO (FeO*) for granitoid rocks from the St Helens map sheet and some associated rocks from the Blue Tier and St Marys map sheets.

○ Dbdc, ■ Dbgsp, ◇ Dbgbsp, ▲ Dba, ● Dbprc, × metasomatised Dbgsp – George River intrusive phase; □ Dbasc – Mt Pierson intrusive phase; + Dbgp, Dpr (St Marys map sheet) – Scamander Tier intrusive phase.

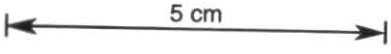

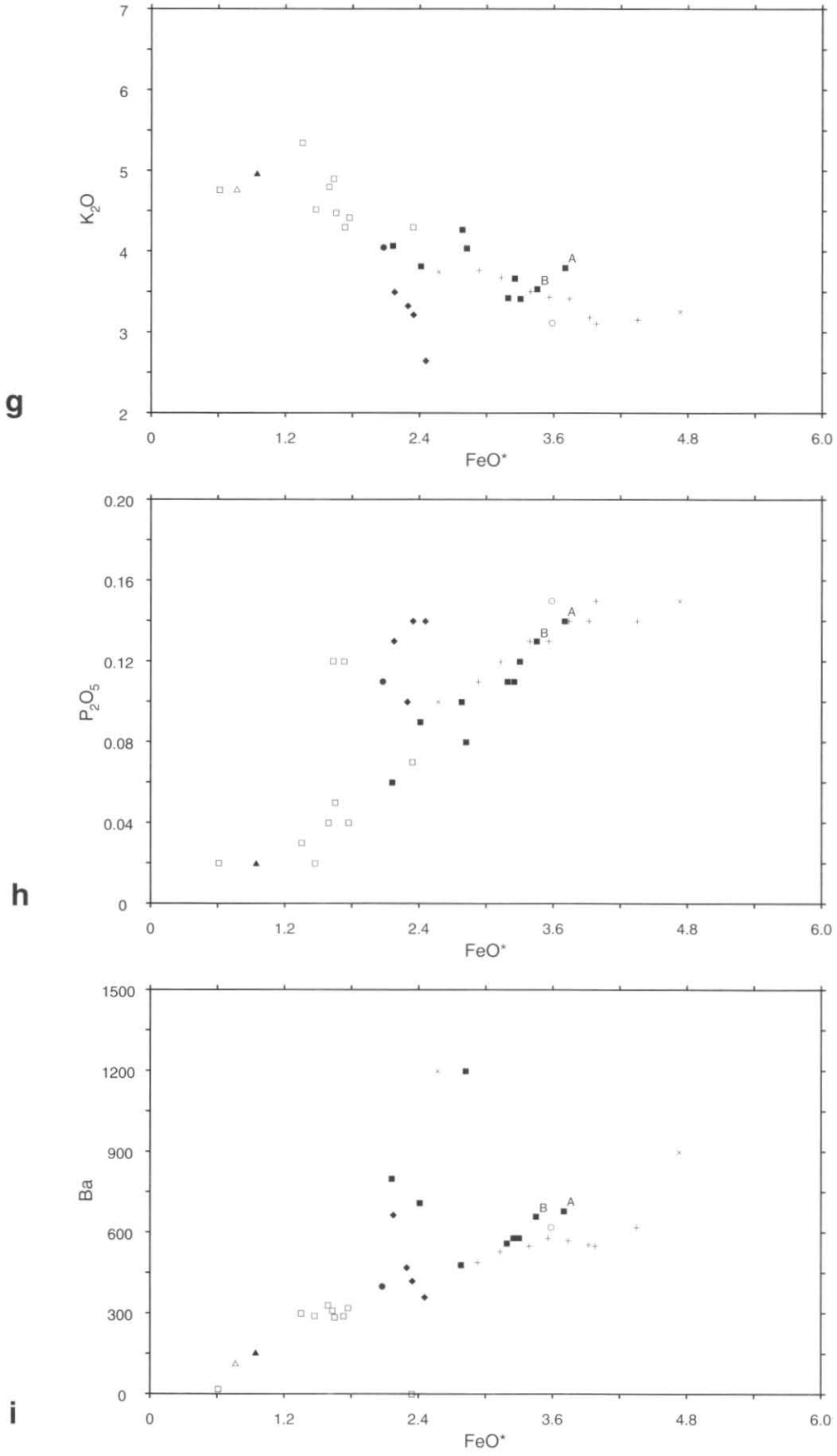

Figure 7g–i. Plots of major and trace elements against total iron as FeO (FeO*) for granitoid rocks from the St Helens map sheet and some associated rocks from the Blue Tier and St Marys map sheets.

○ Dbdc, ■ Dbgsp, ◇ Dbgbsp, ▲ Dba, ● Dbprc, × metasomatised Dbgsp – George River intrusive phase;
□ Dbasc – Mt Pierson intrusive phase; + Dbgp, Dpr (St Marys map sheet) – Scamander Tier intrusive phase.

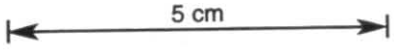

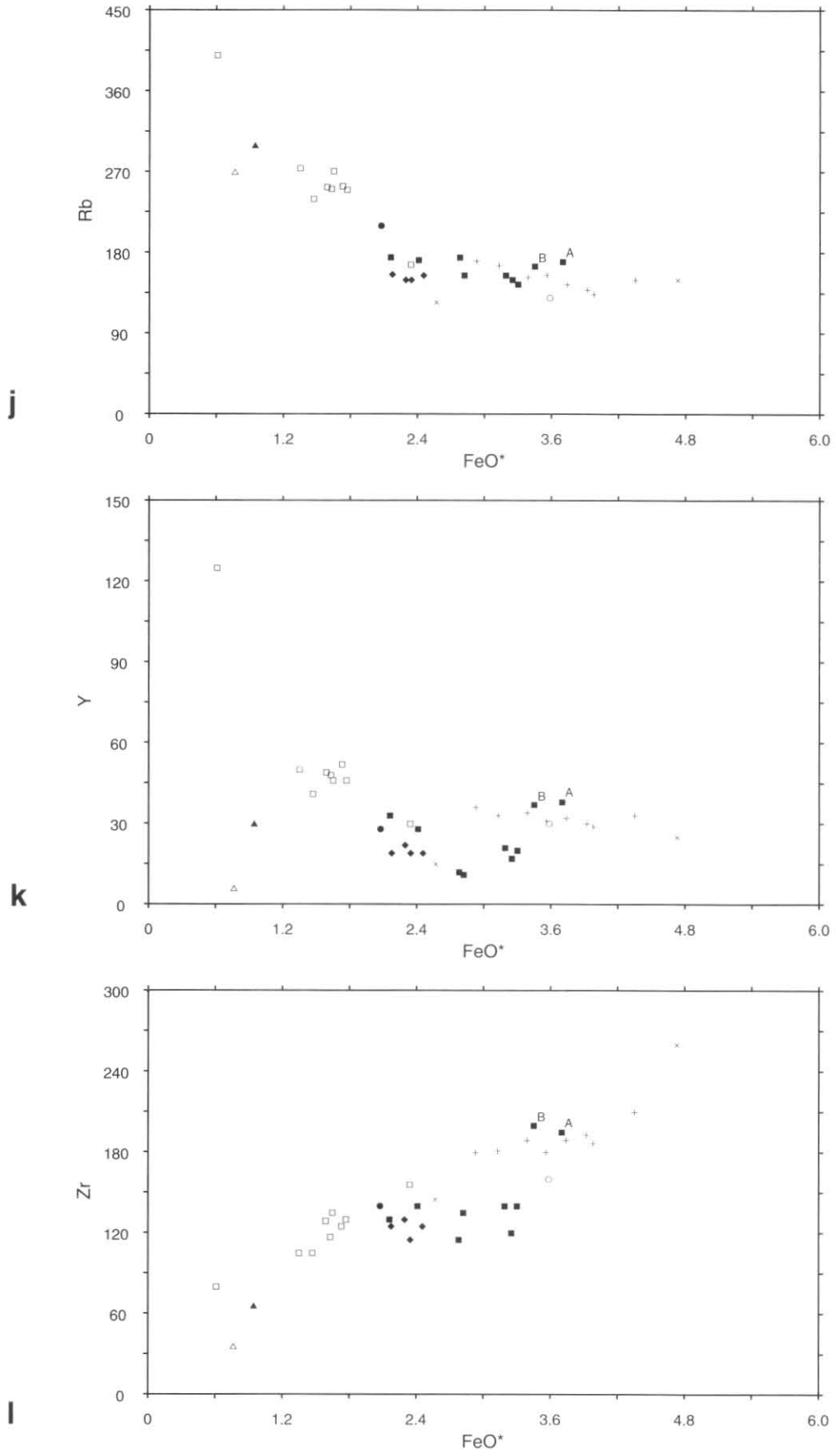

Figure 7j–l. Plots of major and trace elements against total iron as FeO (FeO*) for granitoid rocks from the St Helens map sheet and some associated rocks from the Blue Tier and St Marys map sheets.

○ Dbdc, ■ Dbgsp, ◇ Dbgbsp, ▲ Dba, ● Dbprc, × metasomatised Dbgsp – George River intrusive phase; □ Dbasc – Mt Pierson intrusive phase; + Dbgp, Dpr (St Marys map sheet) – Scamander Tier intrusive phase.

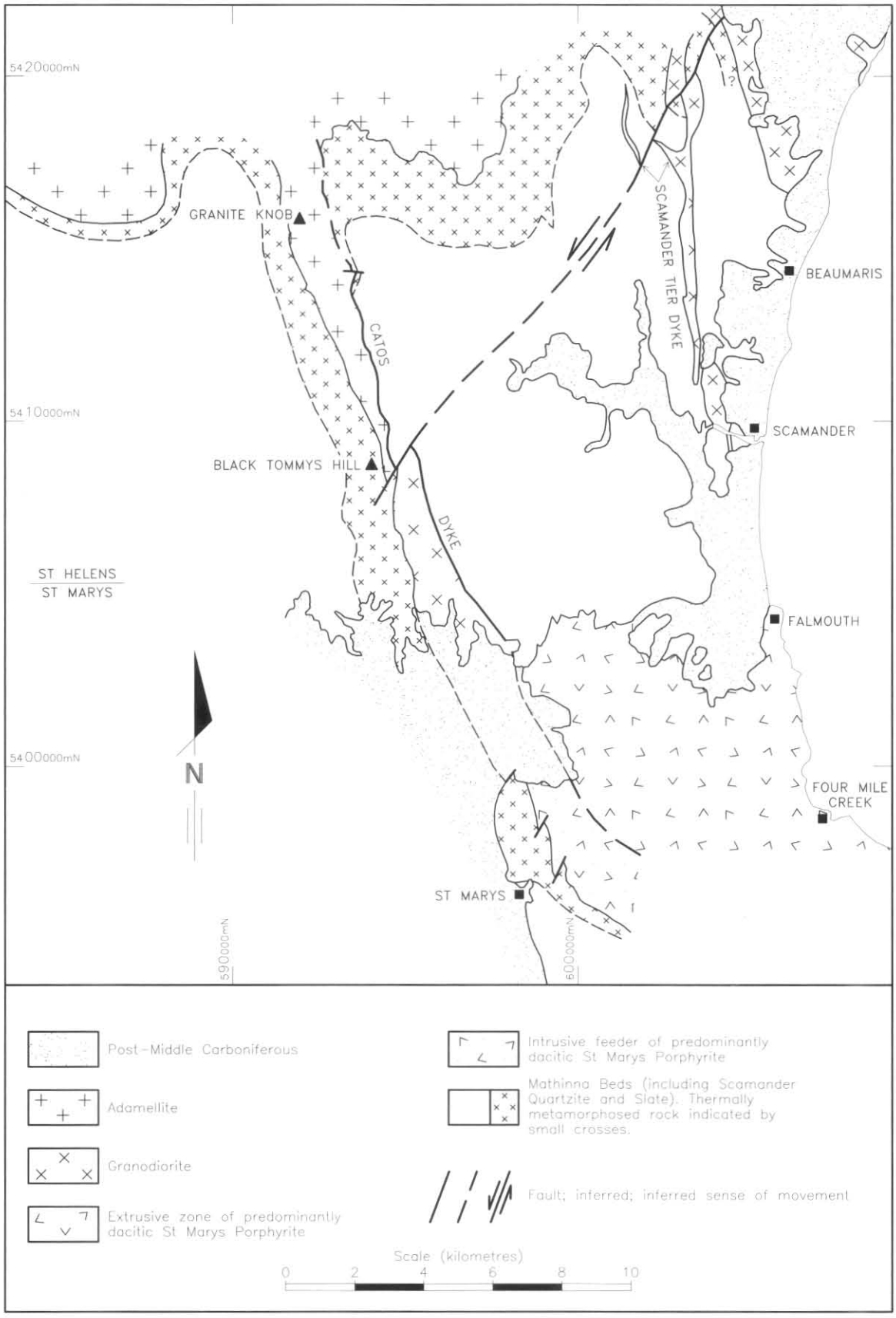

Figure 8. Simplified geology of the southern part of St Helens quadrangle and the northern part of St Marys quadrangle. The latter is from Turner, Calver, Castleden and Baillie (1984).

5 cm

mudstone and sandstone is exposed 2.5 m from the contact. The breccia does not appear to contain igneous material and is mostly poorly foliated. However, slivers of breccia within the igneous material at the contact are aligned parallel to a biotite foliation in the igneous material and the breccia in the slivers contains admixed grains of igneous origin.

The igneous material at the contact at EQ961072 has been strongly 'chilled', probably to the extent of the groundmass being glassy since the present texture is similar to 'snowflake' texture, an early stage of glass recrystallisation. There is a progressive increase in the grain size of the groundmass with distance from the contact (fig. 9) and it appears that an interval between 15 m and 50 m wide was subject to relatively rapid cooling.

Petrography of granodiorite (Dbgp)

The granodiorite in Catos Creek dyke is porphyritic microgranodiorite which shows considerable variation in groundmass grain size (fig. 9). From the chilled eastern margin the quartz, potash feldspar and minor biotite which comprise most of the groundmass increase markedly in grain size towards the centre of the body then decrease less markedly towards the western contact. With increasing grain size the potash feldspar tends to coalesce and become intergranular to the other minerals.

Phenocrysts in the chilled rocks in the immediate vicinity of the eastern contact at EQ961072 are relatively small (up to 4 mm) and comprise subhedral to euhedral quartz, strongly zoned plagioclase and biotite with common anhedral potash feldspar. The quartz phenocrysts have smoothly rounded margins and are usually strongly embayed. At about one metre from the contact the phenocryst grain size is greater, ranging up to about 10 mm. Potash feldspar is less common here than in the contact rocks and amphibole, which is not in the contact rocks, is present.

The relatively high proportion of potash feldspar phenocrysts in the contact rocks at EQ961072 suggests that the modal composition is probably rhyolitic/granitic. In comparison, the sparseness of potash feldspar phenocrysts in rocks one metre from the contact along with the presence of amphibole suggests a dacitic/granodioritic modal composition. Table 11 shows a marginal granitic/granodioritic modal composition for 'chilled' material collected 7 m from the eastern contact of Catos Creek dyke on Catos Rd at EQ948087. Chemically the rock is granodioritic (table 12) as is coarser grained material from EQ952076 which is near the centre of the dyke.

The granodioritic part of Catos Creek dyke is petrographically fairly uniform, apart from the grain size variations. Quartz phenocrysts tend to be rounded and 'globular' throughout the granodiorite but the smoothly rounded grain margins which are a feature of quartz phenocrysts in the chilled margin become progressively more pitted and irregular as the groundmass grain-size increases. Plagioclase is abundant and grains are strongly zoned, usually with the cores replaced by muscovite. Potash feldspar phenocrysts vary considerably in form. In the chilled margin the phenocrysts are much the same size as phenocrysts of other mineral species. However, beyond this zone potash feldspar may occur as sparse, large phenocrysts up to 30 mm across with numerous quartz and biotite inclusions.

Rare orthopyroxene and clinopyroxene occur in the dyke but all grains are partially altered to amphibole. Pyroxene is most common in 'chilled' granodioritic rocks near the eastern contact where the grains have rims of colourless, fibrous amphibole which, in turn, have thin rims of hornblende. In the central part of the dyke a little clinopyroxene is present as cores in hornblende laths and a little fibrous amphibole is similarly preserved. Many amphibole grains which consist entirely of hornblende have inhomogeneously coloured cores which strongly indicate a mineralogically different precursor.

Though hornblende occurs as laths which are conspicuous in hand specimen, much hornblende occurs as roughly equidimensional grains in inclusions (microxenoliths) together with biotite and a little calcic plagioclase. These inclusions resemble the noritic inclusions which occur in the St Marys Porphyrite (Higgins *et al.*, 1986) except that alteration of pyroxene to amphibole is very extensive. Only a small proportion of the total biotite in the granodiorite occurs in inclusions. Most occurs as individual grains either in the groundmass or as phenocrysts.

Accessory minerals in the granodiorite include green chlorite after biotite and muscovite after plagioclase cores. A little calcite, epidote and colourless chlorite are present in some rocks. Pyroxene occurs as inclusions in some plagioclase grains and zircon, apatite and opaque minerals may form inclusions in biotite grains.

Metasedimentary xenoliths are sparsely disseminated in the granodiorite and appear to represent hornfelsed Mathinna Beds and quartz veins. Igneous xenoliths are fairly common in places and can be quite large, up to several metres across (e.g. near EQ953076). These raft-like xenoliths may themselves contain igneous and metasedimentary xenoliths. In general the shapes of xenoliths are highly variable and little evidence of regional alignment was found. The igneous xenoliths are usually porphyritic and tend to be finer grained and more mafic than their host granodiorite. The large raft near EQ953076 is quartz diorite consisting of fibrous amphibole, relict orthopyroxene, biotite and chlorite along with abundant laths of plagioclase and subordinate quartz and potash feldspar. In places (e.g. near EQ943114) there are patches of very coarse-grained material rich in tabular, aligned megacrysts of potash feldspar and containing globular quartz, biotite and rare hornblende. Patches (?rafts) of this type were only recognised north of the fault near Black Tommys Hill. Similar patches occur in Scamander Tier dyke.

Table 11. MODAL ANALYSES BASED ON POINT COUNTING OF SINGLE THIN SECTIONS STAINED FOR POTASSIUM

Intrusion	Catos Creek	Scamander Tier
Position	'chilled' margin	central
Field No.	NM 140	NM 137
Reg. No.	83/22	83/21
AMG	EQ948087	FQ036153
Quartz	8.8 (20.7)	16.6 (13.5)
Plagioclase	34.9 (0.5)	37.0 (2.4)
Altered plagioclase cores (muscovite)	0.3	2.9
K-feldspar	3.7 (14.2)	3 (14)
Biotite	5.8 (5.9)	5.5
Pyroxene	0.9	
Hornblende	2.3	2.8
Chlorite	1.9	2.2
Total groundmass	40.6	29.9
Counts	787	945

Numbers within parentheses represent the amount of the mineral in groundmass.

Chemistry and age of granodiorite

Chemical analyses of two samples of granodiorite are given in Table 12. Sample 83/22 is from north of the fault near Black Tommys Hill whilst sample 83/23 is from south of the fault. Sample 83/22 was collected 7 m from the eastern contact of the dyke on Catos Road and is a fine-grained ('chilled') rock whereas sample 83/23 is

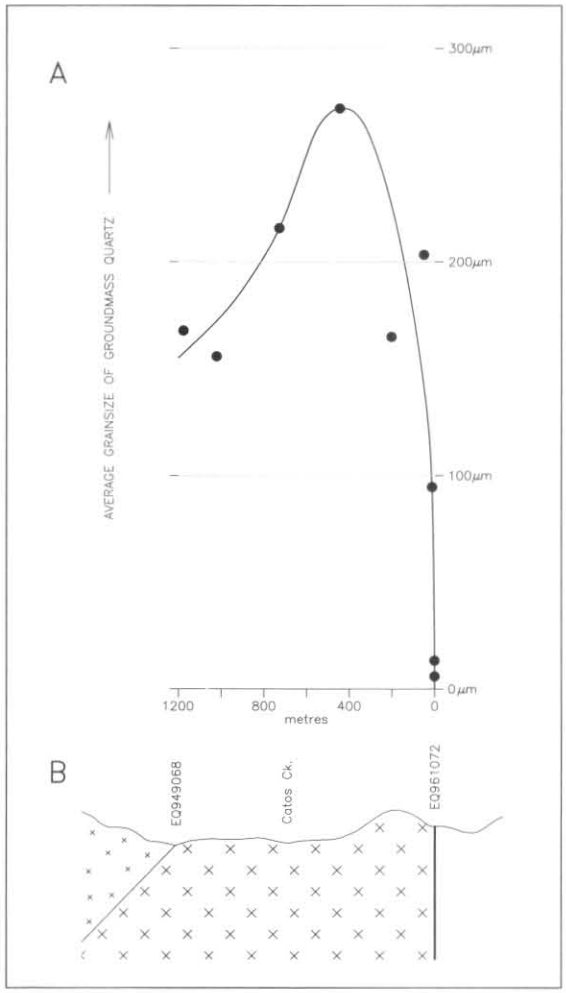

Figure 9. A: Variation in average grain size of groundmass quartz grains across Catos Creek dyke. Average determined by measuring 60 grains in one thin section of each sample. Measurements by Paul Geissler. Samples collected at 0, 1, 15, 60, 220, 440, 740, 1040, 1200 m from the eastern contact.
B: Corresponding geological cross section – the unornamented part represents unmetamorphosed Mathinna Beds, small cross overprint is metamorphosed Mathinna Beds, cross overprint is granodiorite. The eastern contact of the granodiorite is an inferred caldera subsidence fault, the western contact is simply intrusive.

coarser grained material from a fairly central position in the dyke.

Major and trace elements in the two samples are very similar as are the rare earth element, or REE, patterns (fig. 10). The REE patterns are very similar to patterns in the St Marys Porphyrite and in granodiorite in Scamander Tier dyke (Turner *et al.*, 1986) as well as granodiorite in plutons elsewhere in the Blue Tier Batholith (Higgins *et al.*, 1986) thus providing strong evidence of a common parent magma for the various bodies.

Rb-Sr and K-Ar isotopic studies (Turner *et al.*, 1986) of Catos Creek dyke, Scamander Tier dyke and the St Marys Porphyrite indicate that the precise age of 388±1 Ma is shared by all three bodies. In the case of Catos Creek dyke the results were obtained from sample 83/22 and comprised biotite-total rock isochrons of 387 Ma and 388 Ma.

Quartz feldspar porphyry (Dbp)

Two types of porphyry extend along the eastern edge of Catos Creek dyke, to the north of the fault near Black Tommys Hill. Closest to the eastern contact and extending north to near EQ936143 is the narrow band of porphyritic microgranodiorite (Dbgp) which is grouped with granodiorite south of the fault. West of this band there is another narrow band of porphyry which extends north past EQ936143. Both bands of porphyry appear to be discontinuous in places.

The quartz-feldspar porphyry in the inner band resembles the porphyritic microgranodiorite but does not contain hornblende. Unlike the microgranodiorite it contains numerous orthoclase megacrysts in places and these may display strong, local alignment parallel to the trend of the dyke. The microtexture of the quartz-feldspar porphyry is similar to that of the microgranodiorite, particularly with the anhedral to subhedral quartz grains having smoothly rounded, embayed margins. Similar also are the strongly zoned, partially sericitised plagioclase phenocrysts. However, biotite is the only ferromagnesian mineral except for a little secondary chlorite. Neither pyroxene nor hornblende are present. Zircon is an accessory mineral.

Biotite occurs as a phenocryst phase. It also occurs in the groundmass along with quartz and feldspar. The average grain size of the groundmass is less than one millimetre.

Table 12. CHEMICAL ANALYSES OF GRANODIORITIC MATERIAL FROM SCAMANDER TIER DYKE AND CATOS CREEK DYKE

Intrusion	Scamander Tier	Catos Creek	Catos Creek
Position	central	'chilled' margin	central
Field No.	NM137	NM140	NH31
Reg. No.	83/21	83/22	83/23
AMG	FQ036153	EQ948087	EQ952076
SiO_2	67.11	67.81	68.76
TiO_2	0.60	0.61	0.53
Al_2O_3	14.71	14.66	14.34
Tot Fe*	4.55	4.50	4.08
MnO	0.08	0.07	0.07
MgO	1.56	1.63	1.51
CaO	3.62	3.70	3.23
Na_2O	2.79	2.76	2.81
K_2O	3.33	3.24	3.41
P_2O_5	0.17	0.16	0.14
LOI	1.89	1.57	1.48
Total	100.41	100.71	100.36
Ag	<4	<4	n.d.
Sb	<5	<5	n.d.
Sn	18 (17)	16 (12)	4
Th	14	18	n.d.
Sr	250	250	251
U	6	6	n.d.
Rb	150	145	155
Y	33	33	30
Zr	210	190	181
Nb	8	8	10
Mo	<2	<2	n.d.
Pb	17	22	n.d.
As	22	18	n.d.
Bi	<5	<5	n.d.
Ga	16	15	n.d.
Zn	59	57	n.d.
Cu	<6	10	n.d.
Ni	5	5	n.d.
Sc	15	15	15
V	67	64	n.d.
Cr	23	24	n.d.
Co	6	<5	n.d.
Ba	680	610	614

Analyses of 83/21 and 83/22 are by the Department of Mines; analysis of 83/23 is by the University of Tasmania. Tin values shown in parentheses are repeat analyses by the University of Tasmania.

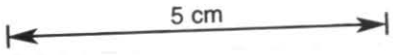

Coarse-grained adamellite (Dbasc)

North of the fault near Black Tommys Hill most of Catos Creek dyke is occupied by very coarse grained adamellite which is not present south of the fault. The age relationships of the adamellite and the much finer grained porphyritic rocks which occur along the eastern margin of the dyke were not clearly established. Patches (?rafts) of very coarse-grained adamellite occur in the porphyritic rocks which may indicate that the adamellite is older. Also, the adamellite locally displays a high degree of deformation that the porphyritic rocks do not appear to have experienced. Thus, on present evidence it seems that the adamellite is older.

Minerals comprising the adamellite include perthitic orthoclase, quartz, plagioclase and fairly minor biotite. Orthoclase is abundant and is very coarse grained with crystals exceeding 20 mm in length. The crystals may be either anhedral or tabular euhedral and they contain inclusions of biotite and quartz. Plagioclase is usually anhedral and displays zoning though the zoning is not as marked as it is in the plagioclase phenocrysts in the porphyritic rocks. Partial replacement of the plagioclase grains by muscovite is common and some muscovite grains are quite large. Biotite is generally fresh with only very minor alteration to chlorite.

Strain related features are conspicuous in the adamellite. In thin section grains of all minerals display undulose extinction. Quartz has been extensively annealed such that it occurs as relatively fine-grained patches which contain coarser remnant grains. Similarly, there are two populations of biotite grains. Earlier, coarser grains are extensively kinked and are largely overgrown and replaced by much finer grains. As a result biotite mostly occurs as fine-grained patches, the shapes of which are controlled by the boundaries of adjacent felsic grains. Most biotite patches have an irregular lenticular form.

In outcrop the strain in the adamellite is expressed as a variably developed, steeply dipping foliation which trends parallel to the trend of the dyke. The foliation is defined by alignment of elongate patches of felsic minerals and biotite and by alignment of orthoclase crystals. At Catos Road the foliation is particularly intense.

Small intrusions in Dbasc

There are numerous small intrusions within the very coarse-grained adamellite in Catos Creek dyke. They contain cream to yellowish granitoids which become pinkish when slightly weathered. Few similar intrusions are present in the porphyritic rocks.

The light coloured granitoids vary considerably in their petrography. Most are fine-grained or medium-grained but coarse-grained material may form thin bands within material of lesser grain size. Some rocks are sparsely porphyritic in orthoclase and globular quartz whilst others are even grained and a few are seriate. Ferromagnesian minerals are a minor constituent in all rocks. In most cases the ferromagnesian mineral is brown biotite whilst in some cases it is green biotite. There are rare, small segregations of well crystallised smoky quartz such as occur near EQ943105. Muscovite is present in some rocks but not in others.

An unusual rock occurs in a small intrusion at the western contact of Dbasc in the Avenue River. It is seriate with fine average grain size and consists of quartz, orthoclase, plagioclase, muscovite, euhedral garnet and green biotite. Some biotite grains are chloritised. The largest orthoclase grains are perthitic and rich in inclusions of quartz, plagioclase and muscovite. The rock is unusual because it contains garnet.

SCAMANDER TIER DYKE

Setting

Unlike Catos Creek dyke, Scamander Tier dyke is fairly symmetrical in cross section. Both its western and eastern contacts are steeply dipping, intrusive and have narrow 'chilled' margins associated with them. There is little evidence of thermal metamorphism in the Mathinna Beds adjacent to the dyke. However, none of the fault associated features which are related to the absence of metamorphism along the eastern edge of Catos Creek dyke was found in the tract south of FQ037200.

North of FQ037200 there is apparent displacement of older features across the dyke which implies that the dyke was emplaced in a fault (McClenaghan, this volume). Whether or not igneous intrusion was contemporaneous with faulting has not been established. However, the apparent absence of breccias similar to those at the eastern edge of Catos Creek dyke suggests that it was not. Scamander Tier dyke's lack of thermal metamorphic aureoles is attributed to the relatively small volume of igneous material in the dyke and to the subvertical attitude of the contacts.

Petrography of granodiorite

The granodiorite in Scamander Tier dyke is porphyritic microgranodiorite similar to the granodiorite in Catos Creek dyke though the groundmass is of coarser grain size. Quartz grains in the groundmass range from an estimated average size of 72 μm in the chilled margins to an estimated average size of 500 μm in the central part of the dyke. Orthoclase grains coalesce as the groundmass grain size increases and the mineral becomes intergranular to other minerals in the groundmass.

In order of abundance (table 11) phenocrysts in the granodiorite comprise plagioclase, quartz, biotite, hornblende and orthoclase. Plagioclase phenocrysts are strongly zoned and tend to be subhedral and euhedral. They may contain clinopyroxene inclusions and are commonly partially sericitised. Quartz phenocrysts are usually rounded and embayed due to resorption. They have a globular form in hand specimen. Quartz in the groundmass is anhedral. Most biotite occurs as individual flakes, both as phenocrysts and in the groundmass, and the flakes may be partially chloritised. Some biotite occurs with hornblende in rare microxenoliths similar to those in Catos Creek dyke. Hornblende usually occurs as individual grains which may be either subhedral laths up to 15 mm long or anhedral. Though no relict pyroxene was found in the hornblende, some grains have differently coloured cores which suggest replacement of a pre-existing mineral.

Orthoclase megacrysts vary in abundance but are more common in Scamander Tier dyke than they are in the granodiorite in Catos Creek dyke. Some megacrysts are conspicuously perthitic in hand specimen whereas others appear uniform. Biotite inclusions are numerous in some megacrysts. In places (e.g. near FQ036153) there are thin layers rich in megacrysts. These megacrysts are well aligned parallel to the layers whereas megacrysts outside the layers are not aligned. The megacrystic layers at FQ036153 are associated with other thin equigranular layers defined by variation in biotite content and with less regular patches of equigranular diorite. Remnant clinopyroxene is common within hornblende grains in the diorite which consists mostly of plagioclase with about 20% by volume of hornblende and pyroxene with no biotite. Relatively large patches of material rich in strongly aligned megacrysts occur in the dyke at Scamander Tier [e.g. FQ036192]. The patches are apparently rafts and resemble patches which occur in Catos Creek dyke.

Sparse xenoliths of hornfelsed Mathinna Beds up to one metre across are present in Scamander Tier dyke as well as small xenoliths of mafic granitoid. Rare examples of the latter display a strong planar/linear cataclastic fabric defined by lenticules of fine-grained biotite and hornblende in fine-grained quartz and feldspar.

Near Scamander the granodiorite shows varying degrees of hydrothermal alteration and there are small fracture controlled sulphide deposits containing silver, lead, zinc and copper. In altered granodiorite from the Scamander mine plagioclase is partially sericitised and contains clinozoisite granules. Hornblende is partially replaced by ?actinolite, calcite and epidote. Biotite is almost completely replaced by chlorite, epidote and opaque mineral. At the eastern contact on the north side of the Scamander River plagioclase is even more extensively replaced by relatively coarse-grained muscovite and calcite is more abundant. At the Beulah South mine plagioclase is totally sericitised and biotite is replaced by muscovite and opaque mineral.

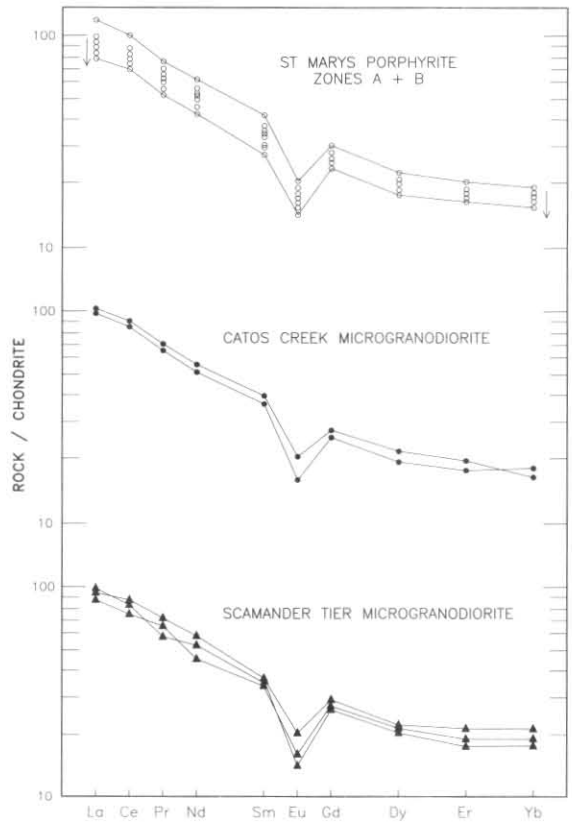

Figure 10. Chondrite normalised REE plots for the St Marys Porphyrite, the Catos Creek microgranodiorite and the Scamander Tier microgranodiorite. Arrows indicate increasing SiO_2 in the St Marys Porphyrite. Data prepared by Higgins in Turner, Black and Higgins, 1986.

Chemistry and age of granodiorite

Major, trace and rare earths elements in granodiorite in Scamander Tier dyke closely match those in Catos Creek dyke (table 12, fig. 10) which indicates a common parent magma. Rb-Sr isotopic studies are consistent in that they show that the ages of granodiorite in the two dykes are indistinguishable. Isotopic data for Scamander Tier dyke was derived from sample 83/21 and comprised a biotite/total rock isochron of 386 Ma and an internal mineral isochron of 386±5 Ma (Turner *et al.*, 1986).

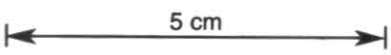

OTHER INTRUSIONS

Granodiorite (Dbgsp) *and diorite* (?Dbdc)

Granodiorite which outcrops around Georges Bay extends south past Dianas Basin and very small, isolated exposures of similar rocks occur further south. The metamorphic aureole associated with the southern part of the main granodiorite mass was not satisfactorily mapped due to the paucity of pelitic material in the poor exposures of Mathinna Beds along the contact.

Around FQ091204 the main granodiorite is medium to coarse grained and fairly equigranular. It consists of plagioclase, quartz, biotite, hornblende and minor orthoclase. Plagioclase grains are subhedral to euhedral, strongly zoned and partially sericitised whilst quartz grains are anhedral and contain numerous plagioclase inclusions. Both biotite and hornblende occur as individual grains but mostly they occur in clusters of grains which resemble the microxenoliths in Catos Creek dyke and Scamander Tier dyke. Some hornblende grains have inhomogeneous cores which suggest a mineralogically different precursor.

Along its western and southern margin the granodiorite is finer grained and tends to be porphyritic. Relatively large, zoned plagioclase phenocrysts together with mainly monocrystalline phenocrysts of hornblende and biotite occur in a groundmass of poikilitic quartz and feldspar.

The small exposures of granodioritic rocks which are isolated from the main mass are also relatively fine grained and porphyritic. In the small intrusion on the coast at FQ089199 there are abundant phenocrysts of cloudy, altered plagioclase which are overgrown by small epidote grains. There are also sparse, rounded and embayed quartz phenocrysts and hornblende phenocrysts. No biotite is present though uncommon chlorite patches surrounded by rims of tremolite/ actinolite may be after biotite. Further north, near the main granodiorite contact, there are small bodies of unusual rocks consisting of quartz, zoned plagioclase, biotite and chlorite which are said to represent mixing of quartz and biotite derived from metamorphosed Mathinna Beds with plagioclase and chlorite derived metasomatically from the country rock (Gee and Groves, 1971).

Rubble outcrop at the northern end of Wrinklers Beach [FQ066119] consists of porphyry which resembles dacitic material in the St Marys Porphyrite. It contains phenocrysts of rounded quartz, zoned plagioclase, biotite, hornblende, orthophyroxene and clinopyroxene in a fine-grained groundmass of quartz, orthoclase, biotite and plagioclase. Bands of coarser grained porphyry are present which contain markedly more orthoclase.

The tiny rubble outcrop of diorite at FQ068156 contains small phenocrysts of altered, cloudy plagioclase overgrown by small grains of clinozoisite. There are also phenocrysts of hornblende but none of quartz, biotite or chlorite. Quartz, orthoclase, plagioclase and fine-grained amphibole comprise the groundmass

Leucocratic muscovite granite (?Dbgm)

At the northern end of Beaumaris Beach [FQ077159] there are several small outcrops of medium-grained, even-grained, pink granite. They are in close proximity to Mathinna Beds outcrops and are probably parts of a small intrusion.

The rock consists of quartz, pale pink orthoclase, plagioclase, well crystallised primary muscovite and minor biotite which is greenish in thin section. Plagioclase grains are unaltered and have a low calcium content (albite or oligoclase).

Dolerite dykes (Devonian(?))

M. P. McClenaghan

Mafic dykes occur at several localities on the St Helens map sheet. At Grants Point [FQ119320] a vertical 2 m wide dyke trends approximately north and at FQ129296 in the St Helens Point area a vertical 14 m wide dyke trends at 20°.

The dykes are fine-grained dark grey rocks consisting of plagioclase, augite and skeletal ilmenite with an intergranular to sub-ophitic texture. Plagioclase shows sericitic alteration and the augite is partly altered to chlorite. Accessory pyrite and apatite is also present. Small granitoid xenoliths are present in the dyke at Grants Point.

The dykes are similar in character to dolerite dykes occurring widely throughout north-east Tasmania and are considered to be part of the same suite. The dykes occur as far north as the Furneaux Group (Cocker, 1977) and as far south as Maria Island (Clarke and Baillie, 1984; referred to as microdiorite (Dm)). The dykes are particularly abundant on the Blue Tier and Eddystone map sheet where they show locally regular trends. The dykes are inferred to be of similar Devonian age to the granitoids as they intrude all granitoid types and on Flinders Island a dolerite dyke is crossed by a quartz-feldspar porphyry dyke (pers. comm., P. W. Baillie and N. J. Turner, 1984) assumed to be of comagmatic with the other granitoids. The geochemistry of the dykes is discussed by McClenaghan (1984).

Jurassic dolerite

J. L. Everard

Jurassic dolerite is confined to a few small areas in the south-west of the quadrangle. The main occurrence is at The Pimple [EQ850081] where it caps a small but prominent hill at an elevation of 430–475 m. There is a similar occurrence about 900 m to the north [EQ848090] on a lower hill at 420–425 m. At both localities the base of the dolerite is obscured by talus, but it has intruded Permian rocks at a level only 50–100 m above the unconformity with the Mathinna Beds.

At the former locality, EQ850081, at the top of The Pimple, the rock is a fine-grained dolerite with closely spaced jointing, and is rather weathered, especially along and adjacent to joint planes. In thin section (sample BJ674, Reg. No. 003887) it consists of a few per cent of raggedly oblong, subhedral orthopyroxene crystals which are only slightly coarser than the remainder of the rock, mainly clinopyroxene, plagioclase and altered quartzo-feldspathic mesostasis. Clinopyroxene, comprising about 40% of the rock, occurs as oblong to equant polygonal subhedra and euhedra mostly 300–600 μm across. Most is augite (biaxial positive, moderate $2V$) and pigeonite (very low $2V$) is rare. Plagioclase laths are typically 200–400 × 50–100 μm (rarely up to 1 mm × 300 μm). Scattered equant angular opaque grains (typically 50–100 μm across) are also present. The fine mesostasis, probably largely quartz, alkali feldspar and iron-titanium oxides, is patchily altered to a cloudy aggregate of very fine sericite and/or epidote, and oxidation products.

The rock is a fine to medium-grained pyroxene-enriched, orthopyroxene-bearing dolerite, characteristic of cumulates in the lower part of a sill. On adjoining map sheets similar textural types are indicated as f to m (St Marys) and fo to mo (Ben Lomond).

Both the petrography and the field relationships strongly suggest that it is the remnant of a more-or-less horizontal, subconcordant sheet, originally much more extensive, which intruded near the base of the Parmeener Supergroup, rather than a dyke or feeder. About 10 km to the SSE dolerite capping the Nicholas Range (Turner *et al.*, 1984) also appears to be the remnant of a sheet on both geological and geophysical grounds (Calver in Turner and Calver, 1987, p. 87), as does dolerite on Tower Hill, 16 km to the WSW of The Pimple (Calver *et al.*, 1988). In both areas, dolerite intrudes Triassic lithic sandstone some 300–400 m stratigraphically higher in the Parmeener Supergroup, implying marked downward transgression if the dolerite at The Pimple was originally part of the same sheet. The nearest Jurassic dolerite feeders are 16–20 km to the south, on or near Fingal Tier (Calver in Turner *et al.*, 1984, Leaman and Richardson, 1981).

Another small area of possible Jurassic dolerite (?Jdl) is shown on the map at EQ912065, about 6 km ESE of The Pimple, on a small knoll of a ridge west of Avenue Road. The area overlaps the unconformity between Mathinna Beds and Permian freshwater sandstone and is surrounded by float of both rock types. Within this area there is no outcrop, but abundant cobble-sized float, mainly of massive, tough but weathered medium- to coarse-grained dolerite. In thin section a typical sample (NH37, Reg. No. 003901) is a coarse-grained dolerite with a subophitic texture, containing both augite and pigeonite (≤2.5 mm), plagioclase, and abundant, poorly crystalline mesostasis. It is typical of Jurassic dolerite from the upper parts of a sill (textural types c or ce). Also present in this area are cobbles of finer grained, well-jointed dolerite and vesicular basalt, the latter probably of Tertiary age (see below). The area is probably a remnant of an old talus or lag deposit. Tongues of dolerite talus derived from the Nicholas Range occur on the St Marys Quadrangle only 2 km to the south (Turner *et al.*, 1984), but evidently there has also been a contribution from a subsequently eroded area of basalt.

Tertiary basalt

J. L. Everard

SUGARLOAF ROAD AREA

INTRODUCTION

The only surface exposure of Tertiary basalt in the quadrangle occurs in the south-west, where an area of about 0.4 km^2 of basalt, resting on Mathinna Beds, caps a small ridge at an elevation of 250–275 m. Typically the basalt is pale grey, coarse-grained, very vesicular and often altered. Vesicles are irregularly shaped, typically 1–2 mm across and lined with dull green to green-brown chloritic alteration products. At the southern end of the area of outcrop, at the base of small south-facing cliffs up to 10 m high near the end of Sugarloaf Road [EQ869052], the basalt is less altered, nearly massive, darker coloured and medium- to fine-grained. At this locality, the base of the basalt is obscured by talus, but the basalt is at least 10 m but less than 25 m thick. There is no evidence for more than a single flow.

About 4 km to the east, on a knoll at an elevation of about 250 m west of Avenue Road [EQ912065] a small area of float of igneous rock (shown as ?Jdl on the colour map) occurs close to the Mathinna Beds/Permian unconformity. The principal rock type is medium- to coarse-grained, massive dolerite, petrographically similar to Jurassic dolerite, but subordinate finely vesicular basalt similar to that described above is also present.

PETROGRAPHY

Coarse-grained vesicular basalt (BJ676)

The specimen (Reg. No. 003909), collected from float near a road junction [EQ869056] is very vesicular and typical of basalt in the vicinity. In thin section, it is a rather

coarse-grained basalt with a dominantly subophitic texture, consisting mainly of unaligned plagioclase laths (300–600 × 50–150 μm) and colourless clinopyroxene subhedra (250 μm–1 mm) which partly surround them. The clinopyroxene is optically biaxial positive and both pigeonite (low 2*V*) and augite (high 2*V*) are present. Accessory opaque minerals include equant grains (typically about 100 μm across), probably mainly ilmenite, and angular elongate to acicular laths (up to 300 × 10 μm), probably mainly titanomagnetite. Minor diffuse patches of black glass, characteristically cloudy due to very fine opaque dust, occur intersertally between plagioclase laths.

No olivine phenocrysts are present, but the thin section has intersected a single equant plagioclase glomerocryst (about 1.5 mm across) which consists of two irregularly and intimately intergrown crystals, differing in optical orientation, both of which contain abundant irregular inclusions of opaque minerals and pyroxene.

Vesicles (typically 500 μm–2 mm long) are very abundant and very irregular in shape. Yellow to deep orange-red oxidation products are associated particularly with vesicle linings, black glass and opaque grains.

Basal, more or less massive, basalt (BJ675)

This nearly massive specimen (Reg. No. 003908) was collected from towards the base of the small cliff at EQ869052. In thin section, it consists of sparsely distributed olivine phenocrysts set in a medium- to fine-grained, dominantly intergranular to intersertal groundmass.

The olivine phenocrysts, which comprise only a few per cent of the rock, are typically equant polygonal euhedra to deeply embayed subhedra, usually 500 μm–1 mm across but up to 2 mm. They occur both as isolated phenocrysts and, less often, as glomerocrysts of two or more crystals.

The groundmass consists mainly of unaligned plagioclase laths (typically 150–300 × 30–70 μm) and mostly intergranular angular subhedra and anhedra (typically 100–200 μm) of clinopyroxene, including both augite and pigeonite. In a few places, subophitic texture is developed. Small equant granules (usually about 100 μm across) of olivine, grading in size up to the phenocrysts, also occur in the groundmass. Opaques range from equant to oblong angular grains (about 100 μm across) to acicular laths (100–200 × 5–10 μm) and include both ilmenite and titanomagnetite. Minor diffuse intersertal patches of glass are black due to densely disseminated dust-sized opaque grains.

A few irregularly shaped vesicles and amygdales filled with colourless to pale-yellow-secondary carbonate, up to 500 μm long, are present. Alteration is restricted to vesicles, amygdales and glassy patches.

The rock differs from BJ676 in the presence of olivine phenocrysts, the finer and dominantly intergranular rather than subophitic groundmass, and its relatively fresh and massive texture.

Vesicular basalt float (NH38)

This very vesicular basalt (Reg. No. 003918) was collected from the area of mixed dolerite and basalt float at EQ912065. The thin section comprises about 30% void, but otherwise consists of sparsely distributed small (500 μm) phenocrysts of olivine, slightly to moderately embayed, in an intergranular to intersertal groundmass of labradoritic plagioclase laths (typically 200–800 × 40–80 μm), angular anhedral granules (50–150 μm) of both augite and pigeonite, olivine granules, and cloudy opaque-rich black glass. A single strongly resorbed, inclusion-ridden plagioclase phenocryst (2 mm × 400 μm–1 mm) is also present. The rock resembles BJ675 in the presence of olivine phenocrysts and the dominantly intergranular texture, but is very vesicular like BJ676. Groundmass grain-size is intermediate between the two.

MINERAL CHEMISTRY

Minerals in samples BJ675 and BJ676 were analysed by JEOL electron microprobe at the University of Tasmania, using the 'spot' mode, in which a volume of diameter 0.5 μm and beam penetration 3–5 μm is analysed. Results, recalculated to 100% and cation formulae are presented in Tables 13, 14.

Olivine

The olivine phenocrysts in sample BJ675 are relatively iron rich (Fo_{73-78}) with only slight normal zoning, and

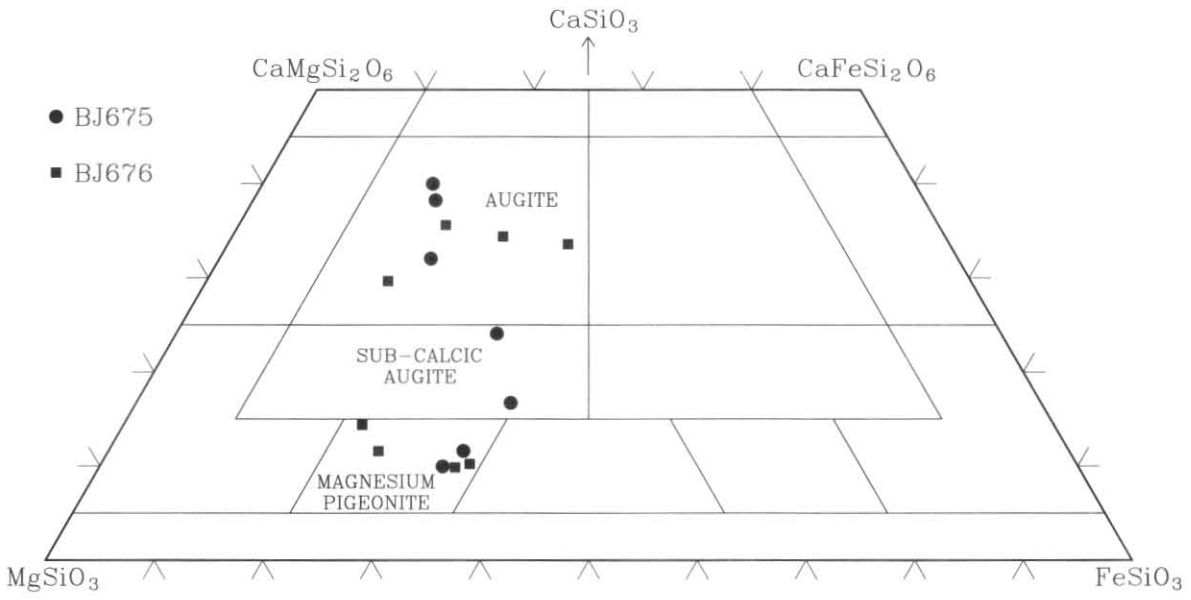

Figure 11. Electron probe microanalyses of pyroxenes from Tertiary basalts in the Sugarloaf Road area, plotted on the pyroxene quadrilateral (Ca:Mg:total Fe+Mn, atomic ratios).

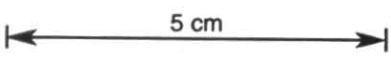

Table 13. ELECTRON PROBE MICROANALYSES, SAMPLE BJ675 (SUGARLOAF ROAD)

	olivine phenocrysts							olivine granules	
	1A(core)	1B(rim)	2A(core)	2B(rim)	3A(core)	3B(rim)	4	5	6
SiO_2	37.78	38.12	38.59	38.17	38.64	38.39	38.33	37.54	37.66
TiO_2	–	–	–	–	–	–	–	–	–
Al_2O_3	–	–	–	–	–	–	–	–	–
Cr_2O_3	–	–	–	–	–	–	–	–	–
ΣFeO	22.29	22.84	20.86	24.01	20.77	22.46	22.21	26.54	25.70
MnO	0.26	0.25	–	0.23	–	–	0.23	0.26	0.29
NiO	0.44	0.37	0.33	–	0.40	0.32	–	–	–
MgO	39.10	38.21	40.23	37.39	40.07	38.83	39.11	35.41	36.17
CaO	0.14	0.20	–	0.20	0.12	–	0.12	0.25	0.18
Na_2O	–	–	–	–	–	–	–	–	–
K_2O	–	–	–	–	–	–	–	–	–
P_2O_5	–	–	–	–	–	–	–	–	–
SO_3	–	–	–	–	–	–	–	–	–
Cl	–	–	–	–	–	–	–	–	–
Total	100.01	99.99	100.01	100.00	100.00	100.00	100.00	100.00	100.00
	Cations calculated on basis of (O) = 4								
Si	0.9864	0.9965	0.9969	1.0007	0.9984	0.9992	0.9965	0.9976	0.9966
Fe as Fe^{II}	0.4867	0.4993	0.4505	0.5264	0.4487	0.4887	0.4830	0.5897	0.5687
Mn	0.0057	0.0055	–	0.0051	–	–	0.0050	0.0059	0.0066
Ni	0.0092	0.0078	0.0068	–	0.0082	0.0067	–	–	–
Mg	1.5217	1.4887	1.5488	1.4613	1.5430	1.5061	1.5155	1.4022	1.4264
Ca	0.0038	0.0056	–	0.0057	0.0033	–	0.0035	0.0071	0.0051
Cation total	3.0136	3.0035	3.0031	2.9992	3.0016	3.0008	3.0035	3.0024	3.0034
100Mg/Mg+Fe	75.8	74.9	77.5	73.5	77.5	75.5	75.8	70.4	71.5

Table 13. ELECTRON PROBE MICROANALYSES, SAMPLE BJ675 (SUGARLOAF ROAD) – *continued*

	augite			sub-calcic augite		pigeonite	
	7	8	9	10	11	12	13
SiO_2	52.46	51.70	51.97	51.45	52.34	52.97	53.15
TiO_2	1.05	1.14	1.03	1.21	0.64	0.59	0.51
Al_2O_3	2.57	2.40	2.00	1.37	0.99	1.10	0.69
Cr_2O_3	0.60	0.64	0.36	–	–	–	–
ΣFeO	9.52	10.36	12.18	18.28	20.84	19.78	19.77
MnO	–	–	–	–	0.24	0.38	0.35
NiO	–	–	–	–	–	–	–
MgO	14.96	15.47	16.89	16.00	16.82	19.42	20.56
CaO	18.84	18.28	15.57	11.69	8.11	5.75	4.97
Na_2O	–	–	–	–	–	–	–
K_2O	–	–	–	–	–	–	–
P_2O_5	–	–	–	–	–	–	–
SO_3	–	–	–	–	–	–	–
Cl	–	–	–	–	–	–	–
Total	100.00	99.99	100.00	100.00	99.98	99.99	100.00
	Cations calculated on basis of (O) = 6						
Si	1.9405	1.9214	1.9310	1.9439	1.9775	1.9772	1.9798
Al^{iv}	0.0595	0.0786	0.0690	0.0561	0.0225	0.0228	0.0202
Al^{vi}	0.0526	0.0267	0.0184	0.0050	0.0218	0.0255	0.0100
Cr	0.0175	0.0189	0.0105	–	–	–	–
Ti	0.0292	0.0319	0.0287	0.0344	0.0183	0.0167	0.0143
Fe as Fe^{II}	0.2944	0.3220	0.3786	0.5775	0.6586	0.6175	0.6159
Mn	–	–	–	–	0.0078	0.0120	0.0111
Mg	0.8250	0.8570	0.9354	0.9012	0.9474	1.0804	1.1412
Ca	0.7469	0.7281	0.6198	0.4734	0.3283	0.2299	0.1983
Cation total	3.9656	3.9846	3.9914	3.9915	3.9822	3.9820	3.9908
100 Mg/Mg + Fe	73.7	72.7	71.2	60.9	59.0	63.6	64.9

grade in size downward to still more iron-rich (Fo_{70-72}) granules in the groundmass. NiO is detectable mainly in the more magnesian analyses, and MnO in the more iron-rich analyses.

Pyroxenes

Both samples contain both augite and pigeonite in the groundmass, with some suggestion of progressive iron-enrichment in each series (fig. 11), as is characteristic of pyroxenes from tholeiitic rocks. Two probe analyses plot as sub-calcic augites, apparently bridging the augite-pigeonite miscibility gap, and may be metastable quench phases, preserved by rapid chilling from high temperatures. The non-quadrilateral components TiO_2 (≤1.21%) and Al_2O_3 (≤2.57)are only minor constituents, but it is noteworthy that both are higher in augites than in pigeonites. Cr_2O_3 (≤0.7%) is detectable only in the more magnesian pyroxenes, both pigeonite and augite. Cation totals are all just below 4, suggesting that little Fe^{III} is present, and virtually all iron is ferrous.

Feldspars

Groundmass plagioclase ranges form sodic andesine (An_{35}) to calcic labradorite (An_{64}), and the phenocryst in sample BJ676 falls within this range (An_{60}). K_2O remains low but increases with Ab (i.e. Na_2O) content. A single analysis of alkali feldspar ($An_{16}Ab_{74}Or_{10}$) could be either calcic anorthoclase or potassic oligoclase.

Iron-titanium oxides

Two compositionally distinct opaque oxide minerals are present, the higher TiO_2 (50–52%) phase apparently corresponding to the rhombohedral ilmenite-hematite series, and the lower TiO_2 (≈26%) phase to the cubic ulvospinel-magnetite (titanomagnetite) series. Fe^{III} content is calculated in Tables 13, 14 by normalising analyses to the appropriate cation and oxygen numbers. Both phases contain small amounts of MgO, MnO and possibly Al_2O_3, whilst SiO_2 and CaO, where detected, are probably due to impurities. Ilmenite in the vesicular basalt sample BJ676 has a higher Mg and Fe^{III} content than in

Table 13. ELECTRON PROBE MICROANALYSES, SAMPLE BJ675 (SUGARLOAF ROAD) – *continued*

	plagioclase				
	14	15	16	17	18
SiO_2	54.16	53.40	57.80	57.94	59.94
TiO_2	-	-	-	-	0.31
Al_2O_3	29.17	29.44	26.17	26.39	24.51
Cr_2O_3	-	-	-	-	-
ΣFeO	0.26	0.33	0.98	0.59	0.81
MnO	-	-	-	-	-
NiO	-	-	-	-	-
MgO	-	-	-	-	-
CaO	12.44	12.69	9.24	9.18	7.02
Na_2O	3.87	4.01	5.47	5.66	6.88
K_2O	0.10	0.12	0.32	0.25	0.45
P_2O_5	-	-	-	-	-
SO_3	-	-	-	-	-
Cl	-	-	-	-	0.08
Total	100.00	99.99	99.98	100.01	100.00
	Cations calculated on basis of (O) = 8				
Si	2.4474	2.4216	2.6083	2.6039	2.6987
Ti	-	-	-	-	excl
Al	1.5534	1.5735	1.3919	1.3978	1.3004
Fe	excl	excl	excl	excl	excl
Ca	0.6025	0.6165	0.4468	0.4419	0.3388
Na	0.3395	0.3528	0.4789	0.4928	0.6008
K	0.0056	0.0071	0.0187	0.0143	0.0257
Cl	-	-	-	-	excl
Cation total	4.9484	4.9715	4.9446	4.9507	4.9644
An	63.6	63.1	47.3	46.6	35.1
Ab	35.8	36.1	50.7	51.9	62.2
Or	0.6	0.7	2.0	1.5	2.7

Table 13. ELECTRON PROBE MICROANALYSES, SAMPLE BJ675 (SUGARLOAF ROAD) – *continued*

	ilmenite			titano–magnetite	glass		
	19	20	21	22	23	24	25
SiO_2	–	–	–	0.35	68.70	68.62	64.31
TiO_2	50.00	49.72	49.63	25.59	3.28	0.79	1.39
Al_2O_3	0.20	–	–	1.68	10.52	14.59	10.97
Cr_2O_3	–	–	–	–	–	–	–
ΣFeO	48.62	49.18	49.09	71.29	3.38	5.15	9.31
MnO	0.46	0.28	0.39	0.35	–	–	–
NiO	–	–	–	–	–	–	–
MgO	0.72	0.65	0.88	0.74	–	0.30	1.04
CaO	–	0.17	–	–	3.57	2.64	4.21
Na_2O	–	–	–	–	1.81	5.38	3.98
K_2O	–	–	–	–	5.47	1.35	2.64
P_2O_5	–	–	–	–	2.63	0.67	1.62
SO_3	–	–	–	–	0.50	0.35	0.41
Cl	–	–	–	–	0.15	0.15	0.13
Total	100.00	100.00	99.99	100.00	100.01	99.99	100.01
	Cations						
Si	–	–	–	excl			
Ti	0.9404	0.9358	0.9328	0.7018			
Al	0.0059	–	–	0.0724			
Fe^{III}	0.1135	0.1284	0.1344	0.5240			
Fe^{II}	0.9035	0.9011	0.8916	1.6508			
Mn	0.0097	0.0060	0.0084	0.0109			
Mg	0.0269	0.0241	0.0328	0.0401			
Ca	–	0.0046	–	–			
$FeTiO_3/FeTiO_3 + Fe_2O_3$	0.949	0.937	0.930	–			
$Fe_2TiO_4/Fe_2TiO_4 + Fe_3O_4$	–	–	–	0.726			

ilmenite : cations calculated on basis of oxygen number (O) = 3, cation total (Z) = 2
titanomagnetite: cations calculated on basis of oxygen number (O) = 4, cation total (Z) = 3

BJ675. Average compositions, calculated by the method of Anderson (1968) are $Ilm_{93.5}Hm_{6.5}$, $Usp_{72.6}Mt_{27.4}$ (BJ675) and $Ilm_{96.0}Hm_{4.0}$, $Usp_{74.8}Mt_{25.2}$ (BJ676). Application of the iron-titanium oxide geothermometer (Buddington and Lindsley, 1964; Spencer and Lindsley, 1981) suggest conditions of crystallisation of about 950°C, $10^{-12.5}$ bars fo_2 and 850°C, 10^{-15} bars fo_2 respectively.

Glass

The small intersertal patches of black glass in both specimens have variable but dacitic compositions, very depleted in MgO relative to ΣFeO by the progressive crystallisation of olivine and augite. The glass largely represents the potential alkali feldspar and quartz in the rock (cf. CIPW norm, table 15).

GEOCHEMISTRY

The least altered, nearly massive sample (BJ675, EQ869052) was analysed for major and trace elements (table 15). CIPW and Rittmann norms were calculated assuming Fe_2O_3/FeO = 0.15 (Brooks, 1976) and normalised to 100% anhydrous (table 16).

The basalt is a strongly fractionated quartz-normative tholeiite. In the normalised total alkali-silica diagram (fig. 12) it plots below the line of Macdonald and Katsura (1964) in the tholeiite field; in the classification of Le Maitre (1984) it is a basaltic andesite rather than a basalt,

Table 14. ELECTRON PROBE MICROANALYSES, SAMPLE BJ676 (SUGARLOAF ROAD)

	augite				pigeonite			
	1	2	3	4	5	6	7	8
SiO_2	52.52	51.75	52.87	53.04	53.82	54.23	52.98	52.99
TiO_2	0.81	1.06	0.72	0.63	0.47	0.35	0.41	0.58
Al_2O_3	1.27	1.45	1.77	1.87	1.18	0.93	0.43	0.56
Cr_2O_3	–	–	–	0.72	0.40	0.25	–	–
ΣFeO	11.97	15.23	17.86	10.57	13.77	15.69	21.04	20.02
MnO	–	–	–	–	0.25	–	0.35	0.33
NiO	–	–	–	–	–	–	–	–
MgO	15.97	13.90	11.32	18.89	22.95	22.68	19.78	20.59
CaO	17.46	16.28	14.79	14.29	7.16	5.87	5.00	4.92
Na_2O	–	–	0.31	–	–	–	–	–
K_2O	–	0.34	0.37	–	–	–	–	–
P_2O_5	–	–	–	–	–	–	–	–
SO_3	–	–	–	–	–	–	–	–
Cl	–	–	–	–	–	–	–	–
Total	100.00	100.01	100.01	100.01	100.00	100.00	99.99	99.99
	Cations calculated on basis of (O) = 6							
Si	1.9570	1.9493	1.9922	1.9465	1.9628	1.9823	1.9859	1.9767
Al^{iv}	0.0430	0.0493	0.0078	0.0535	0.0372	0.0177	0.0141	0.0233
Al^{vi}	0.0129	–	0.0330	0.0272	0.0137	0.0222	0.0050	0.0014
Cr	–	–	–	0.0209	0.0115	0.0071	–	–
Ti	0.0227	0.0308	0.0216	0.0175	0.0129	0.0096	0.0116	0.0163
Fe as Fe^{II}	0.3728	0.4918	0.5992	0.3243	0.4201	0.4798	0.6596	0.6246
Mn	–	–	–	–	0.0078	–	0.0111	0.0104
Mg	0.8867	0.8005	0.6766	1.0332	1.2474	1.2360	1.1051	1.1451
Ca	0.6972	0.6737	0.6355	0.5620	0.2797	0.2301	0.2006	0.1968
Na	–	–	excl*	–	–	–	–	–
K	–	excl*	excl*	–	–	–	–	–
Cation total	3.9923	3.9954	3.9659	3.9851	3.9931	3.9848	3.9930	3.9946
100 Mg/Mg + Fe	70.4	61.9	53.0	76.1	74.8	72.0	62.6	64.7

* K subtracted as $KAlSi_3O_8$, Na subtracted as $NaAlSi_3O_8$

Table 14. ELECTRON PROBE MICROANALYSES, SAMPLE BJ676 (SUGARLOAF ROAD) – *continued*

	plagioclase phenocryst	groundmass plagioclase					
	9	10	11	12	13	14	15
SiO_2	54.39	54.02	54.17	53.98	58.47	59.64	66.40
TiO_2	–	–	–	–	0.16	–	0.17
Al_2O_3	29.08	29.12	29.03	28.74	25.92	25.34	20.26
Cr_2O_3	–	–	–	–	–	–	–
ΣFeO	0.46	0.51	0.42	0.76	0.46	0.51	0.75
MnO	–	–	–	–	–	–	–
NiO	–	–	–	–	–	–	–
MgO	–	–	–	–	–	–	–
CaO	11.76	12.12	11.94	11.96	8.56	7.70	3.06
Na_2O	4.14	4.10	4.28	4.33	6.02	6.36	7.61
K_2O	0.18	0.14	0.16	0.23	0.41	0.45	1.54
P_2O_5	–	–	–	–	–	–	–
SO_3	–	–	–	–	–	–	0.20
Cl	–	–	–	–	–	–	–
Total	100.01	100.01	100.00	100.00	100.00	100.00	99.99
	Cations calculated on basis of (O) = 8						
Si	2.4596	2.4476	2.4527	2.4547	2.6274	2.6686	2.9469
Ti	–	–	–	–	excl	–	excl
Al	1.5497	1.5551	1.5486	1.5402	1.3727	1.3365	1.0597
Fe	excl	excl	excl	excl	excl	excl	excl
Ca	0.5695	0.5883	0.5791	0.5829	0.4123	0.3694	0.1456
Na	0.3631	0.3599	0.3758	0.3816	0.5242	0.5515	0.6548
K	0.0104	0.0078	0.0095	0.0134	0.0236	0.0258	0.0874
S	–	–	–	–	–	–	excl
Cation total	4.9523	4.9587	4.9657	4.9728	4.9601	4.9518	4.8944
An	60.4	61.5	59.6	59.6	42.9	39.0	16.4
Ab	38.5	37.6	39.0	39.0	54.6	58.3	73.8
Or	1.1	0.8	1.4	1.4	2.5	2.7	9.8

since SiO_2* >52%. Trace element values, notably low Nb (Nb/Y<1), Zr, Sr, REE and P_2O_5 are also characteristic of tholeiites.

The rock is very similar both petrographically and chemically (table 16) to another analysed tholeiite from Barnes Road, St Marys Quadrangle [EQ848044], about 2.3 km to the WSW (Everard, 1987*a*). The latter has somewhat lower MgO and 100 Mg/Mg + Fe, suggesting that it is more fractionated, but Ni is slightly higher. Derivation of either from a primary olivine tholeiite requires large amounts (probably >20%) of crystal fractionation, probably of clinopyroxene and plagioclase as well as olivine.

Although the nearby Jurassic dolerite is also quartz-normative and may have a similar 100 Mg/Mg + Fe, it otherwise differs markedly in composition (notably in TiO_2, CaO, Na_2O, Cr, Ni, Rb, Sr and Nb; e.g. Everard, 1987*c* and lacks olivine. Therefore it is considered certain that the basalt is not comagmatic with the Jurassic dolerite.

DISCUSSION

The basalt is almost contiguous to the south with the area of similar tholeiitic basalt on the St Marys Quadrangle (Turner *et al.*, 1984), which extends westward for about 3 km to EQ834042 near the edge of that quadrangle. All the basalt lies at an elevation of about 250 to 275 m and

Table 14. ELECTRON PROBE MICROANALYSES, SAMPLE BJ676 (SUGARLOAF ROAD) – *continued*

	ilmenite			titano-magnetite	glass	
	16	17	18	19	20	21
SiO_2	-	-	-	0.46	67.69	64.67
TiO_2	50.37	51.82	51.62	26.52	1.08	6.56
Al_2O_3	0.20	-	-	1.69	10.97	11.47
Cr_2O_3	-	-	-	-	-	-
ΣFeO	47.92	46.61	46.45	69.74	10.10	8.01
MnO	0.42	0.29	0.29	0.31	-	-
NiO	-	-	-	-	-	-
MgO	1.09	1.27	1.64	1.13	-	-
CaO	-	-	-	0.15	2.26	0.82
Na_2O	-	-	-	-	1.90	2.32
K_2O	-	-	-	-	4.73	5.90
P_2O_5	-	-	-	-	1.18	0.24
SO_3	-	-	-	-	-	-
Cl	-	-	-	-	0.08	-
Total	100.00	99.99	100.00	100.00	99.99	99.99
	Cations					
Si	-	-	-	excl		
Ti	0.9450	0.9731	0.9662	0.7263		
Al	0.0058	-	-	0.0728		
Fe^{III}	0.1042	0.0538	0.0676	0.4746		
Fe^{II}	0.8956	0.9196	0.8992	1.6497		
Mn	0.0088	0.0063	0.0061	0.0095		
Mg	0.0406	0.0472	0.0609	0.0613		
Ca	-	-	-	0.0058		
$FeTiO_3/FeTiO_3 + Fe_2O_3$	0.945	0.972	0.964	-		
$Fe_2TiO_4/Fe_2TiO_4 + Fe_3O_4$	-	-	-	0.748		

ilmenite : cations calculated on basis of oxygen number (O) = 3, cation total (Z) = 2
titanomagnetite : cations calculated on basis of oygen number (O) = 4, cation total (Z) = 3

Table 15. CHEMICAL ANALYSES OF TERTIARY BASALTS, SUGARLOAF ROAD AREA

Field No.	BJ675	M366
Analysis No.	876007	831451
SiO_2	52.67	52.53
TiO_2	1.49	1.54
Al_2O_3	13.98	14.27
Fe_2O_3	1.31	2.19
FeO	9.50	9.69
MnO	0.14	0.19
MgO	7.03	5.99
CaO	8.44	9.08
Na_2O	2.98	2.71
K_2O	0.66	0.50
P_2O_5	0.24	0.19
H_2O	0.94	1.00
CO_2	0.15	0.43
Total S	<0.05	0.02
Total	99.53	100.33
100 Mg/Mg + Fe^{II} (a)	56.9	52.4
(b)	57.1	51.0
(c)	54.0	47.8

(a) as analysed, atomic ratios
(b) assuming $Fe_2O_3/FeO = 0.15$, atomic ratios
(c) all iron as Fe^{II}, atomic ratios

	BJ675	M366
	876007	831451
	Trace elements (ppm)	
Sc	24	23
V	155	145
Cr	320	290
Co	50	48
Ni	180	210
Cu	48	52
Zn	100	125
Ga	16	20
As	<10	n.a.
Rb	16	21
Sr	230	230
Y	26	22
Zr	135	145
Nb	15	12
Mo	2	n.a.
Ag	<5	n.a.
Sb	<5	n.a.
Ba	115	110
La	12	n.a.
Ce	31	n.a.
Nd	16	n.a.
Pb	9	<4
Bi	6	n.a.
Th	<4	n.a.
U	<5	n.a.

BJ675 (876007) : quartz tholeiite, Sugarloaf Road, [EQ869052], St Helens Quadrangle
M366 (831451) : quartz tholeiite, Barnes Road [EQ848044], St Marys Quadrangle. From Everard (1987*b*).
Analyses by Department of Mines Laboratories, Launceston.

probably represents the same flow, or series of flows. Its present total areal extent is about 2.1 km^2, but it has been dissected by Barnes Creek and other streams, and its original extent was probably much greater. The float (lag?) of basalt at a similar elevation at EQ912065 suggests that it formerly extended for at least a further four kilometres to the east.

No feeders were located during field mapping, but a recent airborne geophysical survey (Department of Mines, 1989) detected a very strong magnetic anomaly at EQ853045, just east of Barnes Road on the St Marys Quadrangle, which is considered to indicate the likely feeder. A field inspection of this locality, at the margin of a heathy swamp, was made but the scattered outcrop of massive basalt in the vicinity does not exhibit any special features.

At present the age of the basalt is unknown, but an Early Tertiary age seems likely in view of the degree of erosion and dissection.

Table 16. CIPW AND RITTMANN NORMS OF TERTIARY BASALTS

Field No.	BJ675	M366
Analysis No.	876007	831415
CIPW norms (mass%)		
Q	2.41	4.01
or	3.95	3.01
ab	25.59	23.23
an	23.19	25.57
di	14.61	15.55
hy	24.71	22.97
mt	2.09	2.26
il	2.88	2.96
ap	0.57	0.45
Total	100.00	100.01
mol% an (plag)	46.1	50.9
Rittmann norms (volume%)		
Quartz	3.9	5.7
Plagioclase	57.4	56.5
Pigeonite	35.2	34.3
Magnetite	1.5	1.6
Ilmenite	1.4	1.5
Apatite	0.5	0.4
Total	99.9	100.0

Calculated from major elements, Fe redistributed so that $Fe_2O_3/FeO = 0.15$, normalised to 100% anhydrous.

Basalt occurring a short distance further west on the Ben Lomond Quadrangle (Calver *et al.*, 1988), between EQ834041 and EQ830043, and on the eastern bank of the South Esk River between EQ825035 and EQ825040, is an unrelated, strongly undersaturated olivine nephelinite (Everard, unpublished data).

It is noteworthy that the basalt occupies a low saddle on the watershed between the South Esk River and Barnes Creek, a tributary of the Avenue and Scamander Rivers. The lowest point on the watershed, at EQ857046, has an elevation of 269 m, only 20–25 m above the South Esk River about 3.3 km away. The headwaters of Barnes Creek has a gradient of about 1:30, and is about to begin eroding the alluvial plain of the South Esk near the Beauty Flat bridge site. The upper South Esk River in this vicinity has a gradient of only about 1:750, and thus its capture and diversion to the sea at Scamander is geologically imminent.

ST HELENS AREA

INTRODUCTION

Boring by the Department of Mines within the Tertiary sedimentary deposits west of St Helens has shown that locally basalt occurs near or at their base. Basalt was intersected in 8 out of the 49 holes drilled, but does not crop out at the surface (Jack, 1964).

The Tertiary sediments comprise mixed sands, clays and gravels, and are locally lithified, particularly towards their base. Near St Helens at FQ032249 they are about 80 m thick, extending to about 75 m below present sea level, but further east their maximum thickness is usually 40-45 m. They represent river sediments deposited in the former course of the George River, known as Thureau's Deep Lead (e.g. Montgomery, 1893*a*), and their upper parts have been extensively worked for alluvial tin. The sediments do not represent a single horizon, but occur at a series of surfaces of differing elevations, considered by Jack (1964) to correspond to various Tertiary sea-levels.

The main known occurrence of basalt is 6.5 km WNW of St Helens, where four holes intersected basalt over a cross-channel distance of about 275 m between EQ982271 and EQ984269 (fig. 13). At least two flows are present. The lower flow is about 3 m thick and rests directly on granitic basement at an elevation of about 15 m above present sea-level. It is separated from the upper flow which is up to 10 m thick, by about 3 m of cemented sand and gravel.

About 1.5 km to the NNW near Clio Hill [EQ979286], basalt up to 10 m thick occurs at an elevation of about 45 m in two holes about 90 m apart, beneath about 30 m of clayey sand and gravel.

To the south near Royal Ruby Flat [EQ988254] one of twelve holes intersected basalt at an elevation of about 10 m, towards the bottom of the deepest part of the lead. About one metre of basalt is underlain by a few metres of

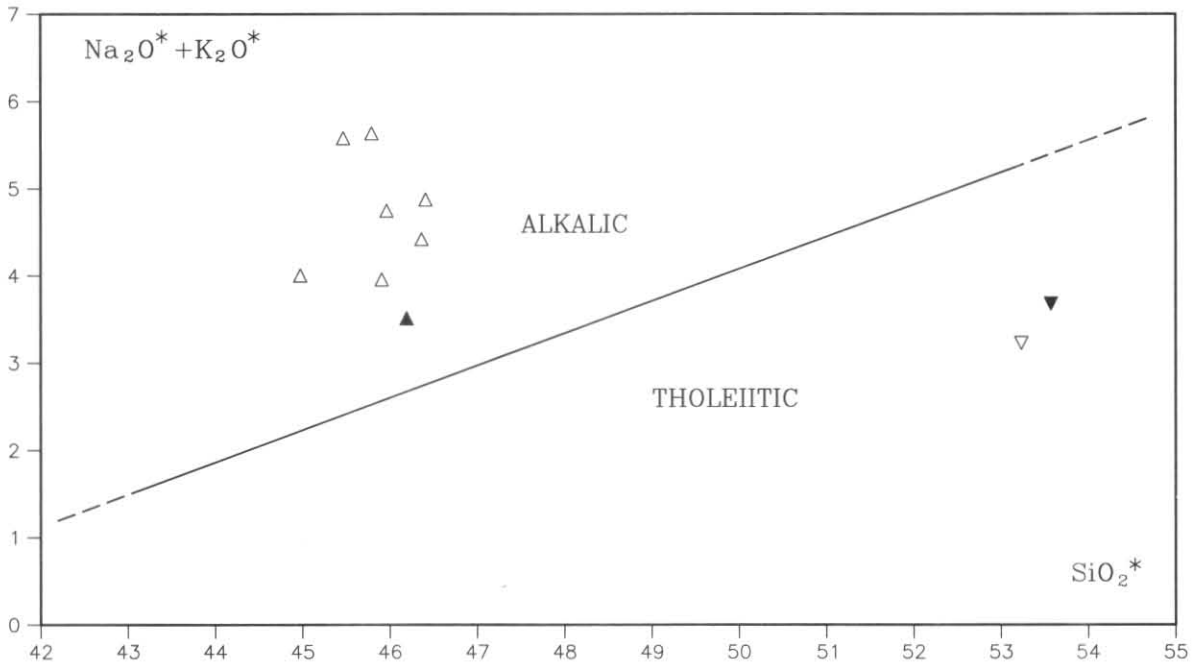

Figure 12. Alkali-silica diagram for Tertiary basalts, St Helens map sheet and adjacent areas. Analyses are recalculated to 100% major elements (anhydrous, CO_2-free, all iron as FeO). Boundary of tholeiitic and alkalic fields (Macdonald and Katsura, 1964) also shown. ▼ BJ675, Sugarloaf Road; ▽ M366, Barnes Road (Everard, 1987b); ▲ 62348, St Helens area (estimate); △ Weldborough Pass area (Brown and McClenaghan, 1982).

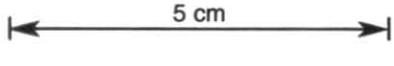

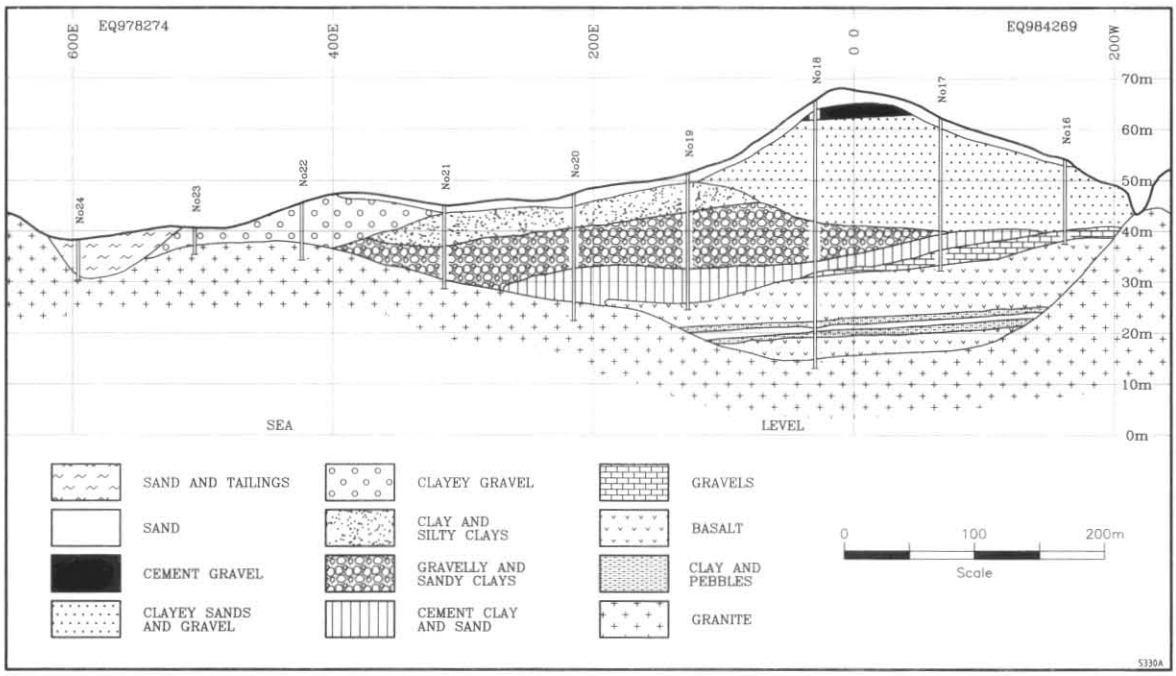

Figure 13. Geological section along bore line No. 3, Thureau's Deep Lead, from Jack (1964).

gravel and cemented gravel, resting on granitic basement.

The above occurrences probably represent the same series of flows. Basalt is absent in a line of holes further east, between FQ005253 and FQ005249. However, there is an isolated occurrence just west of St Helens at FQ032249, where basalt boulders or a very thin flow remnant were found just above granitic basement at about 75 m below present sea-level.

Petrography

A specimen (Reg. no. 62348) of fine-grained, massive dark grey basalt was collected by R. Jack from the top of the upper flow, at a depth of 15 m in hole 16 [EQ984269]. In thin section the rock is clearly an alkali-olivine basalt, and consists of (n = 400) abundant phenocrysts of both olivine (11 vol%) and titanaugite (4%) in a fine-grained intergranular groundmass (85%).

Olivine phenocrysts (typically 500 μm–1 mm, rarely 2 mm) range from equant or shortly oblong, angular or subrounded euhedra to irregular, deeply embayed subhedra and smaller rounded anhedra grading into groundmass. They occur either as isolated phenocrysts or, less commonly, as glomerocrysts of two or more crystals. They are sometimes fresh and colourless, but usually show incipient to partial orange-brown to khaki-brown iddingsitic alteration, especially around rims and fractures, and are sometimes completely altered.

The titanaugite phenocrysts are smaller (typically 250–500 μm, rarely ≤1 mm) and also grade downward in size into the groundmass. They are equant and polygonal, and are usually clumped into glomerocrysts of four to eight crystals, although isolated phenocrysts also occur. There are rare composite glomerocrysts containing both titanaugite and olivine crystals. The titanaugite is biaxial positive and pale pinkish-purple to pale yellow-brown, sometimes with a weak pleochroism. Occasionally an orange-brown iddingsite-like alteration is present.

The fine-grained, somewhat altered groundmass contains rather sparsely distributed plagioclase laths (typically 150– 300 μm × 10–20 μm), equant titanaugite granules (typically 50–200 μm), sparse olivine granules, abundant disseminated angular equant opaques, probably titanomagnetite (10–50 μm) and a very-fine colourless indeterminate mesostasis, probably largely alkali feldspar. No glass is present. Alteration products within the groundmass include khaki-coloured iddingsite and minor pale green chlorite. There is no flow lamination.

MINERAL CHEMISTRY

Minerals in a polished thin section cut from sample 62348 were analysed by electron microprobe on 'spot' mode. Results, recalculated to 100%, and cation formulae are given in Table 17.

Olivine

Olivine phenocrysts show slight to moderate normal zoning, with the composition of cores (mole% forsterite $Fo_{84–88}$) more magnesian than that of rims ($Fo_{86–77}$). The former overlaps with that of upper mantle olivine ($Fo_{88–90}$; e.g. Frey *et al.*, 1978, pp. 468–469). However, because of the euhedral form of many phenocrysts, they are considered to be the liquidus phase of an unfractionated primary magma that has rapidly ascended from the upper mantle, rather than xenocrysts of direct mantle origin.

The composition of the groundmass olivine ($Fo_{74–84}$) is similar to that of the phenocryst rims. Generally higher but variable CaO contents may be due to lower pressure during crystallisation (e.g. Simkin and Smith, 1970). Only the most iron-rich olivines contain detectable MnO.

Titanaugite

On the available data there are no consistent compositional differences between the titanaugite phenocrysts and groundmass titanaugite, into which they grade in size. All are relatively Mg-rich, calcic clinopyroxenes, with appreciable amounts of non-quadrilateral components, notably Al_2O_3 (5.7–11.6%) as well as TiO_2 (2.1–4.0%) and small amounts of Cr_2O_3 (≤0.66%) and Na_2O (≤0.65%). Structural formulae are calculated by normalising the analysis to four cations, distributing iron to Fe^{II} and Fe^{III} so that the oxygen number (O) equals 6 (i.e. total cation charge 12) and allocating aluminium to tetrahedral ($Si + Al^{IV}$) and octahedral sites so that both equal 2. This method is

5 cm

Table 17. ELECTRON PROBE MICROANALYSES, SAMPLE 62348 (ST HELENS AREA)

	olivine phenocrysts							olivine granules			
	1A	3A(core)	3B(rim)	4A(core)	4B(rim)	5A(core)	5B(rim)	6E	7A(core)	7N(rim)	7C
SiO_2	38.56	40.95	39.80	40.09	38.55	40.71	40.29	38.30	39.28	36.63	39.94
TiO_2	-	-	-	-	-	-	-	-	-	-	-
Al_2O_3	-	-	-	-	-	-	-	-	-	-	-
Cr_2O_3	-	-	-	-	-	-	-	-	-	-	-
ΣFeO	20.47	11.41	16.57	14.68	20.76	11.59	13.26	21.30	17.38	28.81	15.01
MnO	0.29	-	-	-	0.33	-	-	-	-	0.55	-
NiO	-	-	-	-	-	-	-	-	-	-	-
MgO	40.68	47.47	43.41	44.98	40.30	47.48	46.22	40.05	43.22	33.54	44.83
CaO	-	0.18	0.22	0.25	0.26	0.22	0.23	0.36	0.12	0.46	0.21
Na_2O	-	-	-	-	-	-	-	-	-	-	-
K_2O	-	-	-	—	-	-	-	-	-	-	-
P_2O_5	-	-	-	-	-	-	-	-	-	-	-
SO_3	-	-	-	-	-	-	-	-	-	-	-
Cl	-	-	-	-	-	-	-	-	-	-	-
Total	100.00	100.01	100.00	100.00	100.00	100.00	100.00	100.01	100.00	99.99	99.99
	Cations calculated on basis of (O) = 4										
Si	0.9943	1.0088	1.0052	1.0037	0.9916	1.0044	1.0021	0.9917	0.9968	0.9878	1.0018
Fe as Fe^{II}	0.4414	0.2350	0.3499	0.3074	0.4489	0.2392	0.2758	0.4611	0.3687	0.6499	0.3148
Mn	0.0063	-	-	-	0.0073	-	-	-	-	0.0127	-
Ni	-	-	-	-	-	-	-	-	-	-	-
Mg	1.5637	1.7428	1.6340	1.6785	1.5583	1.7460	1.7138	1.5456	1.6345	1.3483	1.6758
Ca	-	0.0046	0.0058	0.0067	0.0073	0.0059	0.0062	0.0099	0.0033	0.0134	0.0058
Cation total	3.0057	2.9912	2.9949	2.9963	3.0084	2.9955	2.9979	3.0083	3.0033	3.0121	2.9982
100 Mg/Mg + Fe	78.0	88.1	82.4	84.5	77.6	88.0	86.1	77.0	81.6	74.1	84.2

Table 17. ELECTRON PROBE MICROANALYSES, SAMPLE 62348 (ST HELENS AREA) – *continued*

	titanaugite phenocrysts			titanaugite in groundmass			
	2A	4C(core)	4D(rim)	6G	7E	7G	7J
SiO_2	47.12	45.37	46.15	48.57	46.96	46.88	44.06
TiO_2	2.29	2.54	2.29	2.16	2.50	2.49	3.96
Al_2O_3	8.12	11.59	8.94	5.74	7.47	7.55	9.94
Cr_2O_3	0.66	0.22	0.49	0.23	0.19	–	–
ΣFeO	5.56	6.63	6.70	6.60	6.74	6.89	7.88
MnO	–	–	–	–	–	–	–
NiO	–	–	–	–	–	–	–
MgO	13.05	12.27	12.46	13.46	13.17	13.03	10.94
CaO	22.86	20.73	22.70	22.93	22.56	22.83	22.77
Na_2O	0.36	0.65	0.27	0.31	0.40	0.33	0.46
K_2O	–	–	–	–	–	–	–
P_2O_5	–	–	–	–	–	–	–
SO_3	–	–	–	–	–	–	–
Cl	–	–	–	–	–	–	–
Total	100.02	100.00	100.00	100.00	99.99	100.00	100.01
	Cations calculated on basis of (O) = 6, Z = 4						
Si	1.7420	1.6738	1.7120	1.8005	1.7391	1.7374	1.6485
Al^{iv}	0.2580	0.3262	0.2880	0.1995	0.2609	0.2626	0.3515
Al^{vi}	0.0957	0.1777	0.1030	0.0514	0.0651	0.0673	0.0868
Cr	0.0193	0.0064	0.0144	0.0068	0.0057	–	–
Ti	0.0636	0.0705	0.0639	0.0602	0.0697	0.0694	0.1113
Fe^{III}	0.0413	0.0476	0.0623	0.0431	0.0795	0.0803	0.0749
Fe^{II}	0.1305	0.1569	0.1457	0.1616	0.1292	0.1331	0.1715
Mg	0.7188	0.6747	0.6889	0.7436	0.7272	0.7197	0.6099
Ca	0.9053	0.8196	0.9023	0.9110	0.8949	0.9064	0.9127
Na	0.0255	0.0467	0.0195	0.0224	0.0286	0.0238	0.0330
Cation total	4.0000	4.0001	4.0000	4.0001	3.9999	4.0000	4.0001
100 Mg/Mg + ΣFe	80.7	76.7	76.8	78.4	77.7	77.1	71.2

widely accepted, although very sensitive to analytical error (e.g. Robinson, 1980, pp. 421–422).

Substitution of Ti for divalent ions in the octahedral sites is probably coupled with the substitution of tetrahedral Al^{IV} for Si, equivalent to solid solution with the hypothetical pyroxene component $CaTiAl_2O_6$ (e.g. Yagi and Onuma, 1967; Carmichael *et al.*, 1974, pp. 273–275). However, in these pyroxenes this cannot account for all Al^{IV}, and octahedral Al^{VI} is also significant, suggesting that $CaAlAlSiO_6$ (calcium-Tschermak's pyroxene, CaTs) and $CaFe^{III}AlSiO_6$ (fassaite) are also important components. Na is probably also coupled with Al^{IV} as a minor $NaAlSi_2O_6$ (jadeite) component.

In contrast, titanaugites from the Tertiary alkali-olivine basalts of north-west Tasmania (Everard, 1989) and the Triassic alkali-olivine basalt near St Marys (Everard, 1987*a*) contain generally lower amounts of Al_2O_3 more strongly correlated with TiO_2 and little or no octahedrally co-ordinated Al. The reason for this difference is unclear. Because of the importance of non-quadrilateral components, these analyses have not been plotted in Figure 11.

Feldspar

The small plagioclase laths in the groundmass range in composition from intermediate andesine to sodic bytownite (An_{40-73}) but are probably mainly labradorite. Alkali feldspar is confined to the mesostasis and is too fine-grained to determine optically, but a single analysis suggests sanidine (Or_{43}). The small amount of ΣFeO present in both plagioclase and alkali feldspar may be due to minute inclusions of iron oxide and is common in volcanic feldspar. TiO_2, MgO and SO_3, where present, are also attributed to impurities.

Other minerals

A single opaque phase is present in the groundmass, probably titanomagnetite (i.e. a member of the cubic

Table 17. ELECTRON PROBE MICROANALYSES, SAMPLE 62348 (ST HELENS AREA) – *continued*

	plagioclase					alkali feldspar
	6C	6F	7K	7L	7M	6A
SiO_2	51.77	56.75	58.44	51.37	51.53	64.98
TiO_2	–	0.26	0.39	–	–	0.35
Al_2O_3	30.72	26.84	24.37	30.87	30.96	20.19
Cr_2O_3	–	–	–	–	–	–
ΣFeO	0.41	0.46	1.28	0.46	0.48	0.32
MnO	–	–	–	–	–	–
NiO	–	–	–	–	–	–
MgO	–	0.22	0.85	–	–	–
CaO	13.36	9.83	8.00	13.82	13.79	1.58
Na_2O	3.54	5.14	5.87	2.80	3.10	5.41
K_2O	0.20	0.51	0.81	0.15	0.13	7.18
P_2O_5	–	–	–	–	–	–
SO_3	–	–	–	0.53	–	–
Cl	–	–	–	–	–	–
Total	100.00	100.01	100.01	100.00	99.99	100.01
	Cations calculated on basis of (O) = 8					
Si	2.3569	2.5680	2.6756	2.3494	2.3466	2.9343
Ti	–	excl	excl	–	–	excl
Al	1.6483	1.4316	1.3148	1.6638	1.6620	1.0743
Fe	excl	excl	excl	excl	excl	excl
Mg	–	excl	excl	–	–	–
Ca	0.6518	0.4764	0.3925	0.6770	0.6730	0.0764
Na	0.3124	0.4511	0.5210	0.2482	0.2738	0.4737
K	0.0116	0.0294	0.0472	0.0089	0.0076	0.4134
Cation total	4.9810	4.9565	4.9511	4.9473	4.9630	4.9721
an	66.8	49.8	40.9	72.5	70.5	7.9
ab	32.0	47.1	54.2	26.6	28.7	49.2
or	1.2	3.1	4.9	1.0	0.8	42.9

Table 17. ELECTRON PROBE MICROANALYSES, SAMPLE 62348 (ST HELENS AREA) – continued

	titanomagnetite			apatite
	8A	8B	8C	7H
SiO_2	–	–	–	0.96
TiO_2	24.00	23.35	24.88	–
Al_2O_3	3.46	4.28	3.25	0.19
Cr_2O_3	0.66	1.10	0.45	–
ΣFeO	68.27	66.99	67.56	0.43
MnO	0.72	0.80	0.97	–
NiO	–	–	–	–
MgO	2.89	3.49	2.89	0.29
CaO	–	–	–	55.50
Na_2O	–	–	–	–
K_2O	–	–	–	–
P_2O_5	–	–	–	42.35
SO_3	–	–	–	–
Cl	–	–	–	0.29
Total	100.00	100.01	100.00	100.01
	Cations			
Si	–	–	–	excl
Ti	0.6395	0.6170	0.6641	–
Al	0.1444	0.1775	0.1358	excl
Cr	0.0185	0.0304	0.0126	–
Fe^{III}	0.5581	0.5581	0.5234	–
Fe^{II}	1.4651	1.4106	1.4819	excl
Mn	0.0217	0.0238	0.0291	–
Mg	0.1527	0.1826	0.1531	excl
Ca	–	–	–	3.0059
P	–	–	–	4.9853

titanomagnetite : cations calculated on basis of oxygen no (O) = 4, cation total (Z) = 3
apatite : cations calculated on basis of (O) = 12, (OH, Cl, F) = 1.

ulvospinel-magnetite solid solution series) of composition $Usp_{61}Mt_{39}$ to $Usp_{67}Mt_{33}$, but with appreciable MgO and Al_2O_3 contents. Ilmenite, as is usual in alkali basalts, is apparently absent; this is related to their low silica activity and the presence of titanaugite (e.g. Carmichael, et al, 1974, pp. 274–275).

A single, slightly impure analysis of apatite is also presented in Table 17.

GEOCHEMISTRY

The quantity of sample available was insufficient for a full chemical analysis. However, the major element composition of the basalt was estimated from the groundmass composition (average of three similar electron microprobe seams, each of 300 × 180 μm), the average olivine and titanaugite compositions (table 17),

Table 18. CHEMICAL ANALYSES AND PARTIAL ANALYSES, TERTIARY BASALTS, ST HELENS AND WELDBOROUGH AREAS

	A	B	C	D
SiO_2	47.26	46.2	45.9	45.8
TiO_2	2.27	2.0	2.2	2.5
Al_2O_3	16.06	13.6	14.2	15.2
ΣFeO	9.44	10.3	12.3	12.6
MnO	–	0.15	0.2	0.2
MgO	8.37	13.0	10.4	8.6
CaO	11.60	10.6	10.3	9.6
Na_2O	3.61	3.0	2.9	3.6
K_2O	0.60	0.50	1.0	1.1
P_2O_5	0.79	0.65	0.64	0.8
Total	100.00	100.0	100.0	100.0
100 Mg/Mg + Fe*	64.2	71.8	63.1	58.0

A: Groundmass composition of 62348 : average of three 300 μm × 180 μm microprobe scans.

B: Estimated whole rock composition of 62348 : 82 mass% groundmass + 13 mass% average olivine + 5 mass% average titanaugite.

C: Analysis 735125, Tertiary basalt, Weldborough Pass [EQ812356], recalculated to 100% (Brown and McClenaghan, 1982).

D: Average of seven relatively unaltered basalts, Weldborough Pass area, recalculated to 100% *(ibid)*.

and the modal composition of the rock. MnO was arbitrarily set at 0.15%. Estimates are given in Table 18.

The estimated whole-rock composition (column B) plots in the alkali-olivine basalt field in a total alkali-silica diagram (fig. 12), consistent with petrographic evidence. The Mg number (100 Mg/Mg + Fe^{II}), calculated assuming Fe_2O_3/FeO = 0.15, is 64.2 in the groundmass and, although very dependent on the estimates of the proportion and average composition of olivine phenocrysts, about 71–72 in the whole rock. This suggests that the basalt has a primitive composition, and represents a primary magma derived from partial melting of upper mantle, followed by rapid ascent to the surface without appreciable crystal fractionation. This is consistent with the highly magnesian (Fo_{88}) composition of the cores of the olivine phenocrysts. The low K_2O relative to Na_2O is also noteworthy, but may be attributable to an inaccurate estimate of composition.

DISCUSSION

Petrographically and chemically similar Tertiary basalts occur about 15–20 km to the WNW, near Weldborough Pass in the Ringarooma Quadrangle (Brown *et al.*, 1977; Brown and McClenaghan, 1982). The most similar analysis (column C) and an average of seven analyses (column D) are recalculated to 100% and quoted in Table 18 for comparison. All are sodic alkali-olivine basalts, although somewhat more fractionated (lower MgO and Mg number) than sample 62348. Petrographically, these basalts show some textural variation, but thin sections 72/404 [EQ799352] and 73/518 [EQ804370] in particular closely resemble sample 62348.

The basalts near Weldborough are deeply dissected by erosion, and either rest directly on granitic basement or, south of Weldborough Pass and west of Mt Littlechild, lie on up to 150 m of basaltic agglomerate, suggesting feeders at these localities (Brown and McClenaghan, 1982). There is an outlier of basalt about 3 km to the south-east, around EQ831335. Sutherland and Wellman (1986) have dated these basalts from the Weldborough area, using the K-Ar method, at 46.2 ± 0.6, 47.4 ± 0.5 and 47.2 ± 0.6 Ma (Early Eocene).

The basalts from near the bottom of Thureau's Deep Lead, St Helens Quadrangle, described herein, are considered to be the remnants of flows, now completely concealed beneath younger sediments or removed by erosion, which erupted near Weldborough Pass and flowed eastward for more than 20 km down the valley of the ancestral George River. Spores from a sample of Tertiary sediment collected by M. J. Longman from a creek bank on Thureau's Deep Lead at EQ984269 indicated an Early Oligocene age. As basalt in the adjacent bore hole no. 16 is 7–10 m lower, and there is evidence for an erosional break between extrusion of the basalt and recommencement of sedimentation, this represents a minimum age for the basalt (Jack, 1964), and is consistent with the radiometric ages at Weldborough Pass.

METAMORPHISM OF THE MATHINNA BEDS

M. P. McClenaghan

Regional metamorphism

The Mathinna Beds have undergone partial recrystallisation (Cocker, 1982). Quartz is the dominant detrital mineral with minor feldspar and muscovite comprising less than 10%. The original clay rich matrix has been recrystallised to muscovite and chlorite and the planar alignment of these minerals define the cleavage. The lack of critical rock compositions do not allow a precise assessment of metamorphic conditions however, it appears that the rocks have been subject to low-grade regional metamorphism. Rb/Sr isotope measurements by Cocker (1982) gave a 401±7 Ma age for the Mathinna Beds regional metamorphism.

Contact metamorphism

The Mathinna beds have been contact metamorphosed during the emplacement of the granitoids. The hornfels is medium- to dark-grey recrystallised rock with pelitic horizons showing spotting up to 8 mm in diameter. The spots consist of fine recrystallised quartz and muscovite set in a granoblastic matrix of quartz with minor muscovite, biotite and opaque mineral. The fine-grained muscovite in the spots may be after cordierite. Representative mica compositions from the hornfels are presented in Table 19. The width of the metamorphic aureoles is discussed in the section on structure in the granitoids.

Thermal metamorphic aureole of Catos Creek dyke

N. J. Turner

Near the southern edge of St Helens quadrangle the dip of the western contact of Catos Creek dyke against the

Mathinna Beds can be estimated from the trace of the contact across the steep topography. Dip values of 45°W, 35°W, and 45°W were determined. Combined with the width of 1.7 km for the metamorphic aureole in the Mathinna Beds, these dip values imply an aureole thickness of about 1.2 km.

In comparison, a dip of 45° for the contact of the Mathinna Beds against the Poimena Pluton in Ringarooma quadrangle corresponds to an estimated aureole thickness of about 1.6 km (Turner *in* McClenaghan *et al.*, 1982). The Poimena Pluton represents a very large metamorphosing mass and even though the aureole thickness for Catos Creek dyke is 25% less than for the Poimena Pluton aureole in Ringarooma quadrangle, it seems likely that the metamorphosing mass was still substantial. Thus, Catos Creek dyke probably represents the upper part of a relatively large, subsurface granitoid body.

Close to the western contact of Catos Creek dyke metamorphism in the Mathinna beds corresponds to the pyroxene hornfels facies. Indicative pelitic assemblages comprise poikiloblastic cordierite, relatively uncommon columnar aggregates of andalusite, ?orthoclase, biotite, muscovite, quartz, green to brownish-green tourmaline and opaque minerals. Cordierite is quite fresh in some rocks but exhibits strong retrogression to fine-grained pale green mica in others. A little chlorite is generally present and probably also reflects retrogression, probably of biotite. Thin migmatite veinlets are present in some places [e.g. EQ955086, EQ942099].

The proportions of the various metamorphic minerals vary greatly, as do the textures of the rocks. Quartzose sandstone has been metamorphosed to fine-grained, even grained quartzite whereas siltstone and mudstone metamorphose to mottled or spotted schist. Metamorphism diminishes progressively away from the contact with the outer parts of the aureole being characterised by spotted slate and relatively unaltered sandstone.

Table 19. REPRESENTATIVE MICA ANALYSES FROM HORNFELSED MATHINNA BEDS ROCKS (SDsm)

		muscovite	biotite	
No.		MSH199-2/1	MSH200-1/6	MSH25-1/2
SiO_2		52.45	35.61	34.46
TiO_2		0.39	2.32	2.36
Al_2O_3		29.26	18.41	17.10
Cr_2O_3		0	0	0
Fe_2O_3		0	0	0
FeO		1.64	20.87	21.13
MnO		0	0	0.44
MgO		1.90	9.27	10.15
CaO		0	0	0
Na_2O		0	0	0
K_2O		9.78	9.57	10.47
H_2O		4.57	3.94	3.89
			O = 22	
Tet	Si	6.882	5.416	5.318
	Al	1.118	2.584	2.682
	Σ	8	8	8
Oct	Al	3.408	0.718	0.429
	Ti	0.039	0.266	0.274
	Fe^{+2}	0.180	2.654	2.727
	Cr	0	0	0
	Mn	0	0	0.058
	Mg	0.371	2.100	2.334
	Σ	3.998	5.738	5.822
	Ca	0	0	0
	Na	0	0	0
	K	1.637	1.858	2.061
	Σ	1.637	1.858	2.061
	OH	4	4	4
	Mg	0.67	0.44	0.46

$Mg^* = Mg/(Mg + Fe^{+2})$.
O is the oxygen number used to calculate the structural formulae.

Figure 14. Structural domains in Mathinna Beds from the northern part of the map sheet. Line of structural profile indicated.

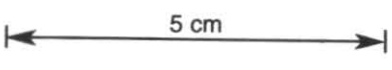

STRUCTURE

Mathinna Beds

NORTHERN PART OF THE ST HELENS MAP

M. P. McClenaghan

The structure of the Mathinna Beds is described by dividing its area of outcrop into a number of domains (fig. 14).

Domain 1 lies in the north-west part of the map sheet and forms part of a sedimentary country rock screen between granitoid bodies. All the rock in the domain is strongly hornfelsed. Bedding in the area strikes west of north and dips steeply east and west (fig. 15). No fold hinges were measured but hinges calculated from adjacent oppositely dipping bedding readings suggest that folds plunge at 3° to 346°. Cleavage has a similar strike to bedding and also dips steeply east and west (fig. 16). It is best developed in the pelitic units. This data is consistent with folds having steep axial surfaces, long relatively planar limbs and sharp closures. Reversals of dip within 100 m indicate folds with wavelengths less than that distance.

Domain 2 is to the south of Domain 1 and includes sedimentary rock forming a screen between granitoid bodies and also rock marginal to a granitoid body. The rocks in the screen area and close to the granitoid body are strongly hornfelsed. Bedding generally strikes north with steep dips to east and west (fig. 17). Cleavage is well developed throughout the domain and generally strikes close to north with steep dips to east and west (fig. 18). As for Domain 1 the data is consistent with folds having steep axial surfaces, long relatively planar limbs and sharp closures.

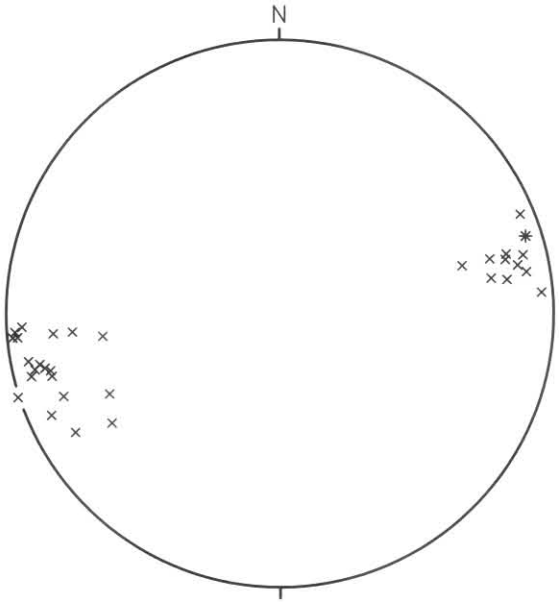

Figure 15. Stereoplot of poles to bedding for Domain 1. × way up unknown; ✳ right way up.

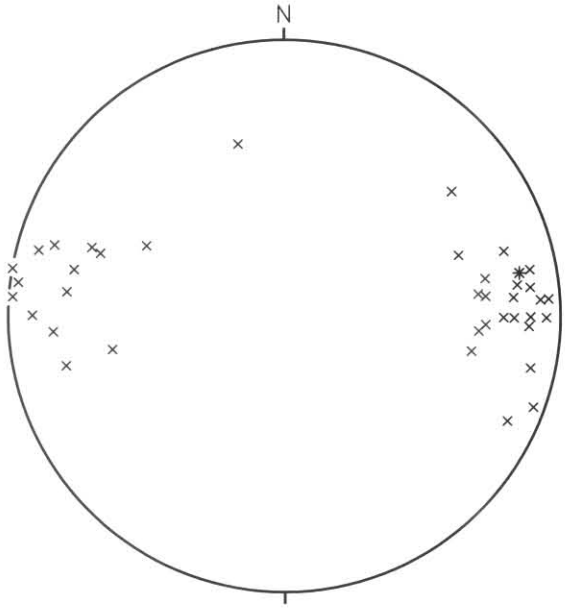

Figure 17. Steroplot of poles to bedding for Domain 2 × way up unknown; ✳ right way up.

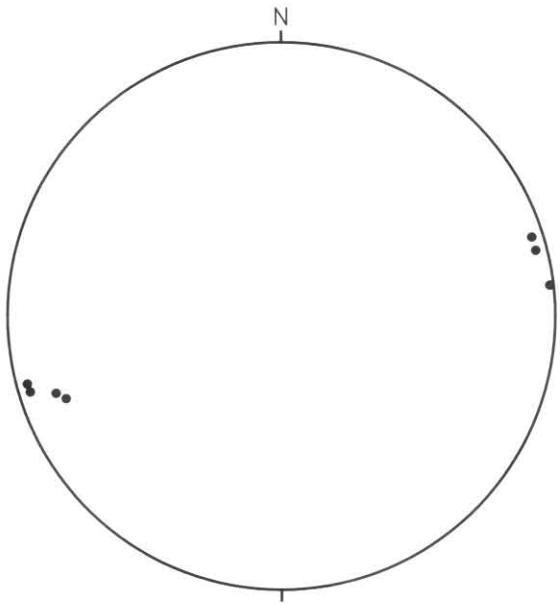

Figure 16. Stereoplot of poles to cleavage for Domain 1.

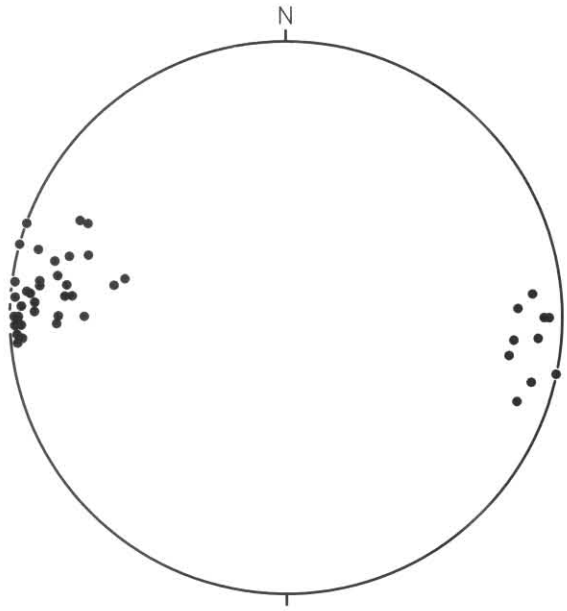

Figure 18. Stereoplot of poles to cleavage for Domain 2.

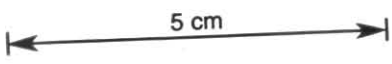

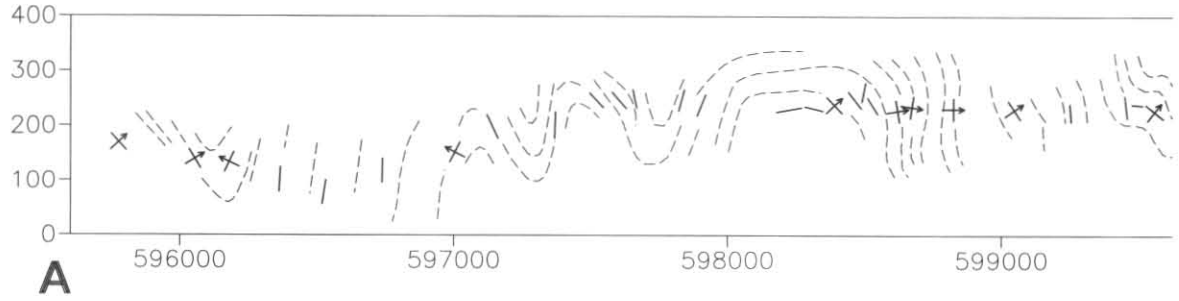

Figure 25. Structural profile along grid line 5415000mN. / bedding attitude; / extrapolated bedding attitude.

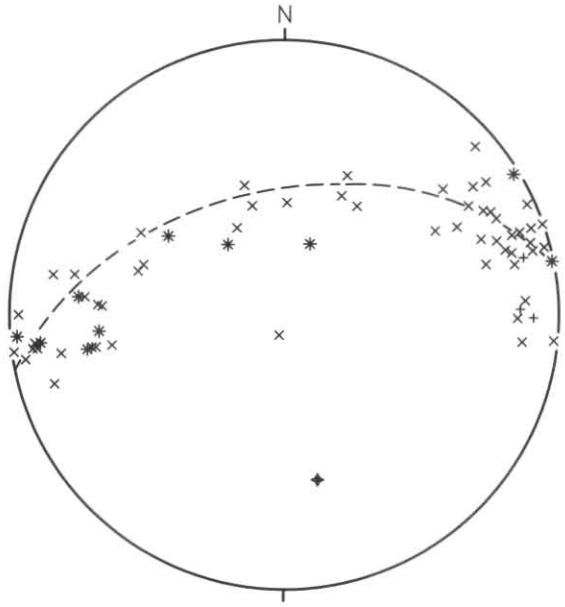

Figure 19. Stereoplot of poles to bedding for Domains 3–6. × way up unknown; ⁎ right way up; + overturned; ✦ statistically-defined fold axis 168°/39°SE. Σ deviation^2 per reading = 0.0814.

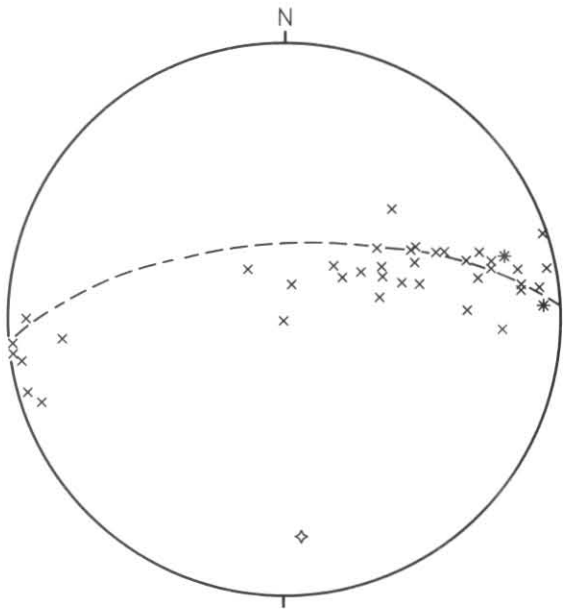

Figure 21. Stereoplot of poles to bedding for Domain 7. × way up unknown; ⁎ right way up; ✧ statistically-definedl fold axis 175°/23°SE. Σ deviation^2 per reading = 0.1337.

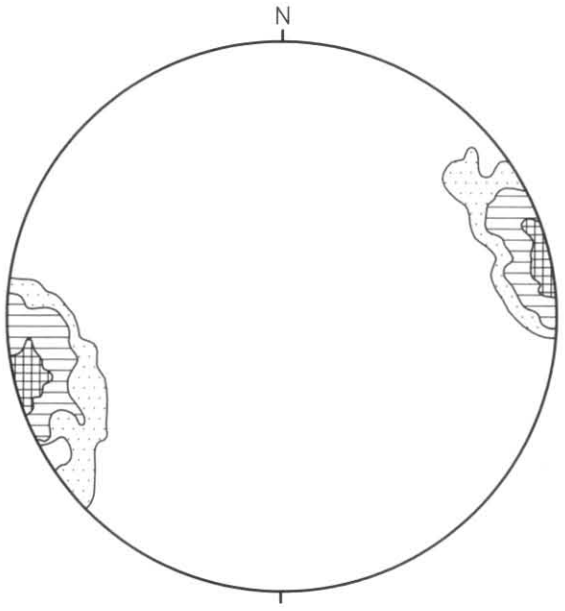

Figure 20. Stereoplot of 71 poles to cleavage for Domains 3–6. Contour intervals: 1–6%, 6–15%, ≥15%.

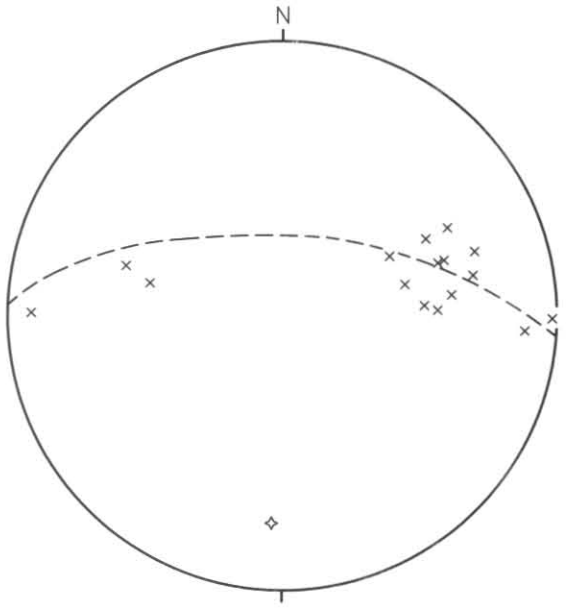

Figure 22. Stereoplot of poles to bedding for Domain 8. × way up unkwown; ✧ statistically-defined fold axis 183°/26°SW. Σ deviation^2 per reading = 0.0879.

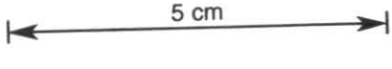

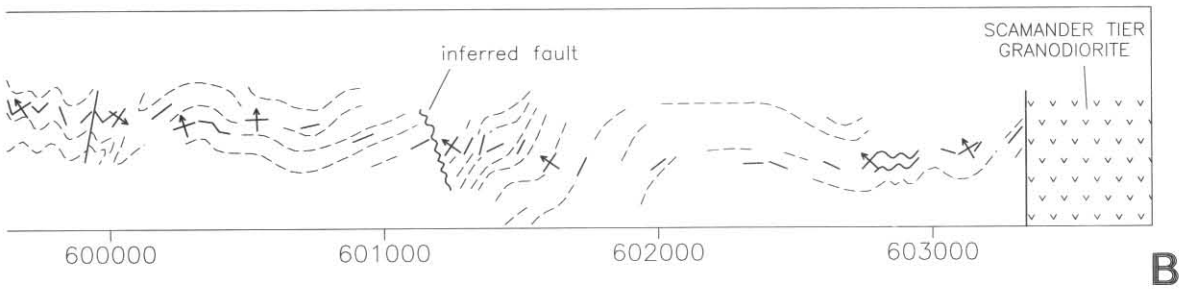

† direction of younging. Profile prepared by P. R. Williams.

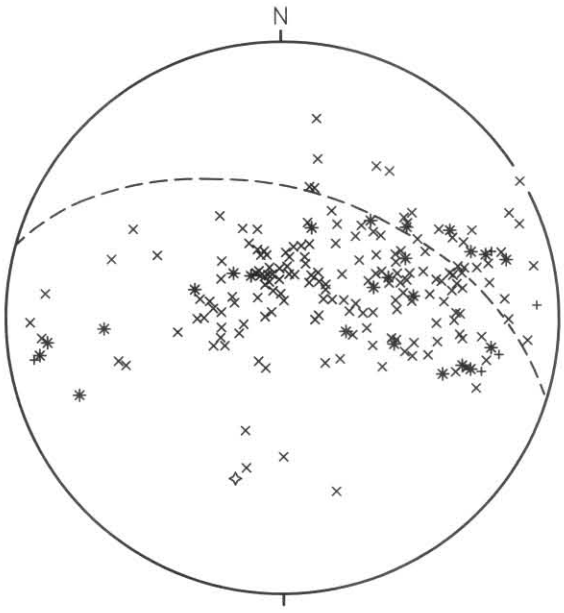

Figure 23. Stereoplot of poles to bedding for Domain 9. × way up unknown; ⁎ right way up; + overturned; ◇ statistically-defined fold axis 197°/40°SW. S deviation^2 per reading = 0.4142.

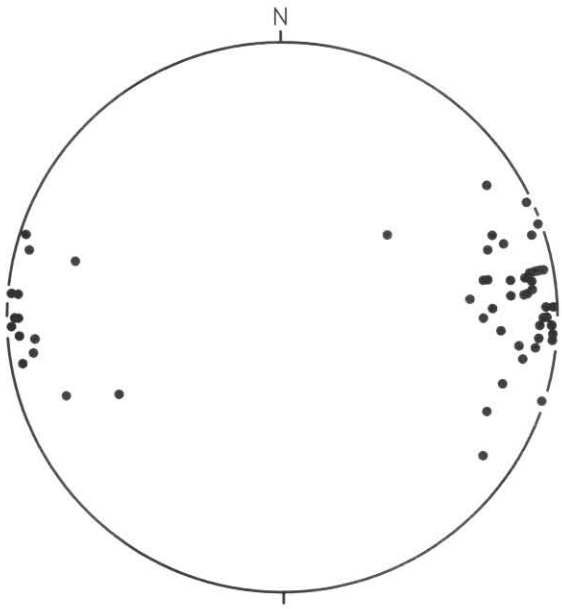

Figure 24. Stereoplot of poles to cleavage for Domain 9.

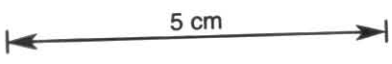

Domains 3, 4, 5 and 6 lie on the southern margin of a large granitoid body which on the basis of outcrop pattern is believed to dip at a moderate south and east angle beneath the Mathinna Beds. Most of the rock within the domains is strongly hornfelsed. Bedding in these domains strikes generally slightly west of north with mostly steep dips east and west, westerly dips being slightly more common (fig. 19). Statistically defined fold axes for these domains plunge slightly east of south at moderate angles and the fold axis for the combined bedding data plunges at 39° to 168° (fig. 19). This direction is consistent with the attitude of hinges of two minor folds (plunge of 31° and 31° to 165° and 162°) from domain 6. Cleavage strikes generally slightly west of north with mostly steep dips to the east and west (fig. 20).

Domain 7 lies north of domain 6 and on the easter margin of a large granitoid body. The granitoid dips at a low angle beneath the domain as is shown by the window of granitoid in Constable Creek at EQ995215. Bedding strikes generally north-west with steep dips to the north-east and gentle to steep dips to the south-west (fig. 21). A statistically defined fold axis to the bedding readings plunges at 23° to 175°. Due to the strong hornfelsing cleavage was not recorded in this domain.

Domain 8 lies 2 km to the east of the domain 7 and also consists of strongly hornfelsed Mathinna Beds. Bedding generally strikes slightly west of north and mostly dips at moderate angles to the south-west (fig. 22). A statistically defined fold axis to the bedding readings plunges at 26° to 183°.

Domain 9 lies at a greater distance from the same granitoid body and is in non-hornfelsed Mathinna Beds. Bedding has variable strike and low to moderate dips. A poorly defined statistical fold axis to the bedding readings plunges at 40° to 197° (fig. 23). Cleavage generally strikes north with steep dips to the east and west with dips to the west being more common (fig. 24).

In domain 6 at EQ985156 and EQ987156 a cleavage occurs (P.R.W) which is steeper than overturned bedding indicating that a second cleavage is present. Folds related to this second event are present in the shallowly dipping area of domain 9 (P.R.W).

A structural profile drawn along an east-west line adjacent to Domains 4, 5, 6 and 9 is presented in Figure 25 (P.R.W). The western part of the profile corresponds to domain 4, 5 and 6 and has folds with steep axial surfaces, long relatively planar limbs an steep closures. Major order folds appear to have wavelengths 0.5–1 km and minor folds of wavelength about 5–10 m also occur. The generally flat bedding in the eastern part of the profile may correspond to a culmination in a large antiformal structure.

SOUTHERN PART OF ST HELENS MAP

N. J. Turner

Data

Structurally fairly homogeneous sub-areas in the southern part of St Helens quadrangle and in the adjacent part of St Marys quadrangle are shown in Figure 26. Lambert projections of data from the sub-areas in St Helens quadrangle are shown in Figures 27–39. These projections contain data additional to that shown on the St Helens map, particularly for Sub-areas 9 and 10A and the northern part of Sub-area 8.

Lambert projections of data from the sub-areas in St Marys quadrangle numbered 3B, 4B and 4C in Figure 26 are respectively shown in Figures 37 and 39, Figures 36 and 39 and Figure 35 of Turner and Calver (1987). Projections of selected data from the St Marys Porphyrite are given for comparative purposes in Figures 40 and 41 of this report.

Dominant folds

In most sub-areas fold limbs display moderate to steep dips and may be overturned towards the east, rarely towards the west. Fold closures are usually tight, commonly in the range 45–90°. The limbs vary considerably in horizontal width ranging from less than 10 m (e.g. parts of Sub-area 10) to more than one kilometre (e.g. Sub-area 5).

Slaty cleavage is associated with the folds, though in parts of Sub-areas 4A, B and C the cleavage can be difficult to discern. The slaty cleavage dips steeply either west or east and fans at fold closures. Cleavage trends and fold axis derived from the Lambert projections of bedding display concordance within the accuracy of the estimations, in contrast to some structural subdivisions in Ringarooma quadrangle (Turner *in* McClenaghan *et al.*, 1982).

Late folds

Axes of the dominant folds in the various sub-areas in the Mathinna Beds plunge SSW to SSE (south-east in Sub-area 2) at shallow angles ranging from 6° to 20°. This variation in orientation between sub-areas may be due to an episode of large-scale kink folding such as occurs in the southern part of St Marys quadrangle (Turner and Calver, 1987) and to the west in the Alberton quadrangle (Goscombe and Findlay, 1989). Late minor structures that are consistent with such an episode include uncommon, locally-developed kink bands, chevron folds and rare, weakly-developed crenulation cleavage (fig. 26). The chevrons and crenulation cleavage indicate that the maximum principal stress was oriented approximately NNE-SSW.

Timing of the late folding event is unclear. The apparent absence of rotated segments in the intrusive, western contact of Catos Dyke suggests that the folding predated the dyke. However, the inferred sinistral transverse movement of the NE-trending fault which cuts Catos Dyke and Scamander Tier Dyke is consistent with a roughly N-S maximum principal stress and may imply a post-dyke age for all strains related to this maximum stress direction.

Relationship of dominant folds to the St Marys Porphyrite

Structures in the Mathinna Beds beneath the extrusive part of the St Marys Porphyrite were described in detail in Turner and Calver (1987). A surprising implication was that a substantial part of the shortening related to short wavelength folds in the Mathinna Beds occurred after emplacement of the St Marys Porphyrite. The further mapping in St Helens quadrangle has not resolved this issue.

Of particular interest is the structural zone in Sub-areas 3A and 3B of Figure 26 which is directly beneath the porphyrite body. In Sub-area 3B in St Marys quadrangle detailed mapping (fig. 34 of Turner and Calver, 1987) has shown a broad, open syncline free of parasitic folds and with little cleavage development. This syncline is unconformably transected by the base of the porphyrite body. Further mapping in St Helens quadrangle has shown that the syncline extends north into Sub-area 3A where the Lambert projection of bedding defines a fold axis plunging 35° to 194° (fig. 29), a result indistinguishable from the fold axis in Sub-area 3B which plunges 34° to 188° (fig. 32 of Turner and Calver, 1987).

The syncline is exposed over an area measuring 3 km transverse to the axis and about 2 km parallel to the axis. Along the axis towards the south the syncline disappears beneath the St Marys Porphyrite. To the north its simple structure dissipates transitionally near the northern edge of Sub-area 3A where short wavelength folds become evident. These folds are common beyond the northern edge of Sub-area 3A. West of Sub-area 3B, in Sub-area 4B, short wavelength folds are also common (fig. 34 of Turner and Calver, 1987). In this case the boundary with Sub-area 3B is sharp rather than transitional, apparently corresponding to a thin breccia interval at EQ994037. Structural relationships east of Sub-areas 3A and 3B are not well established, partly due to poor outcrop, though it is clear that short wavelength folds are present in the area.

Overall, the pattern of folding in the Mathinna Beds below the St Marys Porphyrite and its relationship to the base of the porphyrite body suggests that the simple, SSW trending syncline in Sub-areas 3A and 3B is in a zone that was structurally protected by the porphyrite during the episode which produced the SSW-SSE, short wavelength folds in Sub-areas 4A and 4B. However, it is very difficult to accept that the short wavelength folds are entirely post-porphyrite, particularly since similar structures are cross cut by older(?) granitoid boundaries elsewhere (e.g. north of Sub-area 6). Nevertheless, it is equally difficult to accept that the pattern of short and long wavelength folds below the porphyrite is entirely coincidental.

It is clear from fold structures within the porphyrite (fig. 26, 41, 42) that post-emplacement shortening occurred in response to a maximum principal stress with similar orientation to the WSW-ENE compression indicated by the folds in Sub-areas 4B and 4C. Qualitatively, the amount of shortening in the porphyrite body that is related to the folding appears small in comparison to total shortening in the Mathinna Beds because the folds have relatively long wave lengths and relatively gentle limb-dips (Turner *et al.*, 1984).

There may be an extra component of shortening in the porphyrite body which is due to mylonitic shears though these shears and the folds may be related strains. The geometry of the shears has not been established, nor has an estimate been made of the total displacement caused by them. Similar structures in the Piccaninny Creek Adamellite (Turner and Calver, 1987) and in granodiorite at Piccaninny Point (Gee and Groves, 1974) appear to be related to roughly E-W compression. Thus the mylonitic shears in the St Marys Porphyrite may be related to the folds. The relative abundance of shears in the general area of the axial zone of the fold which cuts the basal contact of the porphyrite appears to support this view.

A full understanding of the relative development of structures in the Mathinna Beds and in the St Marys Porphyrite requires the quantitative assessment of shortening in both units and the careful evaluation of possible décollement movement at, or near, the contact and between Sub-areas 3A and 3B and Sub-areas 4A and

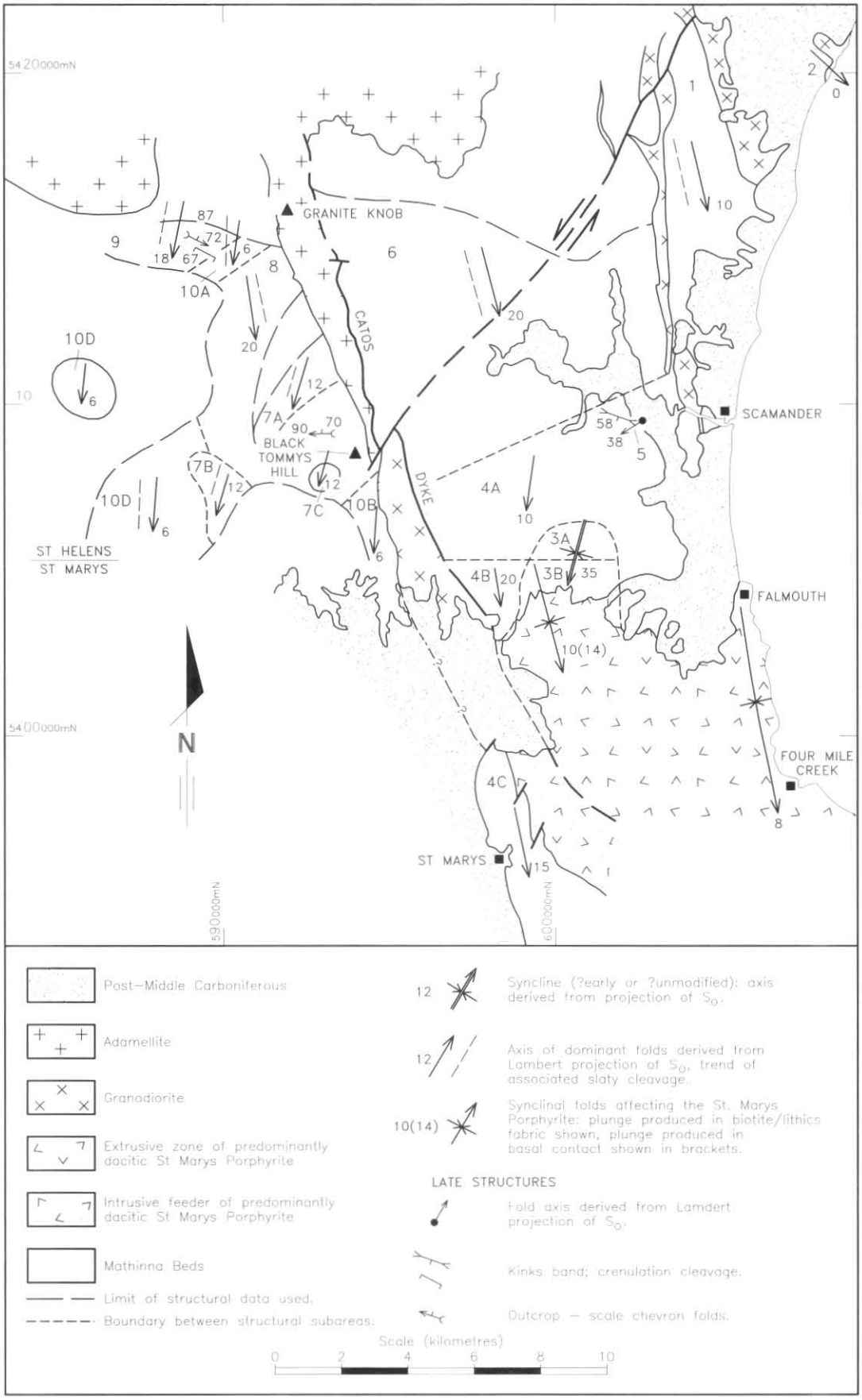

Figure 26. Map showing the major geological units and structural data in the southern part of St Helens quadrangle and the northern part of St Marys quadrangle. Structural sub-areas in the Mathinna Beds are shown along with fold axis and cleavage trends derived from Lambert projections. Lambert projections for the sub-areas in St Marys quadrangle are given in Turner and Calver (1987) as Figure 35 (Sub-area 4C), Figure 36 (Sub-area 4B), Figure 37 (Sub-area 3B) and Figure 39 (Sub-areas 4B, 3B). Data relating to the folds in the St Marys Porphyrite are derived from Turner *et al.* (1984) and projections are shown in Figures 40 and 41 of this report. Chevron folds and crenulation cleavage in the Mathinna Beds represent single field measurements.

4B. Determination of the structural/metamorphic overprinting relationships in the aureole of the porphyrite's feeder, which includes the granodioritic part of Catos Dyke, would probably be complementary in terms of establishing relative timing of events. The possible relevance of relatively highly strained rocks (plate 20 of Turner and Calver, 1987) just above the western segment of the porphyrite's basal contact also needs to be evaluated.

In the Mathinna Beds north-east of Forester, in the Ringarooma quadrangle, there is a structural/ metamorphic sequence which may have its equivalent in the relationships between folds in the Mathinna Beds and in the St Marys Porphyrite. Around Forester the Mathinna Beds display slaty cleavage of generally NW-NNW trend which is overprinted by metamorphic spots in pelites in the aureoles of the nearby granitoids (Turner in McClenaghan *et al.*, 1982). A second, post-metamorphic period of flattening on the same NW-NNW trend is revealed by deflection of external cleavage around the metamorphic spots. This late NW-NNW phase is more precisely revealed by postmetamorphic crenulation in a one kilometre long domain north-east of Forester (fig. 47 of Turner *in* McClenaghan *et al.*, 1982) where an intermediate structural episode of major kink folding caused rotation of the early slaty cleavage to north-east trend. A similar relationship occurs in unmetamorphosed rocks to the north of Forester, in Boobyalla quadrangle (Turner *in* McClenaghan *et al.*, 1982).

The occurrence of pre-granitoid and post-granitoid phases of compression on similar trends is consistent with the similar orientation of structures in the Mathinna Beds and

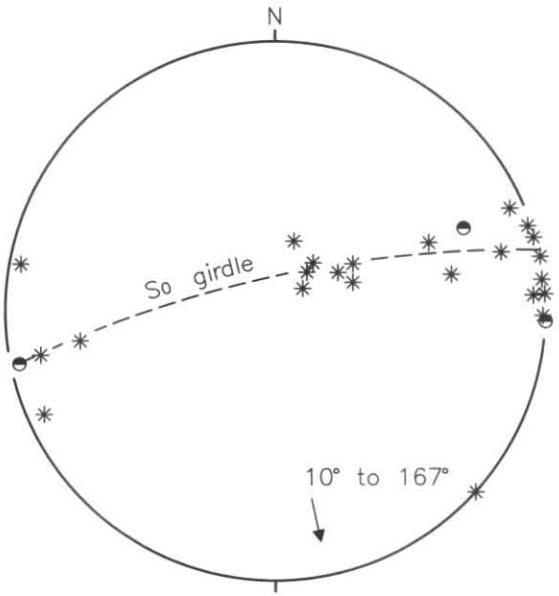

Figure 27. Lambert projection of bedding (✳) and slaty cleavage (◓) measurements in Sub-area 1 of the Mathinna Beds.

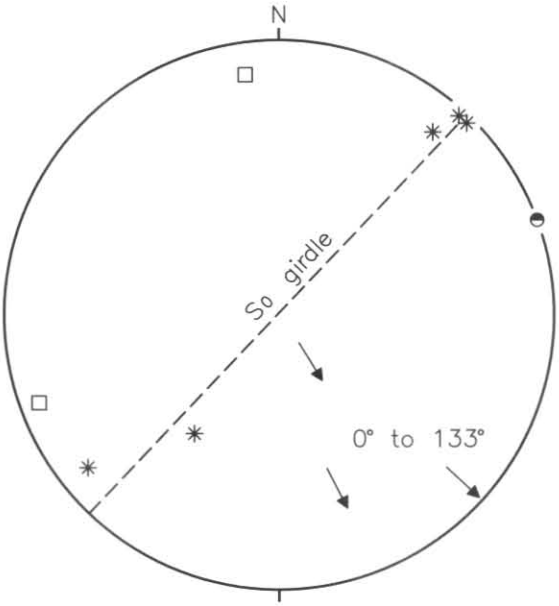

Figure 28. Lambert projection of bedding (✳), slaty cleavage (◓) and folds (□ axial surface, ↑ plunge of axis) in Sub-area 2 of the Mathinna Beds. Locally developed, discordant structures in the Mathinna Beds which are associated with the granodiorite intrusion near EQ691203 are described in detail by Gee and Groves (1971).

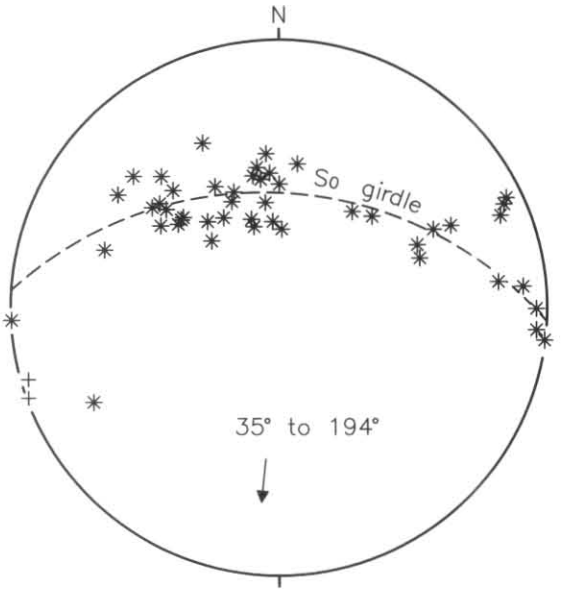

Figure 29. Lambert projection of bedding (✳, + overturned) in Sub-area 3A of the Mathinna Beds.

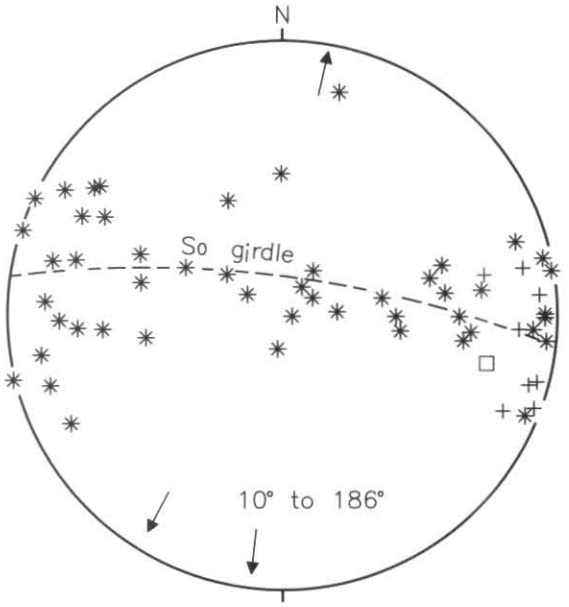

Figure 30. Lambert projection of bedding (✳, + overturned) and folds (□ axial surface, ↑ plunge of axis) in Sub-area 4A of the Mathinna Beds.

5 cm

the St Marys Porphyrite. The later phase would have led to modification of the pre-existing fold pattern in the Mathinna Beds around the porphyrite body. Modification of the simple syncline in Sub-areas 3A and 3B is evident where an extension of the fold affecting the St Marys Porphyrite has tightened its western limb (fig. 26). The amount of modification of fold profiles in Sub-areas 4A and 4B and thus the contribution of any late compressive phase to the overall pattern of folding, is yet to be determined. Since the folds in the Mathinna Beds and porphyrite display similar values of plunge, it seems that most or all of the regional southerly plunge of folds in the Mathinna Beds resulted from tilting which post-dated emplacement of the St Marys Porphyrite.

Deformation associated with intrusion of Dbgsp

The SE-trending structure of Sub-area 2 (fig. 26) is represented in Figure 28. Minor folds which are strongly discordant to this trend occur in a restricted zone of about 200 m length on the coast north of Dianas Basin near EQ691203. The restricted zone is adjacent to the contact with the granodioritic St Helens Pluton and the discordant folds are attributed to lateral pressure exerted by the granodiorite during emplacement (Gee and Groves, 1971).

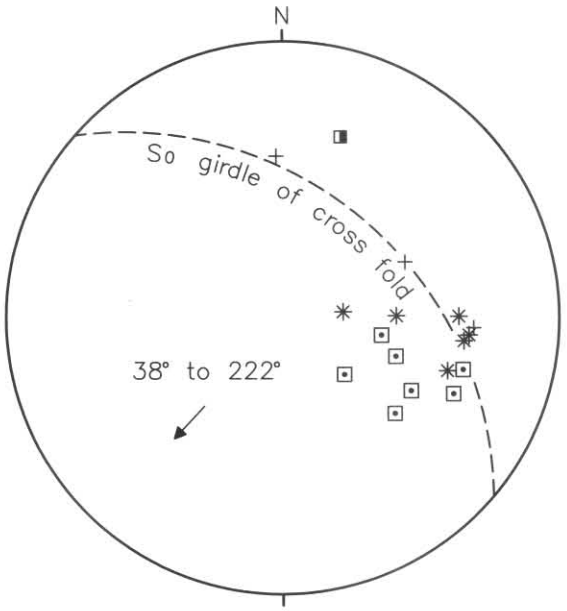

Figure 31. Lambert projection of bedding in Sub-area 5 of the Mathinna Beds. This subarea extends along the Upper Scamander Road from EQ033086 to EQ021101 through a succession which dips and faces west. At EQ029091 there is an open cross fold (+) whose axis is shown in the figure. For about 700 m north-west of this closure the strike is rotated slightly to the north-east (⊡) compared with the strike at either end of the road section (✳). This variation probably also reflects gentle refolding.

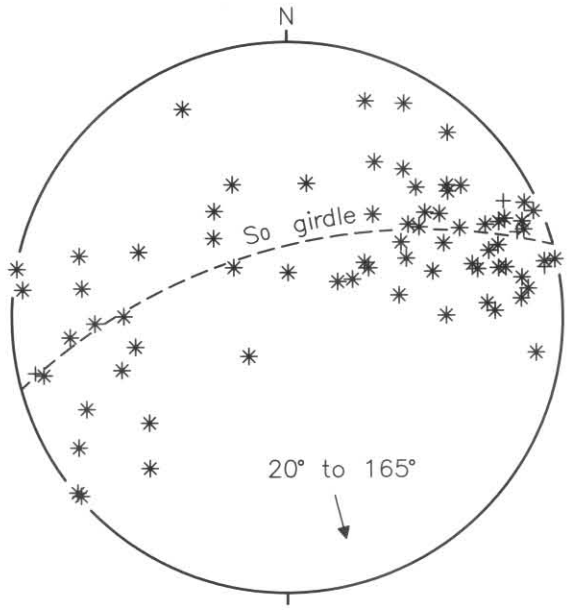

Figure 32. Lambert projection of bedding (✳, + overturned) in Sub-area 6 of the Mathinna Beds.

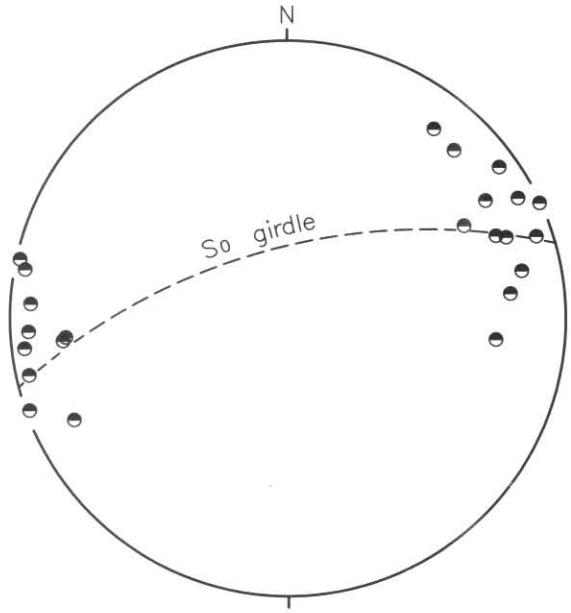

Figure 33. Lambert projection of slaty cleavage in Sub-area 6 of the Mathinna Beds.

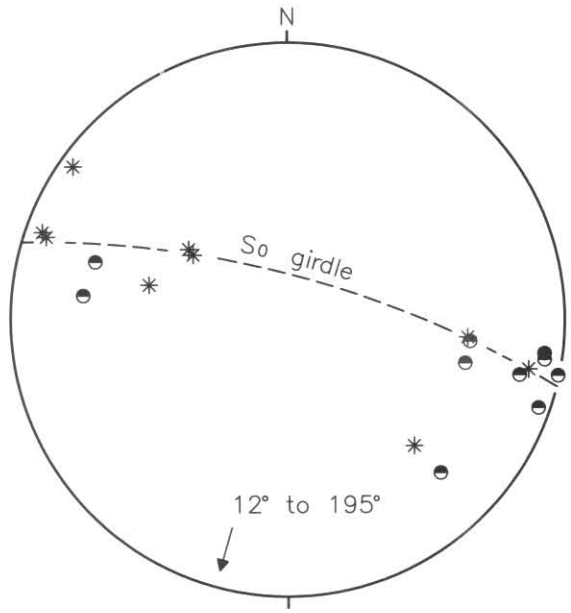

Figure 34. Lambert projection of bedding (✳) and slaty cleavage (◓) in Sub-areas 7A, B, C of the Mathinna Beds. These three sub-areas are grouped on the basis of similar cleavage trends.

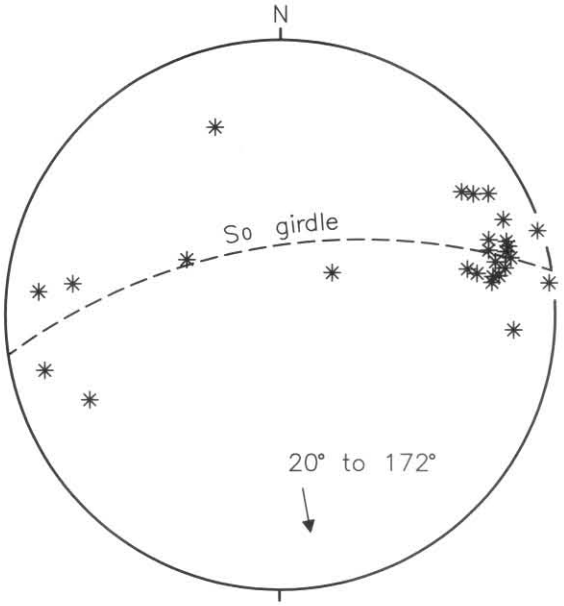

Figure 35. Lambert projection of bedding in Sub-area 8 of the Mathinna Beds.

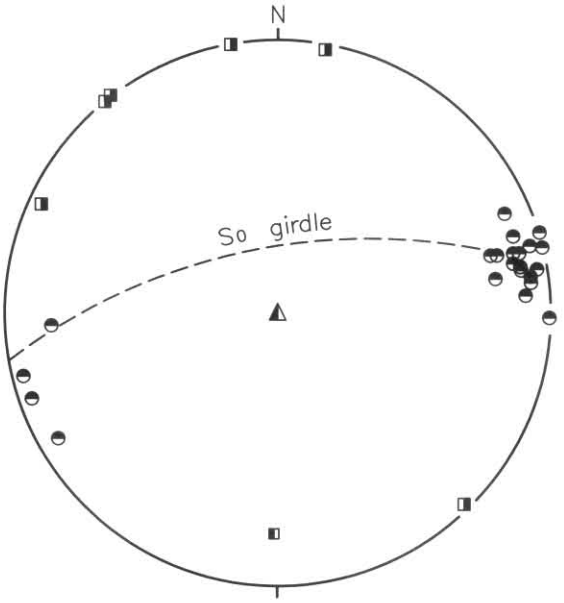

Figure 36. Lambert projection of slaty cleavage (◓), kink bands (◨) and chevron folds (▲ axial surface, ◧ plunge of axis) in Sub-area 8 of the Mathinna Beds.

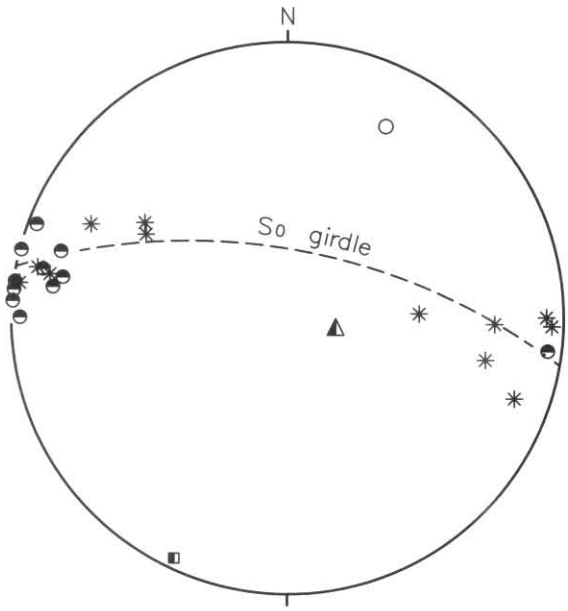

Figure 37. Lambert projection of bedding (✳), slaty cleavage (◓), crenulation cleavage (○) and chevron folds (◧ axial surface, ▲ plunge of axis) in Sub-area 9 of the Mathinna Beds.

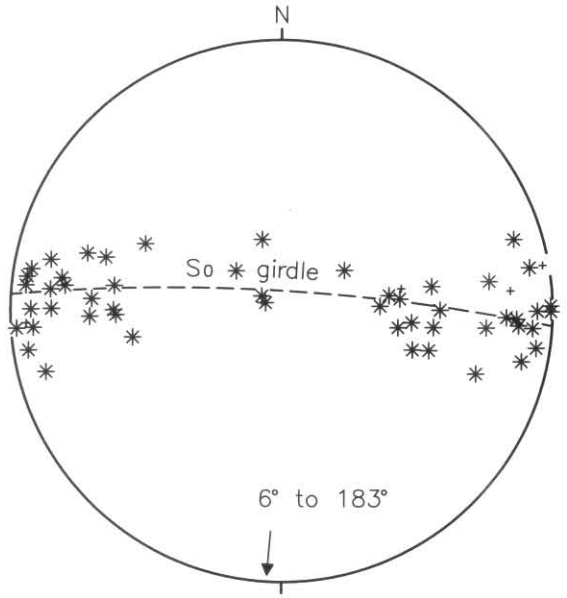

Figure 38. Lambert projection of bedding (✳, + overturned) in Sub-areas 10A, B, C, D of the Mathinna Beds. These four sub-areas are grouped on the basis of similar cleavage trends.

Granitoid rocks

M. P. McClenaghan

INTERNAL STRUCTURE

In the Georges Bay area the very abundantly K-feldspar porphyritic biotite granite (Dbrpc) rock type shows numerous approximate alignments of feldspar phenocrysts on horizontal surfaces defining an apparent lineation. Alignments on non horizontal surfaces were not sufficiently clear to show whether the alignments are the result of a foliation or a lineation. The trend of the apparent lineations has a strong maximum at 100–110° (fig. 42). In the same rocks and in the sparsely porphyritic biotite granodiorite rock type (Dbgbsp) zones of closely spaced approximately vertical jointing occur, with the same maximum trend (fig. 43). These features trend at a high angle to the boundaries between rock types in the Georges Bay area. It is not clear how they were produced.

The sparsely porphyritic biotite-hornblende granodiorite (Dbgsp) rock type, in the area near the Georges River north of St Helens, shows a strongly developed apparent lineation on horizontal surfaces defined by the elongation of quartz aggregates and the alignment of mafic minerals. The alignments have an approximately north-south trend (fig. 44). It was not clear whether they are the result of a foliation or a lineation. They approximately parallel the western intrusive boundary of the granitoid body but are truncated by the later granodiorite (Dbgp) and adamellite (Dbasc) intrusions.

The variably porphyritic biotite-hornblende granodiorite (Dbgp) rock type occurs in dyke shaped bodies and shows

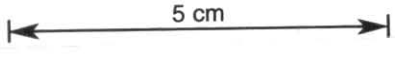

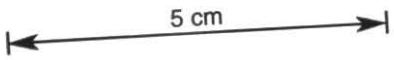

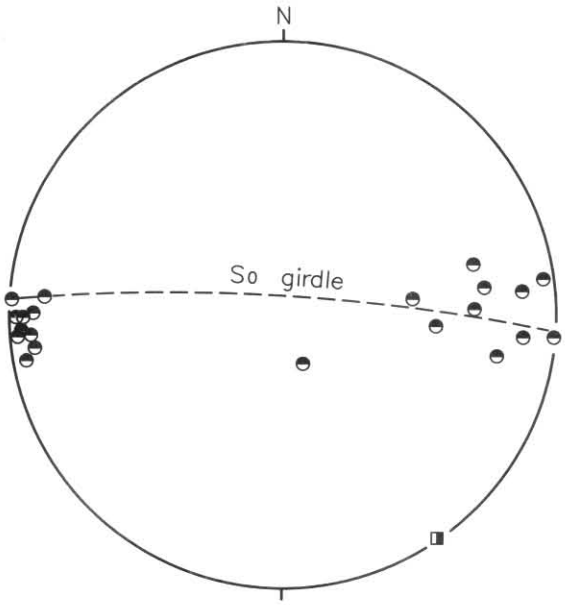

Figure 39. Lambert projection of slaty cleavage (◓) and kink bands (◨) in Sub-areas 10A, B, C, D of the Mathinna Beds. There is possibly slight discordance between average cleavage trend and the fold axis (Figure 38) though both are estimates derived from data showing scatter and are therefore regarded as approximate.

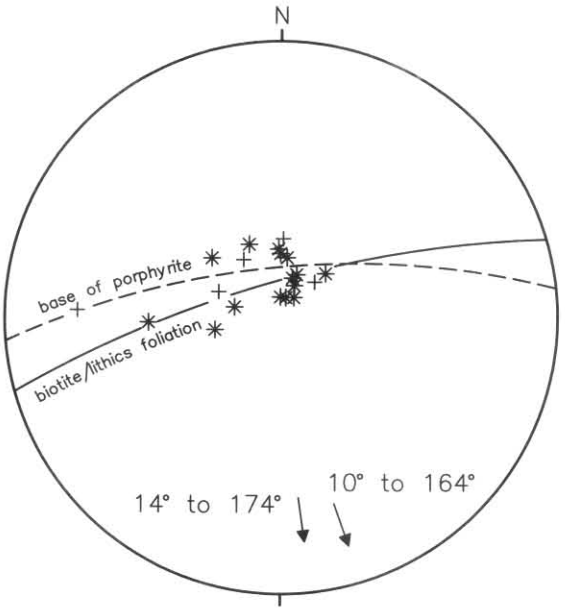

Figure 40. Lambert projection of foliation (✳) in the St Marys Porphyrite near its basal contact with the Mathinna Beds (see Turner *et al.*, 1984). Dips and strikes of the basal contact (+) are also plotted. These were estimated from the trace of the contact on the topography. The two sets of data give slightly different values for the orientation of the axis of the late fold which affects the porphyrite body. This appears to be because the contact and the foliation were initially discordant.

feldspar alignments on horizontal surfaces parallel to the boundary with the surrounding rocks. At a few localities (e.g. FQ065266) the alignments can be seen to have been produced by a steep foliation. These features are probably related to flow.

In the Mt Nisbet [EQ915278] area rapid variations in texture and proportions of Mathinna Beds xenoliths suggest the body has a complex internal structure, possibly involving more than one intrusive pulse.

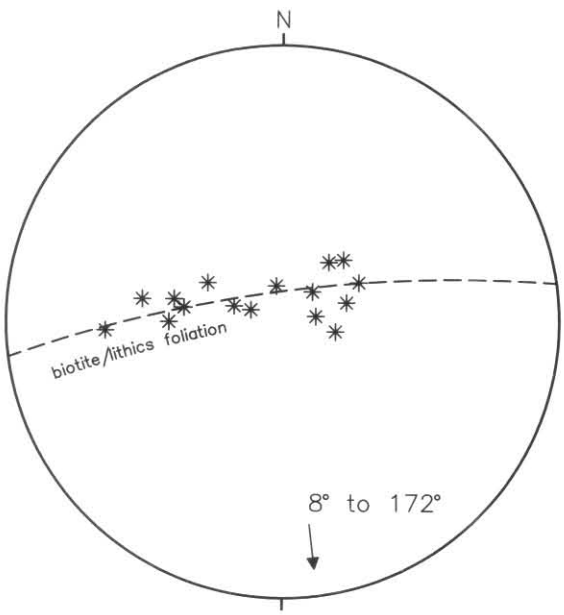

Figure 41. Lambert projection of foliation in the St Marys Porphyrite between Falmouth and Four Mile Creek. The estimated fold axis orientation is very similar to the estimates derived in Figure 40.

The biotite adamellite (Dbasc) shows widespread feldspar alignments on horizontal surfaces defining an apparent lineation. In a few localities (e.g. EQ907223) the feldspars can be seen to define a steep foliation. The general trend of the apparent lineation is slightly east of north-south (fig. 45). On the western margin of the body the lineations are parallel to the contact with the Mathinna Beds. It is possible that the lineations were produced by flow.

The strongly foliated biotite granodiorite (Dbgbf) rock body in the Pyengana area has the fabric defined by the elongation of quartz and feldspar zones and the alignment of biotite. The alignments are parallel to the boundary with the Mathinna Beds and may have been produced by flow or the effects of pressure on the partly consolidated magma against the walls of the intrusion.

The porphyritic biotite adamellite (Dbapc) body in the north-west part of the map sheet shows regular feldspar alignments on horizontal surfaces defining an apparent lineation trending north-west. This direction is at a high angle to the boundary of the body. It is not clear whether the alignment is due to a lineation or a foliation. If the alignments represent lineations the they might be consistent with flow, however a flow foliation would be expected to have produced alignments parallel to the boundary. In the case of foliation the more likely explanation would be that it was produced in partly consolidated magma by a regional stress system.

FAULTING

Three major faults are considered to be present on the map sheet which have provided lines of weakness for later intrusion of granitoids.

The first follows the line of the variably porphyritic biotite-hornblende granodiorite (Dbgp) dyke stretching from Moulting Bay in the north to Scamander in the south. The displacement of the boundary between the sparsely porphyritic biotite-hornblende granodiorite (Dbgsp) and the Mathinna Beds in the area immediately south of St Helens shows that movement must have taken place along the line of the dyke. If the dilation effect of the dyke is discounted the boundary still does not join. At FQ030205 the boundary is well exposed in a stream and can be seen to dip west at a moderate angle. The straight trend of the

dyke across an area of variable topography indicates that it is steep and may be a normal fault. Displacements of this boundary by a normal fault along the line of the dyke indicates a downthrow on the eastern side.

The second fault is postulated to join with the first near Moulting Bay and to trend WNW following the line of a thin dyke of the variably porphyritic biotite-hornblende granodiorite (Dbgp) which is continuous with the dyke along the first fault. Slickensiding is visible in the biotite adamellite (Dbasc) at a number of points on the northern side of the dyke (e.g. FQ003307 and FQ031292). Movement along the line of the dyke is indicated by the termination of the boundary between the sparsely porphyritic biotite-hornblende granodiorite (Dbgsp) and the biotite adamellite (Dbasc) against the dyke at EQ995308. Evidence has been presented to show that the upper surface of the adamellite dips east and south-east at a low angle thus indicating that the granodiorite overlies the adamellite. Since the granodiorite on the south side of the fault is brought against underlying adamellite on the north (apart from the small thickness of granodiorite along the dyke) it must have been downthrown on the south side of the dyke. There is no evidence as to whether the fault continues south-east across Georges Bay.

The third fault is considered to have cut the western part of the biotite adamellite (Dbasc) body and to extend along a line of approximately north-south trend between Mothers Hill [EQ909311] in the north and near Bolpeys Ridge [EQ971051] in the south. Along the southern part of its length the fault line has been intruded by the variably porphyritic biotite-hornblende granodiorite (Dbgp) rock type which forms a broad dyke shaped body in the Catos Creek area and farther north is present as very thin discontinuous bodies extending to near Granite Knob at

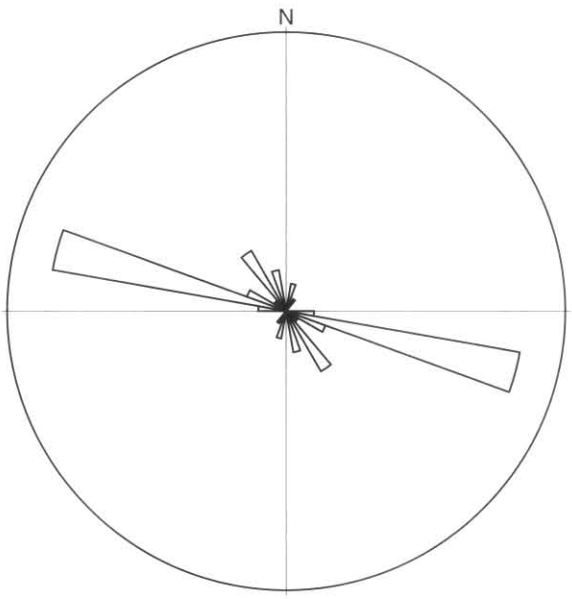

Total readings = 37; circle = 20; segment angle = 10°

Figure 42. Rose diagram of alignments of feldspar phenocrysts in Dbrpc.

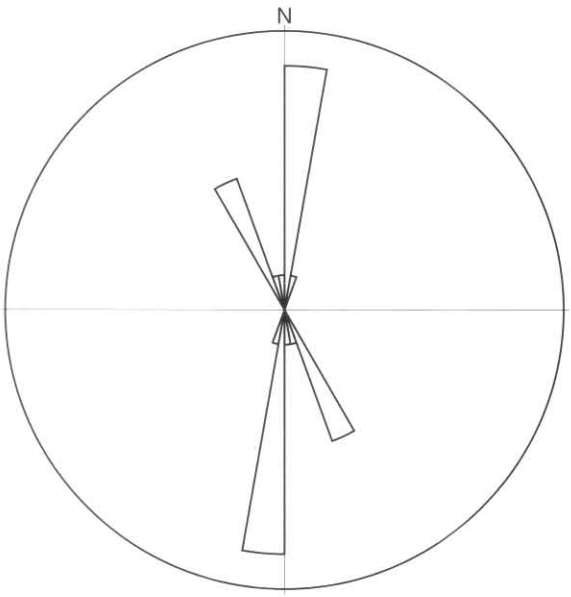

Total readings = 21; circle = 8; segment angle = 10°

Figure 44. Rose diagram of apparent lineation defined by the elongation of quartz aggregates and the alignment of mafic minerals in Dbgsp.

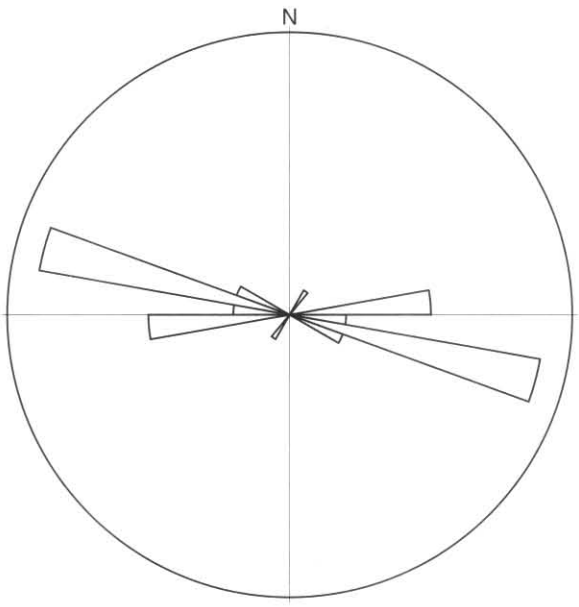

Total readings = 20; circle = 10; segment angle = 10°

Figure 43. Rose diagram of zones of closely-spaced vertical jointing in Dbgbsp.

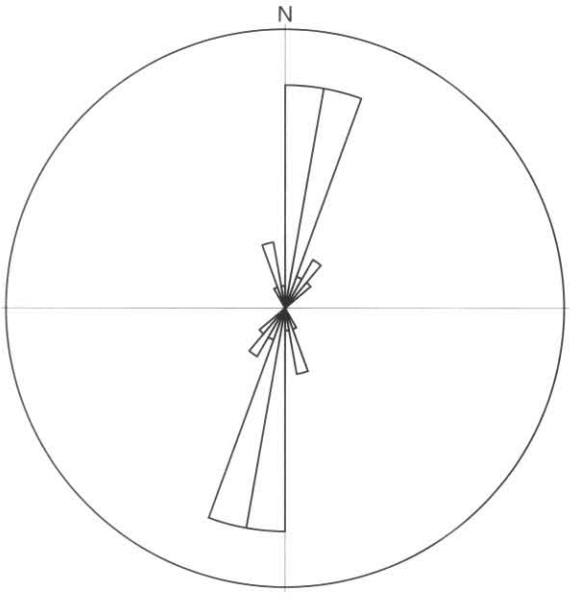

Total readings = 64; circle = 25; segment angle = 10°

Figure 45. Rose diagram of foliation in feldspars in Dbasc.

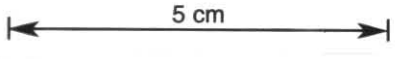

EQ930155. A narrow quartz feldspar porphyry body is also intruded along the line of the fault in that area and is present as a broader body crossing Hogans Road at EQ925184. At the northern end of the postulated fault a 3 km wide wedge shaped body of the variably porphyritic biotite-hornblende granodiorite (Dbgp) rock type occurs which joins with the dyke shaped intrusion along the second fault. In the intervening area the fault is postulated to cross biotite adamellite (Dbasc) and is marked for part of the distance between EQ923187 and EQ911207 by the western edge of the area of pink adamellite with numerous small granite intrusions. At EQ912193 a zone of intense shearing in the adamellite is the result of the fault and at other localities farther south there is evidence for faulting along the eastern margin of the granodiorite intrusions. The fault is inferred to have downthrow on its eastern side since Mathinna Beds overlying the adamellite are brought against the adamellite in the Hogans Road to Catos Creek area.

The virtual absence of a metamorphic aureole in the Mathinna Beds on the eastern side of the granitoid intrusions compared to the broad aureole on the west, between Holloways Hill [EQ940140] and the Catos Creek area indicates that the Mathinna Beds on the eastern side were brought into their present position close to the biotite adamellite (Dbasc) of this area by faulting, after the adamellite was intruded.

The western boundary of the biotite adamellite (Dbasc) body is clearly steep and straight in contrast with the irregular low angle margin of the body on its east and south side. This suggests that intrusion on the western margin was controlled by an existing fault.

The downfaulting of the large block of country to the east and south of the second and third faults is probably related to the extrusion of the St Marys Porphyrite (dacitic, welded, ash-flow tuff) a short distance to the south in the St Marys area. The extrusion of a large volume of material from a high level magma chamber would be expected to have produced a caldera type collapse

REFERENCES

ANDERSON, A. T. 1968. The oxygen fugacity of alkaline basalt and related magmas, Tristan da Cunha. *Am. J. Sci.* 266:704–727.

BAILLIE, P. W. 1984. Geological atlas 1:50 000 Series. Sheet 25 (8516S). Eddystone. *Department of Mines, Tasmania.*

BAILLIE, P. W.; POWELL, C. M.; BANKS, M. R.; HILLS, P. B. 1989. The eastern Tasmanian terrane, *in* BURRETT, C. F.; MARTIN, E. L. (ed.). Geology and mineral resources of Tasmania. *Spec. Publ. geol. Soc. Aust.* 15:234–237.

BAILLIE, P. W.; TURNER, N. J.; COX, S. F. 1979. Tasmanian Geological Atlas 1:50 000 Series. Sheet 24 (8416S). Boobyalla. *Department of Mines, Tasmania.*

BANKS, M. R. 1962. Mathinna Beds in SPRY, A. H.; BANKS, M. R. The geology of Tasmania. *J. geol. Soc. Aust.* 9(2): 182–184.

BROOKS, C. K. 1976. The Fe_2O_3/FeO ratio of basalt analyses: an appeal for a standard procedure. *Bull. geol. Soc. Denmark* 25:117–120.

BROWN, A. V.; MCCLENAGHAN, M. P. 1982. Tertiary basaltic rocks, *in* MCCLENAGHAN, *et al.*, Geology of the Ringarooma – Boobyalla area. *Bull. geol. Surv. Tasm.* 61:92–114.

BROWN, A. V.; MCCLENAGHAN, M. P.; MOORE, W. R.; TURNER, N. J.; MCCLENAGHAN, J.; WILLIAMS, P. R.; BAILLIE, P. W.; CORBETT, K. D.; CORBETT, E. B.; COX, S. F.; GROVES, D. I.; PIKE, G. P. 1977. Geological atlas 1:50 000 series. Sheet 32 (8415N). Ringarooma. *Department of Mines, Tasmania.*

BUDDINGTON, A. F.; LINDSLEY, D. H. 1964. Iron-titanium oxide minerals and synthetic equivalents. *J. Petrology* 5:310–357.

CALVER, C. R.; EVERARD, J. L.; FINDLAY, R. H.; LENNOX, P. G. 1988. Geological atlas 1:50 000 series. Sheet 48 (8414N). Ben Lomond. *Department of Mines, Tasmania.*

CAPP, S. C. E. 1991. The geology of the Evercreach area, NE Tasmania. B.Sc.(hons) thesis, University of Tasmania : Hobart.

CARMICHAEL, I. S. E.; TURNER, F. J.; VERHOOGEN, J. 1974. *Igneous petrology.* McGraw Hill : New York.

CHAPPELL, B. W. 1978. Granitoids from the Moonbi district, New England Batholith, eastern Australia. *J. geol. Soc. Aust.* 25:267–283.

CHAPPELL, B. W.; WHITE, A. J. R.; WYBORN, D. 1987. The importance of residual source material (restite) in granite petrogenesis. *J. Petrology* 28:1111–1138.

CLARKE, M. J.; BAILLIE, P. W. 1984. Geological atlas 1:50 000 series. Sheet 77 (8512N). Maria. *Explan. Rep. geol. Surv. Tasm.*

COCKER, J. D. 1971. *The St Helens Pluton. Petrology and structure.* B.Sc. (hons) thesis, University of Tasmania : Hobart.

COCKER, J. D. 1977. The geology of the St Helens area: petrology and structure of the granitoid rocks in GROVES, D. I.; COCKER, J. D.; JENNINGS, D. J. The Blue Tier Batholith. *Bull. geol. Surv. Tasm.* 55:117–156.

COCKER, J. D. 1982. Rb-Sr geochronology and Sr isotopic composition of Devonian granitoids, eastern Tasmania. *J. geol. Soc. Aust.* 29:139–158.

DAVIES, J. L. 1959. High level erosion surfaces and landscape development in Tasmania. *Aust. Geogr* 7:193–203.

EVERARD, J. L. 1987*a*. Petrology of the Triassic basalt, *in* TURNER, N. J.; CALVER, C. R. Geological atlas 1:50 000 series. Sheet 49 (8514N). St Marys. *Explan. Rep. geol. Surv. Tasm.*:89–121.

EVERARD, J. L. 1987*b*. Petrology of the Jurassic dolerite, *in* TURNER, N. J.; CALVER, C. R. Geological atlas 1:50 000 series. Sheet 49 (8514N). St Marys. *Explan. Rep. geol. Surv. Tasm.*:123–148.

EVERARD, J. L. 1987*c*. Petrology of the Tertiary basalt, *in* TURNER, N. J.; CALVER, C. R. Geological atlas 1:50 000 series. Sheet 49 (8514N). St Marys. *Explan. Rep. geol. Surv. Tasm.*:149–152.

EVERARD, J. L. 1989. Petrology of the Tertiary basalt, in SEYMOUR, D. B. (comp.) Geological atlas 1:50 000 series. Sheet 36 (8015N). St Valentines. *Explan. Rep. geol. Surv. Tasm.*

FORSYTH, S. M. 1989. Tertiary cover rocks in BURRETT, C. F.; MARTIN, E. L. Geology and mineral resources of Tasmania. *Spec. Publ. geol. Soc. Aust.* 15:372–373.

FREY, F. A.; GREEN, D. H.; ROY, S. D. 1978. Integrated models of basalt petrogenesis: a study of quartz tholeiites to olivine and melilitites from south eastern Australia utilizing geochemical and experimental petrological data. *J. Petrology* 19:463–513.

GEE, R.D.; GROVES, D. I. 1971. Structural features and mode of emplacement of part of the Blue Tier Batholith in north eastern Tasmania. *J. geol. Soc. Aust.* 18:41–55.

GEE, R.D.; GROVES, D. I. 1974. Contact structures at a granodiorite intrusion, Piccaninny Point, northeast Tasmanaia. *Pap. Proc. R. Soc. Tasm.* 107:47–52.

GOSCOMBE, B. D.; FINDLAY, R. H. 1989. Mega-kinking in the Mathinna Beds, north-east Tasmania. *Rep. Dep. Mines Tasm.* 1989/42.

GROVES, D. I. 1972. The zoned mineral deposits of the Scamander – St Helens district. *Bull. geol. Surv. Tasm.* 53.

GROVES, D. I. 1977. The geology, geochemistry and mineralisation of the Blue Tier Batholith, *in* GROVES, D. I.; COCKER, J. D.; JENNINGS, D. J. The Blue Tier Batholith. *Bull. geol. Surv. Tasm.* 55:7–116.

GROVES, D. I.; BAKER, W. E. 1971. The cobalt and nickel content of some sulphides from ore deposits in eastern Tasmania. *Tech. Rep. Dep. Mines Tasm.* 14:27–35.

HARRIS, W. K. 1968. Tasmanian Tertiary and Quaternary microfloras. Summary report. *Palaeont. Rep. geol. Surv. S. Aust.* 5/68.

HENDERSON, Q. J. 1939. Report on the geological survey of the country between Scamander and Mathinna. *Unpubl. Rep. Dep. Mines Tasm.* 1939:53–60.

HENDERSON, Q. J. 1941. Scamander copper field. *Unpubl. Rep. Dep. Mines. Tasm.* 1941:5–11.

HIGGINS, N. C.; TURNER, N. J.; BLACK, L. P. 1986. The petrogenesis of an I-type volcanic-plutonic suite: the St Marys Porphyrite, Tasmania. *Contrib. Mineral. Petrology* 92:248–259.

HINE, R.; WILLIAMS, I. S.; CHAPPELL, B. W.; WHITE, A. J. R. 1978. Contrasts between I-type and S-type granitoids of the Kosciusko Batholith. *J. geol. Soc. Aust.* 25:219–234.

JACK, R. 1964. Thureau's deep lead, St Helens. *Tech. Rep. Dep. Mines Tasm.* 8:63–71.

JENNINGS, D. J. 1968*a*. Alluvial tin in the Lower Scamander River valley. *Tech. Rep. Dep. Mines Tasm.* 11:32, 34–36.

JENNINGS, D. J. 1968*b*. Geological investigations and results of drilling for tin, adjacent to the George River. *Tech. Rep. Dep. Mines Tasm.* 12:19–24.

LEMAITRE, R.W. 1984. A proposal by the IUGS Subcommission on the Systematics of Igneous Rocks for a chemical classification of volcanic rocks based on the total alkali silica (TAS) diagram. *Aust. J. earth Sci.* 31:243–255.

LEAMAN, D. E.; RICHARDSON, R. G. 1981. Gravity survey of the East Coast coalfields. *Bull. geol. Surv. Tasm.* 60.

MACDONALD, G. A.; KATSURA, T. 1964. Chemical composition of Hawaiian lavas. *J. Petrology* 5:82–133.

MCCLENAGHAN, M. P. 1984. The petrology, mineralogy and geochemistry of the Pyengana and Gardens granodiorites, the Hogans Road diorite and the dolerite dykes of the Blue Tier Batholith. *Unpubl. Rep. Dep. Mines Tasm.* 1984/04.

MCCLENAGHAN, M. P. 1989. Mid-Palaeozoic granitoids. Eastern Tasmania, *in* BURRETT, C. F.; MARTIN, E. L. (ed.). Geology and mineral resources of Tasmania. *Spec. Publ. geol. Soc. Aust.* 15:257–261.

MCCLENAGHAN, M. P.; TURNER, N. J.; BAILLIE, P. W.; BROWN, A. V.; WILLIAMS, P. R.; MOORE, W. R. 1982. Geology of the Ringarooma–Boobyalla area. *Bull. geol. Surv. Tasm.* 61.

MCCLENAGHAN, M. P.; WILLIAMS, P. R. 1982. Distribution and characterisation of granitoid intrusions in the Blue Tier area. *Pap. geol. Surv. Tasm.* 4.

MCDOUGALL, I.; LEGGO, P.J. 1965. Isotopic age determinations on granitic rocks from Tasmania. *J. geol. Soc. Aust.* 12:295–332.

MONTGOMERY, A. 1893*a*. Report on Thureau's Deep Lead, near George Bay. *Department of Mines, Tasmania.*

MONTGOMERY, A. 1893*b*. Report on the silver-bearing lodes of the Scamander River district. *Rep. Secr. Mines Tasm.* 1892–1893:i-iii.

POWELL, C. M.; BAILLIE, P. W.; CONAGHAN, P. J.; TURNER, N. J. *in press.* The mid-Palaeozoic Mathinna turbidite basin, northeast Tasmania. *Aust. J. earth Sci.* **

RICKARDS, R. B.; BANKS, M. R. 1979. An Early Devonian monograptid from the Mathinna Beds, Tasmania. *Alcheringa* 3:307–311.

ROBINSON, P. 1980. The composition space of terrestrial pyroxenes-internal and external limits, in PREWITH, C.T. (ed.) Pyroxenes. *Rev. Mineral.* 7(9) and 419–495.

SIMKIN, T.; SMITH, J. V. 1970. Minor element distribution in olivine. *J. Geol.* 78:304–325.

SMITH, J. H. 1897. Report on the Scamander mining district in April, 1897. *Rep. Secr. Mines Tasm.* 1896–1897: xxxix–xlii.

SPENCER, K.J.; LINDSLEY, D.H. 1981. A solution model for coexisting iron-titanium oxides. *Am. Mineral.* 66:1189–1201.

STRECKEISEN, A. L. 1973. Plutonic rocks. Classification and nomenclature recommended by the IUGS Subcommission on the Systematics of Igneous Rocks. *Geotimes* 18(10): 26–30.

SUTHERLAND, F. L.; WELLMAN, P. 1986. Potassium-argon ages of Tertiary volcanic rocks, Tasmania. *Pap. Proc. R. Soc. Tasm.* 120:77–86.

TURNER, N. J.; BLACK, L. P.; HIGGINS, N. C. 1986. The St Marys Porphyrite and related dykes – a Devonian intracaldera ignimbrite and its feeder. *Aust. J. earth Sci.* 33:201–218.

TURNER, N. J.; CALVER, C. R. 1987. Geological atlas 1:50 000 series. Sheet 49 (8514N). St Marys. *Explan. Rep. geol. Surv. Tasm.*

TURNER, N. J.; CALVER, C. R.; CASTLEDEN, R. H.; BAILLIE, P. W. 1984. Geological atlas 1:50 000 series. Sheet 49 (8514N). St Marys. *Tasmania Department of Mines.*

TWELVETREES, W. H. 1900. Report on gold mines near Hogan's track. *Rep. Secr. Mines Tasm.* 1899–1900:i–xiii.

TWELVETREES, W. H. 1904. Report on deposits of clay at Georges Bay and elsewhere. *Department of Mines, Tasmania*

TWELVETREES, W. H. 1911. The Scamander mineral district. *Bull. geol. Surv. Tasm.* 9.

URQUHART, G. 1968. Loila Tier tin prospect, Scamander area. *Tech. Rep. Dep. Mines Tasm.* 11:18–23, 25.

WALKER, K. R. 1953. *Geology of the Falmouth–St Helens area.* B.Sc. (Hons) thesis, University of Tasmania : Hobart.

WALKER, K. R. 1957. The geology of the St Helens–Scamander area, Tasmania. *Pap. Proc. R. Soc. Tasm.* 91:23–39.

WALLER, G. A. 1901. Report on the mining district of the Scamander River and St Helens. *Rep. Secr. Mines Tasm.* 1900–1901:268–301.

WHITE, A. J. R.; CHAPPEL, B.W. 1977. Ultrametamophism and granitoid genesis. *Tectonophysics* 43:7–22.

WHITE, A. J. R.; CHAPPEL, B.W. 1983. Granitoid types and their distribution in the Lachlan Fold Belt, south-eastern Australia, in RODDICK, J. A. (ed). Circum-Pacific plutonic terranes. *Mem. geol. Soc. Am.* 159:21–34.

WILLIAMS, E. 1959. The sedimentary structures of the Upper Scamander sequence and their significance. *Pap. Proc. R. Soc. Tasm.* 93:29–32.

YAGI, K.; ONUMA, K. The join $CaMgSi_2O_6$-$CaTiAl_2O_6$ and its bearing on titanaugites. *J. Fac. Sci. Hokkaido Univ.* 4(8):463–483.

Appendix A

ECONOMIC GEOLOGY

N. J. Turner

Introduction

Metallic mineral deposits of economic interest in the St Helens quadrangle comprise small lodes, which contain a variety of metals, and alluvial tin deposits. Construction materials are quarried in many parts of the quadrangle and a little clay has been extracted for brickmaking near Georges Bay.

The lodes include a group of gold occurrences in Mathinna Beds and Devonian adamellite (Dbapc) around Golden Ridge in the western part of the quadrangle. There is also a zoned mineral field comprising a series of tungsten, tin, copper and silver-lead-zinc lodes in the eastern part of the quadrangle in Mathinna Beds, differentiated Devonian adamellite (Dbasc) of the Mt Pierson Pluton and in granodiorite (Dbgp). Minor tin occurrences are present in the Mt Pierson Pluton in the central north of the quadrangle. They appear to be unrelated to the zoned series of lodes.

Zoned mineral field

PRODUCTION AND MINES

Most of the lode deposits in the zoned Scamander–St Helens field were discovered in the latter part of the last century, beginning in about 1884 with the discovery of silver at the Scamander River mine (Secretary for Mines, 1884). The discovery of copper and tin bearing lodes followed and the first leases for tungsten were granted in 1898 (Nye, 1941*b*).

Table A1 summarises the known production data. Statistics from the different source references are in some cases difficult to reconcile except in so far as all sources agree that production has been very low.

In the period since 1960 the mineral field has been re-investigated using modern mineral exploration techniques. Relatively recent work, culminating in 1984, has delineated a resource comprising 3.2 Mt of 0.22% Sn at the Great Pyramid deposit (Ruxton, 1984, Ruxton and Plummer *in* Turner and Taheri, 1990). The deposit is currently held under Retention Licence by the Broken Hill Pty Co Ltd.

GEOLOGY

The lodes

Many accounts have been written of the various lodes in the zoned Scamander–St Helens field. Of notable importance are the accounts by Groves (1972) and Ruxton (1984). The brief notes presented here provide a general introduction to the data which is available.

Table A2 lists the various lodes and their locations, anomalous metals, styles and trends also the main accounts which document their features. There is some disagreement amongst the various accounts as to the geographic positions of some of the lodes and this is reflected in the positions shown on the St Helens map. In particular, the positions shown on the map for Baden Powell, Prices, Carson de Beers, North Orieco and Echo are quite inaccurate. However, the positions given by the AMG co-ordinates in Table A2 are considered to be fairly accurate for all deposits. They were derived by plotting the positions shown on maps in the source references onto the St Helens geological map, cross-checking with the other source references, then determining the co-ordinates to the nearest 100 m. Accuracy has been confirmed by field checks in a number of instances.

In general the lodes are quartz-rich or, less commonly, sulphide-rich and fill fissures that are related either to faults or to tensional fracturing. The faults trend both north-westerly and north-easterly whilst tension fractures predominantly trend NNE–E. The North Scamander lode is unusual in that it is partly the result of replacement of the Mathinna Beds (Ruxton, 1984) whilst the Stony Ford lode also involves alteration, specifically of granodiorite in a shear zone (Twelvetrees, 1902; Cocker, 1977).

Table A1. PRODUCTION FROM THE SCAMANDER – ST HELENS ZONED MINERAL FIELD

Mine	Metal	Period	Quantity *(tonnes)*	Grade
Baden Powell	W	(1) pre-1901	1 (conc.)	-
		(2) pre-1916	0.5 (conc.)	-
		(3) pre-1938	5 (conc. – 70% WO_3)	1.4% WO_3 (estim.)
			2.5 (conc. – 70% WO_3)	1.2% WO_3 (estim.)
Carson de Beers (Prices)	W	(1) pre-1901	1 (conc.)	-
	-	(2) pre-1938	0.75 (conc. – 70% WO_3)	-
Jacobs (Lutwyche)	W	(1) pre-1941	minor	-
	-	(2) pre-1938	2 (conc. – 70% WO_3)	1.9% WO_3 (estim.)
Echo North	W	(1) 1918	minor	-
	-	(2) pre-1952	1	1% WO_3
Great Pyramid	Sn	1928-1936	2.96 (metal equiv.)	0.88% Sn (recov.)
Orieco	Cu, Ag	(1) 1895–1897	122 (picked ore)	28% Cu, 520.4 g/t Ag
		-	305 (stockpile)	10-15% Cu, 306.1 g/t Ag
		(2) 1900	199 (picked ore)	17% Cu, 398 g/t Ag
		(3) 1940–1942	4 (metal equiv.)	-
		(4) total production.	446 (picked ore)	15-28% Cu
Beulah	Ag	1896–1897	52 (picked ore)	2832 g/t Ag
Scamander River	Ag	pre-1893	51 (picked ore)	1010 g/t Ag

Source references: Orieco (1), Beulah - Smith, 1897; Baden Powell (1), Carson de Beers (1), Orieco (2) - Waller, 1901; Baden Powell (2) - Hills, 1916; Jacobs, Echo North (1) - Nye, 1941; Orieco (3) - Mines Dept. mine records; Orieco (4) - Groves, 1972; Scamander River-Montgomery 1893*b*; Jacobs (2), Carson de Beers (2), Baden Powell (3) - Schell, 1938; Echo North (2) - Walker, 1957.

Grade of tin at Great Pyramid is recovery grade. Quantity of production for Great Pyramid and Orieco (3) expressed as the calculated tonnes of metal in the ore produced. Henderson (1941) obtained 'in ground' copper grades ranging 1.82% to 7.51% at the Orieco mine.

Table A2. SCAMANDER – ST HELENS LODE DEPOSITS

Name	AMG	Metals	Style	Trend	References
In Mt Pierson Pluton					
Priory	EQ992309	Sn, As	q, t vein	E	2
Ferntree Hill	EQ932210	Sn, Pb, Zn	g, t vein	-	4, 26
un-named	EQ973177*	As, Cu	q vein	-	-
Echo North	EQ999216	Mo, W, Bi	q, g vein	WNW	7, 15, 17, 24
Echo South	EQ995209	Sn, W, Bi	q, g vein	NW-WNW	15, 17
In Mathinna Beds					
Silver Echo	EQ996228	Cu, Mo, Bi	q vein	NNW	2, 7, 17, 19, 21, 25
Baden Powell	EQ964164*	W, Mo	q vein	NNE-NE	7, 9, 15, 17, 18, 22, 25
Carson de Beers (Prices)	EQ973160	W, Mo	q, t vein	NW	7, 9, 15, 17, 18, 22, 25
Jacobs (Lutwyche)	EQ974155	W, Mo, Bi, Sn	q vein	NNE-NE	7, 9, 12, 15, 17, 18, 22, 25
Fitzgeralds Creek	≈EQ970147	W, As	q vein	ENE	7
Pinnacles West	EQ981147	Sn, Cu, AS	sheeted q vein	NNE-ENE	7, 17
Pinnacles West (south)	EQ982141	Sn, Cu	q vein	-	16
Pinnacles East	EQ984139	As, Pb, Ag, Cu	fractures	NE	7, 17
Great Pyramid (Brocks)	EQ996133*	Sn, Ag, Cu	sheeted q vein	NE	5, 7, 10, 17, 22
Loila Tier	EQ997182	Sn, As, Pb, Ag, Cu	Loila Tier Fault	NE	7, 17, 23
Williams West	FQ004185	As, Pb, Sn, Ag	Loila Tier Fault	NE	7, 17, 23
Williams East	FW006185	As, Sn, Pb, Cu	Loila Tier Fault	NE	7, 17, 23
Orieco North	FQ010143	Sn, Zn, Cu, Pb	Orieco Fault	NW	3, 7, 17
Orieco	FQ012138*	Cu, Zn, Sn, Pb, Ag, As	Orieco Fault	NW	3, 6, 7, 8, 17, 19, 22, 25
Orieco South (Ruxton)	FQ013136	Cu, Zn, Sn, Ag	Orieco Fault	NW	3, 7, 17
Orieco South (Henderson)	≈FQ016134	As, Cu, Zn	Orieco Fault	NW	7, 8
un-named	FQ013135*	gossanous breccia	Orieco Fault	NW	-
Paul Beahrs	FQ022124	Zn, Pb, Cu, Ag	Orieco Fault	NW	7, 8, 17, 22, 25
Dunns	FQ015143*	As, Cu, Sn, Ag	un-named fault	NW	7, 8, 17, 22
Arm	FQ016139	As, Pb, Sn, Cu	un-named fault	NW	17
Cramps	FQ014154	As, Pb, Cu, Ag, Bi	fault	NE	7, 8, 17, 19
Ringarooma Bay	FQ004131*	gossanous breccia	fault	NW	7, 8, 17, 22
North Ringarooma Bay	FQ007134*	Sn, Pb, Zn	?fault	E	7, 17
North Scamander	FQ011118*	Pb, Zn, Cu, Ag, Sn	fracture/ replacement	WNW	7, 17, 19, 22, 25
West Scamander	-	As, Zn, Pb	q vein	-	22
Copper Show Creek	EQ949153	As, Cu, Pb	q vein	NNE	13
un-named	≈EQ953157	Pb, Zn, Ag, As	q vein	NE	13
Upper Scamander Cu	EQ937178	Cu, Pb	joints / fractures	-	13
Ryan-Fitzpatrick	≈EQ946162	AS, Cu	vein	-	13, 25
un-named	EQ956142*	?Cu	-	-	-
un-named	EQ955144*	?Cu	-	-	-
Yarmouth	FQ057144	As, Cu, Au, Ag	q vein	E	3, 7, 17, 19, 20, 22
un-named	FQ049097	As, Au	q vein	E	11
!n granodiorite					
Stoney Ford	FQ012248	Zn, Sn, Cu, monazite	alteration zone	NE-E	2, 14, 17, 21
un-named	≈FQ048236	sulphides, monazite	alteration zone	-	2, 21
un-named	FQ035145	-	-	-	27
Beulah	FQ040105*	Pb, As, Ag, Au	q vein	NNE	3, 7, 11, 17, 19, 22
Beulah South	FQ041101*	As, Zn, Pb, Ag, Au	q vein	NNE	3, 7, 17, 19, 22
Scamander Bell	FQ044100	gossan, Ag	q vein	-	3, 19, 22
Scamander River	FQ047092*	As, Zn, Pb, Ag	q vein	NNE	3, 7, 11, 17, 19, 20, 22

* – position confirmed by ground check; q – quartz; g – greisen; t – tourmaline.

Source references: 1. Anon, 1981; 2. Cocker, 1977; 3. Cromer, 1990; 4. Ellis, 1983; 5. Everard, 1964; 6. Ford *et al*, 1970; 7. Groves, 1972; 8. Henderson, 1941; 9. Hills, 1916; 10. Jack, 1963*a*; 11. Montgomery, 1893; 12. Mortimore, 1970; 13. Mortimore, 1974; 14. Nye, 1933; 15. Nye, 1941*a*; 16. Nye, 1941*b*; 17. Ruxton, 1984; 18. Schell, 1938; 19. Smith, 1897; 20. Thureau, 1886; 21. Twelvetrees, 1902; 22. Twelvetrees, 1911; 23. Urquhart, 1968; 24. Walker, 1957; 25. Waller, 1901; 26. Williams, 1980; 27. Department of Mines – old mineral chart No. 11: St Helens – St Marys mineral area. Metals mainly from Ruxton, 1984.

Twelvetrees (1911), Groves (1972) and Ruxton (1984) assign the name Scamander Bell to the Beulah South prospect. The prospect they describe falls outside the old Scamander Bell leases and matches Smith's (1897) description of Beulah South. Cromer (1990) accurately depicts the relative positions of the prospects.

Veins comprising the wolframite lodes of Baden Powell, Carson de Beers and Lutwyche are relatively thick, up to one metre, and widely spaced at 10–20 m (Ruxton and Plummer, 1984). In contrast the veins which comprise the cassiterite-sulphide lodes at Pinnacles West and Great Pyramid are thin, being commonly less than 5 mm, and closely spaced at less than 20 mm thus forming sheeted vein systems. Veins at North Scamander are even thinner but less closely spaced. In all cases the veins occupy tensional fractures. At Great Pyramid the sheeted vein system is virtually restricted to silicified, sandstone-dominated intervals in the Mathinna Beds (Groves, 1972). This correlation between vein development and competent, quartzitic intervals in the Mathinna Beds is also evident in other places, for example, at the Lutwyche deposit (Mortimore, 1970*a*).

The silicification of the Mathinna Beds at Great Pyramid and elsewhere along the ridge between Pinnacles West and North Scamander is considered to be an effect related to mineralisation (Ruxton and Plummer, unpublished). A fault which runs along the length of the ridge probably acted as a conduit for hydrothermal fluids emanating from underlying granite. Early fluids caused silicification

whilst later fluids deposited metals. The nearby Orieco fault also acted as a conduit.

Ore minerals

The main metallic minerals in the W-Mo lodes are wolframite and subordinate molybdenite. There may also be variable amounts of bismuthinite, cassiterite, scheelite, arsenopyrite, chalcopyrite and pyrite (Groves, 1972).

Primary mineralisation in the Sn-Cu sheeted veins includes cassiterite with pyrite, arsenopyrite, chalcopyrite and pyrrhotite. At Great Pyramid there is a late phase containing magnetite, cassiterite and sphalerite which occupies cross-cutting structures (Ruxton and Plummer, unpublished). Though anomalous in tin (Ruxton, 1984), the fault-associated Orieco lode is sulphide-rich, containing primary pyrite, arsenopyrite, sphalerite, chalcopyrite and galena (Ford *et al.*, 1970). Chalcopyrite is minor but copper grades have been enhanced through replacement of the primary sulphide assemblage by the supergene sulphides chalcocite and covellite. Supergene oxides and carbonates are also present.

Minerals in the primary assemblages of the Pb-Zn-Ag deposits near Scamander (Groves, 1972) include arsenopyrite, pyrite, galena, sphalerite and chalcopyrite. Supergene covellite is present and the silver that was extracted was in the form of the supergene chloride, cerargyrite (Smith, 1897). Supergene scorodite is also present, as it is in most lodes which contain arsenopyrite.

Zonation

Compositional zonation of the lodes which occur between the Mt Pierson Pluton (Dbasc) and Scamander has long been recognised (Twelvetrees, 1911; Groves, 1972). The lodes display a progression from W-Mo to Sn-Cu to Pb-Zn-Ag as the lateral distance from the Mt Pierson Pluton increases. Lodes near the pluton are also characterised by quartz and tourmaline whereas more distant lodes are distinguished by sulphides, sometimes dominant, and quartz. Zonation is most evident between Wolfram Creek and Scamander and is related to the presence along this line of a SE-plunging granite 'ridge' beneath the Mathinna Beds (Ruxton and Plummer, 1984). The zonation is not evident south-west of the Wolfram Creek – Scamander line and becomes greatly constricted to the north-east of the line. More localised zonation is evident along individual faults, for example, from Orieco to Paul Beahrs or from Loila Tier to Williams East.

Fluid inclusion homogenisation temperatures measured in quartz grains (Ruxton and Plummer, 1984) indicate that the W-Mo mineralisation was deposited from hydrothermal fluids of 320–360°C temperature, the Sn-Cu mineralisation from fluids of 200–320°C temperature and the Pb-Zn-Ag mineralisation from fluids of 160–240°C temperature (see also Ruxton and Plummer, unpubl.; in Turner and Taheri, 1990). This decrease in temperature of deposition is consistent with progressively increasing vertical distance from the inferred source of the hydrothermal fluid, that is, the plunging subsurface 'ridge' formed by the marginal phase of the Mt Pierson Pluton.

Mt Pierson Pluton

The pink, marginal phase of the Mt Pierson Pluton (McClenaghan, this volume) is known as the Constable Creek Sheet (Groves, 1972; Groves and McCarthy, 1978) or the Constable Creek Granite (Cocker, 1977). It is the uppermost part of the Mt Pierson Pluton and ranges in composition from adamellite to alkali feldspar granite. Around Wolfram Creek there is a vertical zonation in the Constable Creek granite from biotite/minor muscovite adamellite to biotite/coarse grained muscovite granite to biotite/muscovite/tourmaline greisen with minor fluorite in the apices of the 'ridge' (Ruxton and Plummer, 1984). There are also fairly extensive patches of greisen in the 'window' of Constable Creek granite around EQ595213 which contains the Echo mines (Mortimore and Rattigan, 1970). Quartz veins with greisen margins occur at Echo North and Echo South and respectively contain W, Mo, Bi and Sn, W, Bi.

The metalliferous quartz veins at the top of the Constable Creek granite in the Echo 'window' are representative of the lowest part of the zoned sequence Wo-Mo, Sn-Cu, Pb-Zn-As. There seems little doubt that they were formed from late stage fluids associated with the crystallisation of the differentiated Constable Creek granite. Further, it seems entirely reasonable that the upward passage of these fluids into the chemically unreactive country rocks led to the deposition of the other lode deposits at successively higher levels by progressively cooler fluids. However, Cocker (1977) exercises caution, pointing to the apparently younger age of the Scamander Tier Granodiorite relative to the Mt Pierson Pluton and thus highlighting the requirement for a long-lived hydrothermal system to allow the lodes in the granodiorite to be deposited by fluids generated by differentiation in the top of the Mt Pierson Pluton.

In addition to the fluid phase associated with the Constable Creek granite there were metalliferous fluids derived from an apparently different source which deposited lodes in the deeper parts of the Mt Pierson Pluton. Around EQ932210 near Ferntree Hill, just below the transitional base of the Constable Creek granite, there are greisen and tourmaline veins containing cassiterite and anomalous lead and zinc (Williams, 1980; Ellis, 1983). A cassiterite and arsenopyrite bearing, quartz/tourmaline vein system at EQ592307, which is known as the Priory lode (Cocker, 1977), is also well below the level of the Constable Creek granite. Another deep feature is a pipe-like body of siliceous (?)breccia with associated tourmalinised microgranite and quartz/ tourmaline veins at EQ950277, close to Copplestone Hill (Hall, 1979; Williams, 1980). These rocks are anomalous in tin and are the likely source of eluvial cassiterite in nearby soils. Another deep source of cassiterite in the Mt Pierson Pluton is indicated by eluvial cassiterite in the valley of Saxelby Creek (Williams, 1980).

In conclusion, the features in the lower part of the Mt Pierson Pluton support the existence of at least one hydrothermal system additional to the system associated with the Constable Creek granite. It seems likely that the lodes and alteration in the granodiorite (Dbgp) near Scamander are related to the Constable Creek granite system though the age relationships of the granodiorite and the Mt Pierson Pluton remain a problem to be resolved.

Alluvial tin deposits

PRODUCTION AND MINES

The discovery of alluvial tin in the St Helens quadrangle was made in 1874 (Anon, 1989) on the Royal Ruby Flat which occupies an area around EQ993251 in the district that was referred to generally as Georges Bay. The Georges Bay district included the country near Georges Bay itself and west from the town of St Helens to Goshen. Virtually all the alluvial tin produced from the St Helens quadrangle was mined in the part of the Georges Bay district west from Royal Ruby Flat. No mines are operating at present.

There are few quantitative records of production of alluvial tin from mines in the St Helens quadrangle between 1874 and 1902. (Reports of the Secretary for Mines, 1884–1902). Judging from the large number of lease (section) applications in the Georges Bay district in

the period immediately following discovery, the mining of alluvial tin developed quickly. In the years ending 30 June 1886 and 30 June 1887 there were respectively 578 and 656 tons of ore concentrate shipped from St Helens. These amounts would include concentrate derived from eluvial operations on Blue Tier as well as from the alluvial Georges Bay operations.

Production appears to have been steady until 1894 when reduced tin prices and drought had a strongly adverse affect. By 1898 alluvial mining had come to a virtual standstill but mining conditions improved in 1899 and steady production resumed. In the calendar year 1902 about 36 tons of concentrate were produced in the Georges Bay district.

Department of Mines records for the period 1902 to 1984 show that cassiterite concentrates containing about 1830 tonnes of metallic tin were won from alluvial mines in the Georges Bay district. The major producers in the period 1902–1984 are listed in Table A3.

GEOLOGY

The major alluvial tin mines in the St Helens quadrangle were within a belt of Tertiary and younger deposits (Ts – McClenaghan, this volume) which extends from Terryvale Marsh [EQ918255] north along the Power Rivulet then east along the south bank of the Georges River before turning south through the lower parts of Saxelby Creek, Golden Fleece Rivulet and Argonaut Creek then east through Royal Ruby Flat to Medeas Cove. The belt has long been recognised as an infilled valley (Thureau, 1888) and has been described by Montgomery (1893*b*), Waller (1901), Nye (1933) and, in more detail, by Jack (1964*b*) who drilled a series of five transverse profiles across the belt. Some additional drilling was carried out later (Jennings, 1967).

The old valley is filled with lenticular fluviatile or estuarine units of sandy clay, sand and gravel with basalt in the lower part of the succession. Sediments above the basalt are probably of early Oligocene age (Harris, 1968). Except in the near surface sediments, cassiterite is mostly only present in trace amounts and never reaches commercial grades. Thus, there are no deep leads in the valley infill so the name of Thureau's Deep Lead, by which the fossil valley has come to be known, is inappropriate (Jack, 1964*b*).

Commercial grades of cassiterite are confined to the near surface sediments with mine workings sometimes attaining 6 m in depth but usually averaging 1.5 m–3.7 m (Nye, 1933). Commercial grades of cassiterite are also regionally restricted with little east of Royal Ruby Flat and the great bulk of material occurring in the 6 km interval from Royal Ruby Flat to near the Thureau's Deep Lead Mining Co. workings (table A3). The cassiterite occurs as concentrations in surface soils, in the beds of present creeks and in fossils creeks incised in the upper surface of the sediments which fill the old valley (Waller, 1901). Other alluvial minerals associated with the cassiterite are ilmenite, spinel (pleonaste), zircon and sapphire (Nye, 1933). Hall (1979) cites local information indicating the presence of significant gold. Cassiterite occurs as the ruby tin variety and as the resin or black variety.

The restriction of commercial grades of cassiterite to shallow depths may reflect relatively late unroofing of the cassiterite source (Nye, 1933). Alternatively it may reflect reworking of a substantial thickness of initially low grade sediments with resultant concentration of cassiterite (Jack, 1964*b*). The presence of probable marine deposits (Cpl – Turner, this volume) at elevations of up to 110 m in St Helens quadrangle is consistent with there having been extensive reworking of the fluviatile/estuarine sediments. Elevated sea level may also have exercised control on cassiterite distribution through its function as the base level of erosion. Specifically, by determining in which portion of the valley there was deposition of the cassiterite being carried in the main stream and in tributary streams entering the valley.

In creeks to the south of the old valley there are cassiterite deposits of commercial grade in relatively thin Quaternary alluvium. Such deposits have been worked in Launceston Creek near EQ956222 and downstream also in Constable Creek near EQ970196 and downstream. Similar, small deposits occur north of the old valley system at the Albion [FQ006320] and nearby [EQ599315]. In the south there were other minor deposits in Carter Creek near EQ923184.

Groves (1977) favoured the relatively distant tin lodes on the Blue Tier as the ultimate source of the cassiterite in Thureau's Deep Lead. However, Cocker (1977) considered the pattern of old tin workings in the Georges Bay district to be consistent with derivation of cassiterite from the mineralised marginal phase (Constable Creek granite) of the Mt Pierson Pluton. More cogent arguments for the local derivation of cassiterite are presented by Williams (1980) and Ellis (1983) who demonstrate the presence of mineralised bedrock on the drainage divide (Ferntree Hill) between Carter Creek, Launceston Creek and Derwent Creek. Other indications of local sources for the alluvial tin deposits are provided by the presence of eluvial cassiterite in the valley of Saxelby Creek and near Copplestone Hill (Hall, 1979; Williams, 1980), also by the coarse grain size of the cassiterite in Constable Creek (K. Richardson, ex-leaseholder, pers. comm.). The cassiterite-bearing Loila Tier lode is within the catchment of Constable Creek.

The Blue Tier lodes were apparently the source of cassiterite in the Quaternary deposits of the Groom and Ransom Rivers, upstream from Goshen. Cassiterite in subeconomic Quaternary alluvium in the valley of the Scamander River (Jennings, 1968; Ward, 1972) was probably derived from nearby lode deposits such as the Great Pyramid and Pinnacles.

Gold deposits

PRODUCTION, MINES AND PROSPECTS

Around Golden Ridge in the central western part of St Helens quadrangle there are a number of prospects based on small lodes from which a little gold has been produced (table A4). Twelvetrees (1900*a, b*) and Groves (1972) describe the workings on the various prospects as well as the style and mineralogy of the lodes. Davidson and Roach (1990) and Randell (1991) provide a substantial body of new data but their reports are not open file documents at present. Further new information which is not cited in this summary is contained in Capp (1991). Alluvial gold production in the area around Golden Ridge appears to have been negligible.

The positions of the prospects given by the AMG co-ordinates in Table A4 are more accurate than the positions shown on St Helens map. Most positions in Table A4 are derived from Twelvetrees (1990*a, b*) in combination with the lease (section) charts for the area. One result of improved accuracy has been to show that the Double Event prospect is on the upper slope of a hill east of Hogans Road rather than west of the road as shown in Groves (1972) and St Helens map. Smaller inaccuracies are associated with the plotted positions of the other prospects on St Helens map.

In some cases confusion may arise from the same names having been applied to both specific excavations and to blocks of leases. For example, the Brilliant Creek workings 'proper' are just south of Brilliant Creek, near the old battery (Twelvetrees, 1900*a*), but the Brilliant Creek leases extended from there to the top of Golden

Table A3. ALLUVIAL TIN PRODUCTION IN THE GEORGES BAY DISTRICT IN THE PERIOD 1902–1984

Mine or Company	Period	Production – concentrate *(tonnes)*	Sn metal *(tonnes)*	Locality
Royal Ruby	1902–1909	112	?72.65	EQ 993251
Thureau's Deep Lead Mining Co.	1902–1910	60	?39.00	EQ 969285
Hunt	1903–1907	16	?10.36	Derwent Creek [EQ927261]
	1927–1940	-	49.2	-
Argonaut	1913–1933	-	631.92	EQ978266
Georges Bay	1923–1942	-	183.83	Saxelby Creek [EQ962248]
Siamese Tin Syndicate Ltd	1933–1939	-	430.09	EQ969285–EQ993251
Goshen Tin Mines N. L.	1937–1962	-	387.24	Launceston Creek [EQ956222] Groom River [EQ916312] Thureau's D. L. area [EQ969285] and other areas
Other	1961–1983	-	18.07	St Helens quadrangle
?Others	1961–1984	-	4.78	?St Helens quadrangle

AMG co-ordinates provide a guide to the positions of workings that were usually areally extensive.
Source – DMMR mine records.

Ridge around EQ859156, adjacent to the New Golden Ridge workings. North of Brilliant Creek the Brilliant leases contain many pits and other small workings. Of these, there are only a few with specific names such as Gruebers shaft and Carneys shaft on the crest of Golden Ridge. Multiple, scattered excavations are also a feature of other prospects. At the New Carthage prospect there are the Trafalgar shaft, the Carthage adit, the Beahr adit and small, un-named excavations.

GEOLOGY

The lodes

The lodes around Golden Ridge are hosted by adamellite (Dbapc) and by thermally metamorphosed Mathinna Beds. Double Event and New Carthage (Trafalgar) are in adamellite in the vicinity of the contact whilst the other lodes are in the thermal aureole of the adamellite. The apparent width of the aureole is greater, at least locally, than shown on St Helens map as there are spotted hornfels in the creek near the Queen of the Earth prospect (Groves, 1972). Variation in apparent aureole width between Queen of the Earth and the ridge to the north may be due to the aureole edge dipping generally south-east.

The un-named shaft at EQ890156 is beyond the edge of the aureole. The shaft is located in a block of old leases that were registered for gold but no distinctive mineralisation was found on the dumps, only white, vuggy, vein quartz. Another un-named shaft at EQ851053 is in thermally un-metamorphosed Mathinna Beds. No mineralisation was found nor reports relating to the prospect. The leases around EQ826129 were registered

Table A4. GOLD LODES AND ALLUVIAL GOLD OCCURRENCES IN THE WESTERN PART OF THE ST HELENS QUADRANGLE

Prospect	AMG	Product *(tonnes)*	Grade *(g/tonne)*	Reference
Brilliant (main lode)	EQ857154	102	unknown	1, 7
	-	sample	9.95 Au	1
White Lode (just E of Brilliant main lode)	-	61–102	unknown	1
	-	sample	82.65*	1
New Golden Ridge	EQ860156	-	-	3
Blinding	EQ856158	-	-	4
Golden Ridge workings	EQ864154–EQ867157	samples	1.53–19.90	1,7
	-	sample	14.99 Au, 50.0 Ag	1
	-	2	32.14 Au	1
	-	1	27.49 Au	1
	-	1	41.14 Au	1
	-	sample	3.06 Au, tr.Ag	1
	-	150	0.51 Au	8
	-	sample	13.14 Au, 4.78 Ag	8
Queen of the Earth	EQ877151	5	38.27 Au	2, 7
	-	50	33.10 Au	1
	-	196	22.4 Au	9
New Carthage (Trafalgar)	EQ882164	sample	49.99 Au, 49.99 Ag	1
	-	45	122.45 Au, 122.45 Ag*	1
Double Event	EQ879175	sample	131.63 Au*	1, 7
	-	sample	4.97 Au	1
un-named shaft (Au)	EQ890156	-	-	6
un-named leases (Au)	EQ826129	-	-	7
un-named shaft (?Au)	EQ851053	-	-	6, 7
alluvial	EQ912162	-	-	5
alluvial	EQ940095	-	-	8
alluvial	EQ937096	-	-	8

* Unconfirmed values reported to Twelvetrees, 1900*a*.
Source references: 1. Twelvetrees, 1900*a*; 2. Twelvetrees, 1900*b*; 3. Randell, 1991; 4. Davidson and Roach, 1990; 5. DMMR data base 'Mirloch'; 6. Located during mapping; 7. DMMR Lease Charts; 8. Henderson, 1939; 9. Groves, 1972.

Table A5. CONSTRUCTION MATERIALS

Grid Ref.	Occupier	Locality	Reserves	Status	Rock Name	Unit
FQ035173	Forestry Commission	Loilatier Road	MED	FOP	granite	Dbgp
FQ066270	Portland Council	St Helens	MED	ABN	granite	Dbgp
FQ075310	Barnett, A. J.& I. G.	Binalong Bay	SML	ABN	granite	Dbgsp
FQ078303	Portland Council	Binalong Bay	NOT	ABN	granite	Dbgsp
EQ985315	Portland Council	Ansons Bay R	NOT	ABN	granite	Dbasc
FQ088235	Portland Council	Stieglitz	NOT	FOP	sand	Ts
FQ024229	Stieglitz	Flagstaff Creek	NOT	FOP	sandstone	Mathinna Beds
EQ862310	Portland Council	Pyengana Sdl	SML	FOP	granite	Dbapc
FQ010238	-	Constable Creek	MED	FOP	gravel	Ts
FQ053091	PWD	Scamander	NOT	ABN	gravel	?
EQ847296	Haley	Pyengana	SML	FOP	siltstone	Mathinna Beds
FQ050083	PWD	Scamander	MED	ABN	gravel	Cpl
EQ902294	Portland Council	Goshen	NOT	ABN	granite	Dbasc
EQ905295	Singline	Goshen	NOT	FOP	granite	Dbasc
EQ987323	Singline	Ansons Bay Road	SML	ABN	granite	Dbasc
FQ057217	Portland Council	Parkside	MED	ABN	gravel	Ts
FQ041076	-	Scamander	NIL	ABN	gravel	Cpl
FQ043078	-	Scamander	SML	ABN	gravel	?Mathinna Beds
EQ996111	-	Scamander	SML	FOP	phyllite	Mathinna Beds
EQ940078	Forestry Commission	Catos Road	SML	ABN	phyllite	Mathinna Beds
EQ945067	Forestry Commission	Catos Road	SML	ABN	phyllite	Mathinna Beds
EQ996313	Portland Council	Ansons Bay Road	NOT	ABN	granite	Dbasc
FQ002308	Portland Council	Ansons Bay Road	NOT	ABN	granite	?Dbasc
EQ880165	-	Trafalgar Flat	NOT	ABN	hornfels	Mathinna Beds
EQ999233	Forestry Commission	St Helens	NOT	ABN	hornfels	Mathinna Beds
EQ921182	Portland Council	Carters Road	NOT	ABN	granite	Dbasc
EQ914188	-	Carters Road	NOT	ABN	granite	Dbasc
EQ933233	Portland Council	Argonaut Road	NOT	ABN	granite	Dbasc
EQ937232	Portland Council	Argonaut Road	NOT	ABN	granite	Dbasc
EQ942245	Portland Council	Argonaut Road	NOT	ABN	granite	Dbasc
EQ929190	Portland Council	Hogans Road	NOT	ABN	granite	Dbasc
FQ045115	Forestry Commission	Coach Road	MED	ABN	siltstone	Mathinna Beds
FQ038293	Portland Council	George River	NOT	ABN	granite	Dbasc
FQ020238	-	Medeas Cove Road	SML	ABN	gravel	Ts
FQ024248	Portland Council	Fleece River	NIL	FOP	gravel	Ts
FQ016242	-	Constable Creek	NOT	ABN	granite	Dba
EQ843104	Forestry Commission	Hogans Road	SML	NEW	conglomerate	Parmeener SG
EQ840088	Forestry Commission	Hogans Road	SML	ABN	sandstone	Parmeener SG
EQ842102	Forestry Commission	Hogans Road	SML	NEW	conglomerate	Parmeener SG
FQ051186	Forestry Commission	Dianas Basin	MED	NEW	gravel	?Mathinna Beds
EQ960280	Forestry Commission	Bog Creek	MED	NEW	granite	Dbasc
EQ997273	PWD	Aeson Creek	MED	FOP	granite	?Dbgsp
FQ107267	PWD	Point Road	MED	OCC	granite	Dbgbsp
EQ843075	Forestry Commission	Pimple Road	MED	NEW	conglomerate	Parmeener SG
EQ848065	Forestry Commission	Pimple Road	MED	NEW	phyllite	Mathinna Beds
EQ845060	Forestry Commission	Pimple Road	MED	NEW	phyllite	Mathinna Beds
EQ943086	Forestry Commission	Black Tommys Hill	SML	NEW	granite	?
EQ938237	Forestry Commission	Girdys Hill	LGE	-	granite	Dbasc
EQ902315	Forestry Commission	Groom River	SML	NEW	granite	Dbapc
EQ989281	Forestry Commission	Tasman Highway	NOT	NEW	gravel	Ts
FQ083237	Portland Council	Stieglitz	NOT	FOP	sand	Ts
FQ093239	Portland Council	Stieglitz	NOT	FOP	sand	Ts
FQ090240	Portland Council	Stieglitz	SML	FOP	sand	Ts
EQ901294	Portland Council	Goshen	NOT	FOP	granite	Dbasc
FQ039077	-	Scamander	SML	ABN	gravel	Cpl
FQ013250	Burns, P. L.	Argonaut Road	-	-	sand	?Qha
FQ089241	Burns, P. L.	Stieglitz	-	-	sand	Ts
FQ010248	Burns, P.L.	Medeas Cove	-	-	sand	Ts
FQ088241	Griffiths, T. C.	Stieglitz	-	-	sand	Ts
FQ019242	Riley, R. C.	Medeas Cove	-	-	sand	Qha
FQ030082	Trotter, G. D. & C.	Scamander Road	-	-	sand	?Cpl
EQ945316	Griffiths, T. C.	Apteds Creek	-	-	granite	Dbgp
EQ936179	APPM Forest Products	Carters Creek	-	-	siltstone	Mathinna Beds
EQ900163	Bradbury, R. N. & HYD	Beahrs Creek	-	-	siltstone	Mathinna Beds
EQ945315	Forestry Commission	Apteds Creek	-	NEW	granite	Dbgp
EQ849052	Forestry Commission	Pimple Road	-	NEW	conglomerate	?

Reserves: NOT = not established; NIL=<1000 t; SML (small) = 1000–10 000 t; MED (medium) = 10 000–1 000000 t; LGE (large) = 1 000 000–1 000 000 000.
Status: FOP – fully operational; ABN – abandoned; OCC occasional use; NEW – new.
Source: DMMR Construction Materials Register.

for gold but no reports describing workings or mineralisation have been found.

At the New Carthage prospect the lode intersected by Beahr adit comprised arsenopyrite in ENE-trending quartz veins at the adamellite/Mathinna Beds contact (Twelvetrees, 1900*a*; Henderson, 1935). Minor associated sulphides were galena, chalcopyrite and pyrite (Groves, 1972) with supergene scorodite. The lode is transitional into sericitised and chloritised adamellite containing disseminated sulphides carrying gold. There is a further transition to unaltered adamellite.

Arsenopyrite is abundant in the NNE-trending quartz vein lode at Queen of the Earth where it is accompanied by minor pyrite, sphalerite and galena. Sulphides are present in minor amounts in quartz veins in the Golden Ridge workings and include arsenopyrite, pyrite and supergene covellite. However, no sulphides are known in the quartz vein lodes at Double Event and Brilliant which trend ENE and N-NNE respectively.

In general, the quartz veins in the lodes around Golden Ridge are thin and impersistent and the gold mineralisation is patchy. Reputable assays of up to about 50 g/tonne Au have been obtained (Table A4) from lode material with unconfirmed claims of substantially higher values (Twelvetrees, 1900*a, b*). Variable silver is present and may be combined with gold in electrum (Twelvetrees, 1900*a*).

Alluvial gold

Henderson (1939) found minor alluvial gold in tributaries of the Avenue River near EQ940095 and EQ937096, which drain metamorphosed Mathinna Beds, but considered the remainder of the drainage system to be barren. Little alluvial gold appears to have accumulated in the youthful drainage system downstream of the lodes around Golden Ridge.

Heavy minerals in beach and dune sands

Heavy minerals are generally present in only small amounts in the beach sands of the St Helens quadrangle (Denholm, 1968). They are also low in the extensive dunes south of St Helens Point. The greatest abundance is in beach sands near the mouth of the Scamander River where the heavy mineral suite includes zircon, rutile, garnet and opaque minerals comprising over 90% ilmenite. Best grades of about 1% combined zircon and ilmenite occur in small pockets.

Heavy minerals derived from beach shingle near FQ136297 at St Helens Heads include coarse-grained cassiterite and cassiterite also occurs in beach shingle near FQ091323, close to Binalong Bay (Chesnut, 1966). Cassiterite is present in beach sands along the southern edge of Georges Bay but not in commercial quantities (Waller, 1901).

Clay

Twelvetrees (1904) described a formation of light grey clay exposed at, and just above, high-water mark along part of the south-east shore of Georges Bay near Parnella. Boring and shaft sinking related to tin prospecting in adjacent areas established up to 10 m of uniform clay extending over a wider area.

Crude tests suggested that the clay would fire a white colour and be suitable for fine pottery and stoneware. Blake (1928) summarises the earlier information on the Georges Bay clay and classifies it as a kaolinic or silico-feldspathic clay suited for the manufacture of china, granite-ware and fine pottery generally.

A little clay was quarried for brickmaking near the Recreation Ground at St Helens in the 1880s and from a locality at the southern end of Georges Bay early in this century (Peter Burns, St Helens History Room, pers. comm).

Construction materials

Materials for road construction are quarried at many places in the St Helens quadrangle and most rock types are utilised. Table A5 contains an extract of data from the DMMR data base 'Conmat' which shows position of quarries to 1986, rock type, occupier and operational status.

REFERENCES

ANON. 1981. *North Scamander prospect. Report on drilling, July to September, 1981.* Broken Hill Pty Co. Ltd. [TCR 82-1680a].

ANON. 1989. *Portland before 1932.* St Helens History Room : St Helens [originally published in *The Examiner, Launceston*: 12.3.1932].

BLAKE, F. 1928. Clay and sand deposits of Tasmania. *Unpubl. Rep. Dep. Mines Tasm.* 1928(2):45-50.

CHESNUT, W. S. 1966. *Report on reconnaissance prospecting of offshore exploration licence (E.L. 5/65).* Broken Hill Pty Co. Ltd. : Melbourne. [TCR 66-417].

COCKER, J. D. 1977. The geology of the St Helens area: petrology and structure of the granitoid rocks in GROVES, D. I.; COCKER, J. D.; JENNINGS, D. J. The Blue Tier Batholith. *Bull. geol. Surv. Tasm.* 55:117–156.

CROMER, W. C. 1990. *EL 76/87 Scamander, eastern Tasmania. Year 2 Annual Report.* May 1989–May 1990 Seabed Resources N.L. [TCR 90-3120].

DAVIDSON, G.; ROACH, M. 1990. The geology, geophysics and mineralisation of the Golden Ridge area, north east Tasmania, *in* RANDELL, J. P. 1991. *EL 58/88 – Golden Ridge Joint Venture. Annual exploration report for the period 7.4 1990–7.4 1991.* Billiton Australia. [TCR 91-3232].

DENHOLM, L. S. 1968. *Final report on Scamander H. M. beach sand prospect, Scamander, Tasmania. S.P.L. No. 33.* New Consolidated Gold Fields (A'sia) Pty Ltd. [TCR 68-496].

ELLIS, P. D. 1983. *Final report 1982-1983. Exploration Licence 11/78. George River, Northeast Tasmania.* EMR 60/83, CSR Ltd. [TCR 83-1990].

EVERARD, G. 1964. Petrological examination of specimens from Pyramid Mine, Upper Scamander. *Tech. Rep. Dep. Mines Tasm.* 8:133–135.

FORD, R. J.; GROVES, D. I.; KLOMINSKY, J. 1970. Oxidation at the Orieco copper mine, eastern Tasmania. *Proc. australas. Inst. Min. Metall.* 235:87–92.

GROVES, D. I. 1972. The zoned mineral deposits of the Scamander – St Helens district. *Bull. geol. Surv. Tasm.* 53.

GROVES, D. I. 1977. The geology, geochemistry and mineralisation of the Blue Tier Batholith, *in* GROVES, D. I.; COCKER, J. D.; JENNINGS, D. J. The Blue Tier Batholith. *Bull. geol. Surv. Tasm.* 55:7–116.

GROVES, D. I.; BAKER, W. E. 1971. The cobalt and nickel content of some sulphides from ore deposits in eastern Tasmania. *Tech. Rep. Dep. Mines Tasm.* 14:27–35.

GROVES, D. I.; MCCARTHY, T. S. 1978. Fractional crystallisation and the origin of tin deposits in granitoids. *Mineralium Deposita* 13:11–26.

HALL, G. C. 1979. *Exploration of EL 11/78, George River prospect, St Helens district, Tasmania.* EMR 86/79, CSR Minerals and Chemical Division. [TCR 79-1407].

HARRIS, W. K. 1968. Tasmanian Tertiary and Quaternary microfloras. Summary report. *Palaeont. Rep. geol. Surv. S. Aust.* 5/68.

HENDERSON, Q. J. 1935. Notes on the Trafalgar leases, Upper Scamander district. *Unpubl. Rep. Dep. Mines Tasm.* 1935: 51–53.

HENDERSON, Q. J. 1939. Report on the geological survey of the country between Scamander and Mathinna. *Unpubl. Rep. Dep. Mines Tasm.* 1939:53–60.

HENDERSON, Q. J. 1941. Scamander copper field. *Unpubl. Rep. Dep. Mines. Tasm.* 1941:5–11.

HILLS, L. 1916. Tungsten and molybdenum. Part 1. North-eastern and eastern Tasmania. *Miner. Resour. geol. Surv. Tasm.* 1.

JACK, R. 1964*a*. Great Pyramid tin mine, Upper Scamander. *Tech. Rep. Dep. Mines Tasm.* 8:25–45.

JACK, R. 1964*b*. Thureau's deep lead, St Helens. *Tech. Rep. Dep. Mines Tasm.* 8:63–71.

JENNINGS, D. J. 1968*a*. Alluvial tin in the Lower Scamander River valley. *Tech. Rep. Dep. Mines Tasm.* 11:32, 34–36.

JENNINGS, D. J. 1968*b*. Geological investigations and results of drilling for tin, adjacent to the George River. *Tech. Rep. Dep. Mines Tasm.* 12:19–24.

MONTGOMERY, A. 1893*a*. Report on Thureau's Deep Lead, near George Bay. *Department of Mines, Tasmania.*

MONTGOMERY, A. 1893*b*. Report on the silver-bearing lodes of the Scamander River district. *Rep. Secr. Mines Tasm.* 1892–1893:i-iii.

MORTIMORE, I. R. 1970*a*. *Memorandum report on the Lutwyche prospect, Wolfram Creek area. E.L. 6/68, N. E. Tasmania.* Geophoto Minerals Report 1970/82, Geophoto Resources Consultants. [TCR 70-689].

MORTIMORE, I. R. 1970*b*. *Memorandum report on geochemical sampling in the Copper Show Creek prospect E.L. 6/68, N. E. Tasmania.* Geophoto Minerals Report 1970/83, Geophoto Resources Consultants. [TCR 70-690].

MORTIMORE, I. R. 1971. *Preliminary diamond drilling, Upper Scamander anomaly. E.L. 6/68 north east Tasmania.* Geophoto Minerals Report 1971/44, Geophoto Resources Consultants. [TCR 71-819].

MORTIMORE, I. R.; RATTIGAN, J. H. 1970. *Memorandum report on Constable's Creek drilling EL 6/68, St Helens district, Tasmania.* Geophoto Minerals Report 1970/3, Geophoto Resources Consultants. [TCR 70-701].

NYE, P. B. 1933. Geological notes on the St Helens district. *Unpubl. Rep. Dep. Mines Tasm.* 1933:71–771.

NYE, P. B. 1941*a*. Lease 11866/M (southern portion of western Pinnacle). *Unpubl. Rep. Dep. Mines Tasm.* 1941–1942:55–57.

NYE, P. B. 1941*b*. The tungsten resources of Tasmania. *Unpubl. Rep. Dep. Mines Tasm.* 1941–1942:61–81.

RANDELL, J. P. 1991. *EL 58/88 – Golden Ridge Joint Venture. Annual exploration report for the period 7/4 1990–7/4 1991.* Billiton Australia. [TCR 91-3232].

RUXTON, P. A. 1984. *E.L. 12/78 – Scamander. Progress report on exploration during the period 1/9/83–1/8/84.* Billiton Australia. [TCR 84-2218].

RUXTON, P. A.; PLUMMER, G. (unpublished). *Anatomy of a zoned WO_3-Mo, Sn, Cu, Pb-Zn-Ag-Au system – the Scamander Mineral Field, north east Tasmania.*

RUXTON, P. A.; PLUMMER, G. 1984. Economic geology and fluid inclusion history of the Scamander Mineral Field and Great Pyramid tin deposit, NE Tasmania, *in* BAILLIE, P. W.; COLLINS, P. L. F. (ed.). *Mineral exploration and tectonic processes in Tasmania.* Geological Society of Australia, Tasmanian Division : Hobart.

SCHELL, H. Z. 1938. *Report on mineral sections, Upper Scamander district, Tasmania.* [TCR 37-072].

SECRETARY FOR MINES. 1884–1902. *Reports.* Government Printer : Hobart.

SMITH, J. H. 1897. Report on the Scamander mining district in April, 1897. *Rep. Secr. Mines Tasm.* 1896–1897: xxxix–xlii.

THUREAU, G. 1886. Report on the Scamander silver and gold deposits. *Parliamentary Pap. Tasm.* 73.

THUREAU, G. 1888. Reports written to private prospectors. See MONTGOMERY, 1893.

TURNER, N. J.; TAHERI, J. 1990. *Tin and tungsten deposits and related Devonian granitoids. 10th Australian Geological Convention, Excursion Guide E2.* Geological Society of Australia, Tasmanian Division : Hobart.

TWELVETREES, W. H. 1900*a*. Report on gold mines near Hogan's track. *Rep. Secr. Mines Tasm.* 1899–1900:i–xiii.

TWELVETREES, W. H. 1900*b*. Report on the Queen of the Earth gold mine and neighbourhood. *Rep. Secr. Mines Tasm.* 1899–1900:xcvi–cvi.

TWELVETREES, W. H. 1902. Report on the tin mines of the Blue Tier, County of Dorset. *Rep. Secr. Mines Tasm.* 1901–1902:91–122.

TWELVETREES, W. H. 1904. Report on deposits of clay at Georges Bay and elsewhere. *Department of Mines, Tasmania*

TWELVETREES, W. H. 1911. The Scamander mineral district. *Bull. geol. Surv. Tasm.* 9.

URQUHART, G. 1968. Loila Tier tin prospect, Scamander area. *Tech. Rep. Dep. Mines Tasm.* 11:18–23, 25.

WALKER, K. R. 1957. The geology of the St Helens–Scamander area, Tasmania. *Pap. Proc. R. Soc. Tasm.* 91:23–39.

WALLER, G. A. 1901. Report on the mining district of the Scamander River and St Helens. *Rep. Secr. Mines Tasm.* 1900–1901:268–301.

WARD, C. W. 1972. *Final report – Scamander River.* Cominco Exploration Pty Ltd. [TCR 72-842].

WILLIAMS, R. E. 1980. *Progress report on exploration of EL 11/78, Georges River prospect, St Helens district, Tasmania.* EMR 69/80, CSR Ltd Minerals Division. [TCR 80-1482].